# Optimal Scheduling of Self-healing Distribution Systems Considering Distributed Energy Resource Capacity Withholding Strategies

Meysam Aboutalebi [1], Mehrdad Setayesh Nazar[1], Miadreza Shafie-khah[2], and João P. S. Catalão[3,*]

[1] *Shahid Beheshti University, Tehran, Iran*
[2] *School of Technology and Innovations, University of Vaasa, 65200 Vaasa, Finland*
[3] *Faculty of Engineering of the University of Porto and INESC TEC, 4200-465 Porto, Portugal*
[*] *catalao@fe.up.pt*

**Abstract**

This paper presents a multi-stage day-ahead and real-time optimization algorithm for scheduling of system's energy resources in the normal and external shock operational conditions. The main contribution of this paper is that the model considers the non-utility electricity generation facilities capacity withholding opportunities in the optimal scheduling of system resources. The real-time simulation of external shock impacts is another contribution of this paper that the algorithm simulates the sectionalizing of the system into multi-microgrids to increase the resiliency of the system. The optimization process is categorized into two stages that compromise normal and contingent operational conditions. Further, the normal operational scheduling problem is decomposed into three steps. At the first step, the optimal day-ahead scheduling of system resources and the switching of normally opened switches are determined. At the second step, the optimal real-time market scheduling is performed and the switching of normally closed switches is optimized. At the third step, different extreme shock scenarios are simulated in the real-time horizon and the effectiveness of sectionalizing the system into multi-micro grids are assessed. Finally, at the contingent operational conditions, the optimal topology of the system and scheduling of energy resources are determined. The proposed method was successfully assessed for the 33-bus and 123-bus test systems. The algorithm were reduced the expected cost of the worst-case contingencies for the 33-bus and 123-bus systems by about 97.89% and 88.11%, respectively. Further, the average and maximum values of the 123-bus system capacity-withholding index for real-time conditions reduced by about 67.40% and 71.05%, respectively.

**Keywords:** Resiliency; Demand response program; Optimal Scheduling; Multi-microgrids; Reconfiguration; Capacity Withholding.

## Nomenclature

**Abbreviation**

| | |
|---|---|
| ARIMA | Autoregressive Integrated Moving Average |
| CWI | Capacity-Withholding Index |
| DA | Day-Ahead |
| DER | Distributed Energy Resources |
| DRP | Demand Response Program |
| DSO | Distribution System Operator |
| ESS | Electrical Energy Storage |
| MILP | Mixed Integer Linear Programming |
| MINLP | Mix Integer Non-Linear Programming |
| MT | Micro Turbine |
| NUDERs | Non-utility DERs |
| PHEV | Plug-in Hybrid Electrical Vehicle |
| SFE | Supply Function Equilibrium |

**Sets**

| | |
|---|---|
| I | Set of buses in normal operational condition |
| K | Set of buses in contingent operational condition |
| T | Set of time intervals |
| S | Set of scenarios |
| Z | Set of system topology in normal conditions |
| *NOSDA* | Set of normal operation states in day-ahead horizon |
| *NOSRT* | Set of normal operation states in real-time horizon |

**Parameters**

| | |
|---|---|
| $\alpha, \beta$ | Parameters of the demand curve |
| $c^{NUDER}$ | Cost of electricity purchased from non-utility DER ($/kWh) |
| $c^{L}$ | Price of electricity sold to the consumers ($/kWh) |
| $c^{grid}$ | Price of electricity transacted with the upward market ($/kWh) |
| $c^{MT}$ | Operational cost of microturbine ($/kWh) |
| $c^{down}/c^{up}$ | Startup/shutdown cost of microturbine ($) |
| $c^{RD}$ | Re-dispatch cost of microturbine ($/kWh) |
| $c^{pul}$ | Emission cost of microturbine ($/kg) |
| $c^{ES}$ | Operational and maintenance costs of energy storage ($/kWh) |
| $c^{RER}$ | Operational and maintenance costs of renewable energy resource facilities ($/kWh) |
| $v$ | Emission factor of microturbine (kg/kWh) |

| | |
|---|---|
| $P^{PV}$ | Forecasted photovoltaic electricity generation (kW) |
| $\Delta P^{PV}$ | Forecasting error of photovoltaic electricity generation (kW) |
| $P^{WT}$ | Forecasted wind turbine electricity generation (kW) |
| $\Delta P^{WT}$ | Forecasting error of wind turbine electricity generation (kW) |
| $P^{L}$ | Forecasted electrical load (kW) |
| $\Delta P^{L}$ | Forecasting error of electrical load (kW) |
| $P^{crit}$ | Critical electrical load (kW) |
| $P^{ncrit}$ | Non-critical electrical load (kW) |
| $CLPE$ | Critical load percentage coefficient |
| $\eta_{dch}/\eta_{ch}$ | Charge/discharge efficiency of energy storage |
| $\pi_{dch}/\pi_{ch}$ | Charge/discharge efficiency of PHEV |
| $cap$ | Capacity of energy storage (kW) |
| $st$ | Status of PHEV connected to network (binary parameter) |
| $T_h$ | Scheduling horizon |
| $T_p$ | Time duration of scheduling interval |
| $Prob$ | Probability of scenario |
| $\varphi$ | Price of electricity market |
| $\theta$ | Quantity of distribution system load |
| $\varpi$ , $\zeta$ | Parameters of non-utility distributed generation submitted bid |
| $N$ | Number of non-utility DERs |
| $a$ | Non-utility DERs generation cost multiplier |
| $\Delta U$ | Ramp rate of microturbine |
| $W$ | Weighting factor |

**Variables**

| | |
|---|---|
| $P^{NUDER}$ | Electric power purchased from non-utility DER (kW) |
| $\Delta P^{NUDER}$ | Change in electric power purchased from non-utility DER (kW) |
| $P^{L}$ | Electric power sold to the consumers ($/kW) |
| $P^{MT}$ | Generated electricity of microturbine (kW) |
| $P^{grid}$ | Transacted electricity with upward market (kW) |
| $\Delta P^{grid}$ | Change in transacted electricity with upward market (kW) |
| $P^{ES}$ | Electrical power of energy storage (kW) |
| $\Delta P^{ES}$ | Change in electrical power of energy storage (kW) |
| $SOC$ | State of charge of energy storage |
| $P^{PHEV}$ | Electrical power of PHEV (kW) |
| $E^{PHEV}$ | Electrical energy of PHEV (kWh) |
| $\lambda^{dch}/\lambda^{ch}$ | Binary decision variable of energy storage charge/discharge |

| | |
|---|---|
| $\gamma^{dch}/\gamma^{ch}$ | Binary decision variable of PHEV charge/discharge |
| $\tau$ | Binary decision variable for commitment of microturbine |
| $X$ | Binary decision variable of boundary line |
| $Y$ | Non-critical load supply decision variable |
| $D$ | Duration of deferrable non-critical load commitment |
| $Q_0^{Lt}$ | Normal level of operational condition |
| $Q_{min}^{Lt}$ | Minimum level of operational condition |
| $RI$ | Resiliency index |
| $\Delta\theta^{distort}$ | Capacity distortion of the market |
| $\Delta\theta^{withheld}$ | Capacity withheld of the market |
| $\Delta\lambda^{distort}$ | Lagrangian multipliers associated with power balance constraints in the distortion of market |
| $\Delta\lambda^{withheld}$ | Lagrangian multipliers associated with power balance constraints in capacity withheld of market conditions |
| $\psi$ | Binary variable of system topology state |

## 1. Introduction

Microgrids are the main components of smart grids that utilize Distributed Energy Resources (DERs) to increase the efficiency of energy conversion, reduce environmental pollutions, and enhance the operational flexibility of energy infrastructures. The optimal operational scheduling of microgrids is highly considered in recent papers to improve operational paradigms, reduce costs, increase reliability, and resiliency of systems. Microgrids can be optimally scheduled by different operational paradigms based on the DERs locations, communication infrastructure design, and other technical and economic parameters [1].

The resiliency of the distribution system can be improved by coordinating the operational scheduling of microgrids in external shock conditions to mitigate the impacts of catastrophic events and utilizing the DERs to continue the energy supply [2]. The utilization of Demand Response Programs (DRPs), Electrical Storage Systems (ESSs), and Plug-in Hybrid Electric Vehicles (PHEVs) in microgrids can highly improve the resiliency of the distribution system based on the fact that these energy resources can be dispatched in emergency conditions and they can deliver their energy to the other microgrids. An optimal resilient operation of microgrids that considers the coordinated operation of distributed energy resources in normal and emergency conditions is an important issue in the operational scheduling of distribution systems.

Over the recent years, different optimal scheduling processes and frameworks are presented for microgrids that consider normal operation conditions and external shock conditions. As shown in Table 1, the literature can be categorized into the following categories.

The first category considers the optimal operational scheduling of microgrids in normal conditions that the microgrids transact energy with the upward electricity market. However, the optimal resilient scheduling of the system was not considered in these papers. The algorithms and formulations of these papers are

explored in this survey to consider their methods and frameworks in the development of the present paper formulation and framework.

Ref. [3] presented a coordinated operational paradigm for multi-microgrids that considered the uncertainty of energy resources. Combined heat and power units and thermal energy storages were committed in the Day-Ahead (DA) scheduling horizon. The proposed method utilized a two-stage Mixed Integer Linear Programming (MILP) process. The results showed that the stochastic modelling of parameters led to an increase in the operational costs of the IEEE-33 bus test system by about 7.132%. However, the external shock impacts on the system and capacity withholding procedures were not considered.

Ref. [4] introduced stochastic optimal scheduling of DERs of microgrids. The thermal loads and security constraints were considered in the model and the user comfort levels were modelled. The simulation was carried out for the 37-bus test system and the results presented that the proposed method reduced the operational costs of the microgrid. The real-time operational scheduling of the system and capacity withholding process were not modelled.

Ref. [5] assessed a two-stage model for optimal scheduling of a microgrid. The model utilized a probabilistic optimal power flow method and minimized the operational costs and environmental emissions. The imperialist competitive algorithm was used to optimize the problem and the proposed method successfully reduced the operational and pollution costs. Ref. [6] developed a two-stage optimization framework that considered the PHEVs and responsive loads and minimized the operational and pollutant costs. The intermittent electricity generation facilities were modelled and the particle swarm optimization process was used to find the optimal values of objective functions. The operational costs and emissions were reduced by about 8.61% and 0.61%, respectively. Refs. [5-6] did not consider the sectionalizing process of the system in the contingent conditions, the capacity withholding of non-utility facilities, and the impacts of external shocks on the system.

Ref. [7] introduced an optimization approach for scheduling multi-carrier energy systems. The model considered the interruptible loads as a reserve and the augmented ε-constraint method was used to solve the problem. The method reduced the operating costs by about 0.38% concerning the base case. Ref. [8] proposed a tri-objective function optimization algorithm that minimized the operating costs and emission pollutions and maximized the customer satisfaction level. The shuffled frog-leaping algorithm was utilized for optimization and five case studies were assessed the proposed method. Ref. [9] explored an algorithm for minimizing operating costs, loss of load, and deviation of electricity consumption and generation. The ε-constraint optimization method was applied on the 83-bus test system and four case studies were compared. Refs. [7-9] did not model the non-utility capacity withholding process, sectionalizing of system, and real-time operational scheduling of system.

Ref. [10] assessed an optimal day-ahead scheduling algorithm for microgrids that minimized the operating costs, load curtailment, and coordinated the deferrable loads using the ε-constraint method. A 24-node microgrid was used to assess the model and four scenarios were considered. Ref. [11] introduced an

algorithm for energy management of microgrids considering hydrogen energy storage. The uncertainties of renewable energy generation and loads were considered using the Monte Carlo method. The non-dominated Pareto solutions were considered as the optimal solutions. Refs. [10-11] did not model the resilient operational scheduling of the system, the capacity withholding of non-utility generation facilities in the external shock conditions, and the sectionalizing of the system.

Ref. [12] proposed a stochastic optimization programming approach for optimal scheduling of microgrids considering plug-in electric vehicles, virtual power plants, and demand response programs. The time-of-use and real-time pricing methods were considered. Ref. [13] considered the impacts of battery storage stations on the planning and operational scheduling of microgrids considering the hydro storages, distributed generations, and photovoltaic systems. The model considered the intermittent power generation facilities and electric vehicle charging uncertainties. Ref. [14] modelled the reconfiguration process of distribution systems considering intermittent electricity generation facilities, demand response programs, and energy storage systems. However, Refs. [12-14] did not consider the capacity withholding of non-utility generation facilities in the external shock conditions, the self-healing operational scheduling of the system, and the sectionalizing of the system.

The second category of papers determines the resilient operational scheduling of microgrids in normal and external shock conditions and utilizes the concept of a self-healing framework to improve the resiliency of microgrids. These papers propose the optimal DERs scheduling and electric system switching for pre-event and/or post-event conditions.

Ref. [15] introduced an optimization process to increase the resiliency of the distribution system using sectionalizing of a network. The rolling horizon method was utilized to determine the optimal DA scheduling of DERs and responsive loads. The stochastic optimization algorithm was carried out and the operational costs of the 123-bus test system were minimized in the normal operational conditions; meanwhile, the restoration process in extreme conditions was assessed. Ref. [16] presented a framework for optimal resilient operational scheduling of networked microgrids. A resiliency index was proposed and the uncertainties of intermittent electricity generation facilities and market prices were modelled using a robust optimization process. Different case studies were performed and the proposed method reduced the shed load by about 78.36%. Refs. [15-16] did not model the capacity withholding of non-utility generation facilities in the contingent conditions and optimal scheduling of energy resources in a real-time horizon.

Ref. [17] evaluated an algorithm for increasing the resiliency of networked microgrids. The method utilized an index to assess the resiliency level of the system and an analytical hierarchical process was used to evaluate the resiliency index. Results showed that the resiliency index was increased by about 25.38%. Ref. [18] proposed a planning and scheduling framework for increasing the resiliency of the distribution system using graph theory and the Tabu search algorithm. The proposed model minimized load-generation imbalance, disconnected loads, and energy losses as different objective functions. The method

simultaneously reduced the objective functions for a test system. Refs. [17-18] did not consider the real-time simulation of external shocks and the capacity withholding process of non-utility generation facilities. Ref. [19] introduced a networked microgrids optimal scheduling process that utilized the nested energy management framework to mitigate the impact of external shocks. The method improved the resiliency of the system using multiple nested microgrids that minimized the operational costs of the system and considered the privacy of consumers. The algorithm used the MILP process to find the optimal DA scheduling of the system and the results showed the viability of the algorithm. Different scenarios were considered for the simulations and the demand response process reduced the shed load by about 57.3% concerning the base case. Ref. [20] proposed a framework for determining the model of microgrid formation that maximized the restored loads. An iteration based linear approximation was considered to solve the Mixed Integer Non-Linear Programming (MINLP) model. Refs. [19-20] did not model the real-time optimal scheduling of energy resources and the uncertainties of external shocks and intermittent energy generations. Further, the capacity withholding process of non-utility energy generation devices was not modelled.

Ref. [21] presented a resiliency-based modelling framework for restoration strategies of electric distribution systems. A resiliency measure was considered to model the response-time components and define the set of feasible restoration policies. The model was assessed for a test system with a 180-component system consisted of lines, laterals, and transformers. Ref. [22] assessed a two-stage optimization process that considered the optimal scheduling of microgrids and distribution systems. At the first stage, the microgrids optimized their DERs commitment schedule and at the second stage, the distribution system utilized the capacity of microgrids to recover the energy service of unserved loads using the resiliency index. The MILP model was used for the optimization algorithm. Two methods consisted of centralized and hierarchical optimization processes were considered. The centralized approach showed better results and it reduced the unserved energy more than the hierarchical method. Refs. [21-22] did not consider the real-time reconfiguration of the system, the capacity withholding of non-utility generation facilities, and simulation of shocks, and the intermittent electricity generation uncertainties.

Ref. [23] introduced a two-stage optimization framework to coordinate the microgrids and distribution system using graph theory. The first stage optimized DA scheduling of microgrids energy resources and the second stage determined the optimal coordination of microgrids. The effectiveness of the method was assessed for the 33-bus test system. The graph theory model reduced the operational costs of the system by about 3.53%. Ref. [24] considered a two-stage optimization algorithm for improving the resiliency of the distribution system that utilized the optimal formation of microgrids and commitment of DERs. The uncertainties of energy resources were modelled and a stochastic optimization process was used. The proposed method successfully restored the shed loads using multi-microgrids. Refs. [23-24] did not model the real-time simulation of external shock impacts and their uncertainties. Further, the capacity withholding processes of non-utility generation devices were not modelled.

Ref. [25] proposed a three-stage optimization process that improved the resiliency of the distribution system. At the first stage, the hardening preparation process was considered and at the second stage, the optimal switching actions were performed to increase the system resiliency. Finally, in the third stage, the final steps of service restoration were performed. Ref. [26] utilized an optimization algorithm to supply the critical loads in emergency conditions and increase the resiliency of the system. The process considered adjustable loads and a non-linear optimization algorithm was performed. The minimization of load shedding and maximization of served non-critical loads were considered. Refs. [25-26] did not explore the simulation of external shocks in the real-time operational scheduling and the capacity withholding of non-utility generation facilities.

Ref. [27] assessed an optimization process that clustered the electric system into multi-microgrids in contingent conditions to increase the resiliency of the system. The multi-objective functions were energy not supplied, reactive power not supplied, energy loss, and voltage deviations. The optimization process utilized fuzzy satisfaction and the Pareto optimality method and the algorithm was assessed for the 33-bus and 69-bus test systems. Ref. [28] developed an optimization model to minimize load curtailments in the contingent condition of the electrical system considering uncertainties. A robust optimization procedure was performed to determine the optimal scheduling of system resources and evaluate the worst-case conditions. Refs. [27-28] did not consider the real-time operational scheduling of energy resources in the normal and contingent conditions, and the capacity withholding process of non-utility generation facilities. Table 1 shows the comparison of the proposed framework with the other papers. An algorithm that simultaneously schedules the utility-owned and non-utility owned distributed energy resources in day-ahead and real-time horizons for normal and contingent conditions considering the impacts of capacity withholding of non-utility is less frequent in the previous papers. Further, the proposed method evaluates the impacts of external shocks of system conditions for the real-time horizon and simulates the sectionalizing process of the distribution system into multi-microgrids to reduce the impacts of shocks.

The main contributions of this paper can be summarized as:

- The proposed algorithm considers the capacity withholding process of non-utility owned electricity generation facilities in the optimal scheduling of system resources using the capacity-withholding index. The capacity-withholding index detects the probable capacity withholding opportunities of non-utility distributed energy resources that may tend to the lower level of system resiliency,
- A resiliency index is utilized to evaluate the vulnerability level of the system in the day-ahead and real-time horizons for external shock conditions considering the values of capacity withholding index,
- The algorithm explores the external shocks impacts on the system, minimizes the impacts of the worst-case contingencies, and utilizes an optimization process to sectionalize the distribution system into multi-microgrids, and reschedule the system resources,
- The algorithm reconfigures the distribution system in the day-ahead and real-time normal operational conditions to mitigate the capacity withholding and the impacts of probable external shock impacts.

Table 1: Comparison of the proposed method with other papers.

| Ref. | | 3 | 4 | 5 | 6 | 7 | 8 | 9 | 10 | 11 | 12 | 13 | 14 | 15 | 16 | 17 | 18 | 19 | 20 | 21 | 22 | 23 | 24 | 25 | 26 | 27 | 28 | Proposed Approach |
|---|---|---|---|---|---|---|---|---|---|---|---|---|---|---|---|---|---|---|---|---|---|---|---|---|---|---|---|---|
| Real-time simulation of external shocks | | × | × | × | × | × | × | × | × | × | × | × | × | × | × | × | × | × | × | × | × | × | × | × | × | × | ✓ | ✓ |
| Multi-microgrid formation | | × | × | ✓ | × | × | × | × | × | × | × | × | × | ✓ | ✓ | ✓ | ✓ | ✓ | × | × | ✓ | ✓ | × | × | × | × | × | ✓ |
| DA and RT Reconfiguration | | × | × | × | × | × | × | × | × | × | × | × | × | × | × | × | × | × | × | × | × | × | × | × | × | × | × | ✓ |
| Method | MILP | ✓ | × | × | × | × | × | × | × | × | ✓ | × | × | × | × | × | × | ✓ | × | × | × | × | × | × | × | × | ✓ | × |
| | MINLP | × | × | × | × | ✓ | × | × | × | × | × | ✓ | ✓ | ✓ | × | × | × | × | ✓ | × | × | × | × | × | × | ✓ | × | × | × |
| | Heuristic | × | ✓ | ✓ | ✓ | × | ✓ | ✓ | ✓ | ✓ | × | × | × | × | ✓ | ✓ | ✓ | × | × | ✓ | ✓ | ✓ | ✓ | ✓ | × | ✓ | × | ✓ |
| Model | Deterministic | ✓ | × | ✓ | × | ✓ | ✓ | ✓ | ✓ | × | × | × | × | × | × | ✓ | ✓ | ✓ | ✓ | × | ✓ | ✓ | ✓ | ✓ | ✓ | ✓ | ✓ | × |
| | Stochastic | × | ✓ | × | ✓ | × | × | × | × | ✓ | ✓ | ✓ | ✓ | ✓ | ✓ | × | × | × | × | × | × | × | × | × | × | × | × | ✓ |
| Objective Function | Revenue | ✓ | × | ✓ | × | × | × | × | × | × | × | × | × | × | ✓ | × | × | × | × | × | × | × | × | × | × | × | × | ✓ |
| | Gen. Cost | ✓ | ✓ | ✓ | ✓ | ✓ | ✓ | ✓ | ✓ | ✓ | ✓ | × | × | ✓ | ✓ | ✓ | ✓ | ✓ | × | × | ✓ | ✓ | × | ✓ | × | ✓ | ✓ | ✓ |
| | Storage Cost | ✓ | ✓ | × | × | × | × | × | × | × | ✓ | ✓ | ✓ | × | × | × | × | × | × | × | ✓ | ✓ | × | × | ✓ | × | × | ✓ |
| | Secu. Costs | × | ✓ | × | ✓ | × | × | × | × | ✓ | × | × | × | ✓ | × | ✓ | × | × | ✓ | ✓ | × | × | ✓ | ✓ | × | ✓ | ✓ | ✓ |
| | PHEV cost | × | × | × | ✓ | × | × | ✓ | × | × | ✓ | ✓ | ✓ | × | × | × | × | × | × | × | × | × | × | × | × | × | × | ✓ |
| | DRP costs | × | ✓ | × | ✓ | ✓ | ✓ | ✓ | ✓ | ✓ | ✓ | × | × | × | × | × | × | ✓ | × | × | × | ✓ | × | × | × | × | × | ✓ |
| | WT | × | × | × | ✓ | ✓ | × | × | × | × | ✓ | × | × | × | ✓ | × | × | × | × | × | × | ✓ | × | × | ✓ | × | × | ✓ |
| | PV | × | ✓ | × | ✓ | × | × | × | × | × | ✓ | × | × | × | ✓ | × | × | × | × | × | × | ✓ | × | × | × | × | × | ✓ |
| DA-Market | | ✓ | ✓ | ✓ | ✓ | ✓ | ✓ | ✓ | ✓ | ✓ | ✓ | × | ✓ | ✓ | ✓ | × | ✓ | ✓ | × | × | ✓ | × | × | ✓ | × | × | × | ✓ |
| RT- Market scheduling | | × | × | × | × | × | × | × | × | × | × | × | × | × | × | × | × | × | × | × | × | × | × | × | × | × | × | ✓ |
| Uncertainty Model | PHEV | × | × | × | ✓ | × | × | ✓ | × | × | ✓ | ✓ | ✓ | × | × | × | × | × | × | × | × | × | × | × | × | × | × | ✓ |
| | DRP | × | × | × | × | × | × | × | × | × | × | × | × | × | × | × | × | × | × | × | × | × | × | × | × | × | × | ✓ |
| | DA Market price | ✓ | × | × | × | × | × | × | × | × | × | × | × | × | × | × | × | × | × | × | × | × | × | × | × | × | × | ✓ |
| | RT Market price | × | × | × | ✓ | × | × | × | × | × | × | × | × | × | × | × | × | × | × | × | × | × | × | × | × | × | × | ✓ |
| | External Shock | × | × | × | × | × | × | × | × | × | × | × | × | × | × | × | × | × | × | × | × | × | × | × | × | × | × | ✓ |
| | Loads | ✓ | ✓ | ✓ | ✓ | × | × | × | × | ✓ | × | × | × | × | ✓ | × | × | × | × | × | × | × | × | × | × | × | × | ✓ |
| | Intermittent electricity generation | ✓ | ✓ | ✓ | ✓ | ✓ | × | × | × | ✓ | ✓ | ✓ | ✓ | × | ✓ | × | × | × | × | × | × | × | × | × | × | × | × | ✓ |

The paper is organized as follows: The formulation of the problem is introduced in Section II. In Section III, the solution algorithm is presented. In section IV, the case study is presented. Finally, the conclusions are included in Section V.

## 2. Problem Modelling and Formulation

As shown in Fig.1, the Distribution System Operator (DSO) has photovoltaic systems, wind turbines, electrical energy storages, and microturbines. It transacts electricity with the upward electricity market, non-utility electricity generation facilities, responsive loads, and plug-in electric vehicles. Further, the non-utility electricity generation facilities owners may submit their bids in the day-ahead and real-time horizon, transact energy with the DSO, and sell their surplus electricity to the distribution system. However, the owners of these facilities may withhold their electricity generation in contingent conditions of the distribution system to gain more profit and this process may lead to an increase in the electricity prices and reduce the resiliency level of the distribution system. Thus, the DSO should consider the capacity withholding impacts of the non-utility electricity generation facilities on its operational scheduling practices.

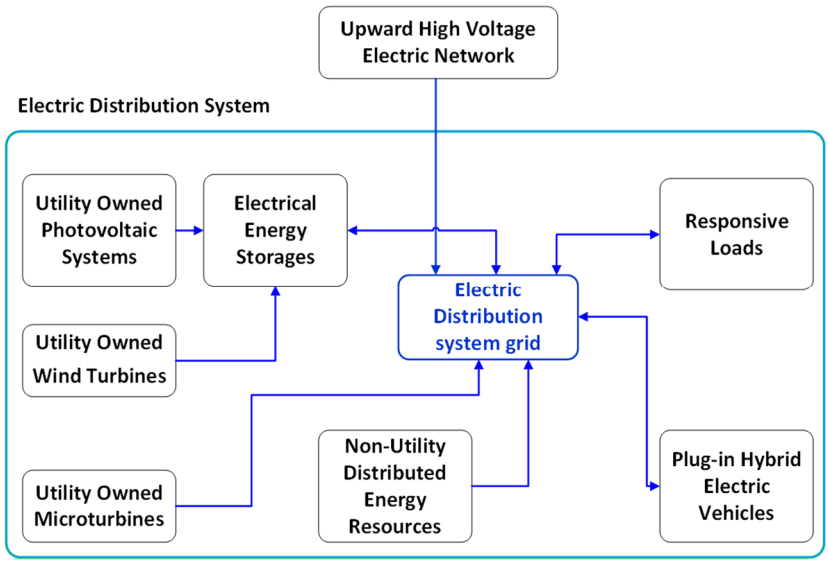


Fig. 1. Electrical distribution system distributed energy resources.

This paper presents optimization processes to optimize the day-ahead and real-time operational scheduling of the self-healing distribution system considering the capacity withholding of non-utility generation facilities.

The proposed optimization processes are decomposed into two stages that consist of normal and contingent conditions, respectively. The first stage problem (normal operational condition) consists of three steps that are day-ahead optimization problem, real-time optimization problem, and simulation of contingent conditions in the real-time horizon, respectively.

At the first step, the DSO optimizes the scheduling of distributed energy resources and switching of normally opened switches in a day-ahead normal state considering the capacity withholding process of non-utility electricity generation facilities. In the second step, the DSO updates its database and optimizes the

normal state real-time operational scheduling. In the third step, the DSO simulates the impacts of external shocks impacts on the system and explores the resiliency level.

The second stage problem considers the optimal scheduling of energy resources and switching of normally closed switches in external shock conditions. If the external shock state is detected, the DSO sectionalizes its system into multi-microgrids and performs the remedial actions in the second stage problem.

### *2.1. Uncertainty Modelling*

Considering the uncertainties associated with plug-in hybrid electric vehicles, day-ahead electricity prices, real-time electricity prices, loads, and intermittent electricity generations, the scenario generation and reduction processes are utilized in this paper. In stochastic programming, each uncertain parameter is modelled as a stochastic process. These stochastic processes are characterized by their corresponding probability distribution functions [29, 30]. The scenario generation process is utilized to discretize the distribution functions. Thus, the objective functions of optimization problems are transformed into random variables, and the expected values of objective functions are calculated. In the present paper, the Auto-Regressive Integrated Moving Average (ARIMA) models have been performed to take the uncertainties of plug-in hybrid electric vehicles, day-ahead electricity prices, real-time electricity prices, loads, and intermittent electricity generations into consideration [29, 30]. However, the curse of dimensionality of the generated scenarios may lead to computational problems. Thus, the scenario reduction method should be performed. The forward selection algorithm proposed in [30] is used to reduce the scenarios. Further, the Monte Carlo stochastic process simulation procedure simulates the location and intensity of the external shocks and demand response program contribution scenarios. Different scenarios are generated for the non-utility electricity generation bidding scenarios. The bidding curves of non-utility generation are generated based on a price-based unit commitment procedure that maximizes the profit of non-utility electricity generation facilities for different day-ahead and real-time horizons. Then, the ARIMA model is utilized to generate different scenarios of the bidding curves. Finally, the scenario reduction process is performed [29, 30].

### *2.2. Capacity withholding index*

The DSO should detect the capacity withholding process, prevent it through an ex-ante way (pre-event), and penalize it. The aggregate demand function can be written as (1) [31, 32]:

$$\varphi = -\alpha\theta + \beta \quad \alpha > 0 \tag{1}$$

Where $\alpha$ and $\beta$ are the parameters of the demand curve. The $\varphi$ and $\theta$ are the price and quantity of load, respectively. It is assumed that in the SFE (supply function equilibrium) game model each non-utility distributed generation unit that submits its bid in the following form [31, 32]:

$$\varpi = \frac{1}{\sigma}(\pi - \zeta) \quad \sigma > 0 \tag{2}$$

Where $\varpi$ and $\zeta$ are the parameters of non-utility distributed generation submitted bid.

The Capacity-Withholding Index (CWI) of Refs. [32, 33] is considered to detect the withholding process of the non-utility distributed energy resource that can be presented as (3) [32-33]:

$$CWI = \frac{\Delta\theta^{distort}}{\Delta\theta^{withheld}} = \left(\frac{1}{1+\sum_{i=1}^{N}\frac{\alpha}{a_i}}\right)\left(\frac{\sum_{i=1}^{N}\left(\frac{\theta_i^e}{a_i\hat{A}_i}+\frac{\Delta\lambda_i^{distort}}{a_i}\right)}{\sum_{i=1}^{N}\left(\frac{\theta_i^e}{a_i\hat{A}_i}+\frac{\Delta\lambda_i^{withheld}}{a_i}\right)}\right) \tag{3}$$

Where $\Delta\theta^{distort}$ and $\Delta\theta^{withheld}$ are the capacity distortion of the market and capacity withheld of the market, respectively. $\Delta\lambda^{distort}$ and $\Delta\lambda^{withheld}$ are the Lagrangian multipliers associated with power balance constraints in the distortion of market and capacity withheld of market conditions, respectively. $N$ and $a$ are the number of non-utility DERs and their generation cost multiplier, respectively. The $e$ index stands for the Oligopoly market equilibrium point. Further, $\hat{A}$ can be presented as (4) [31, 32]:

$$\hat{A}_i = 1/\alpha + \sum_{j=1, i\neq j}^{N} 1/\sigma_j \tag{4}$$

### *2.3. Optimal operation in normal conditions*

The optimal operation in the normal condition problem determines the commitment schedule of utility-owned and non-utility owned distributed energy generation facilities. This process minimizes the operational and emission costs considering system constraints and capacity withholding of non-utility distributed generation units.

#### *2.3.1. Optimal operation in day-ahead normal conditions*

The optimal scheduling of the system in normal conditions is carried out for the day-ahead horizon using the rolling-horizon technique. The DSO receives the non-utility electricity generation bids and performs a unit commitment process for the scheduling of energy generation facilities considering the capacity withholding process and different real-time operating scenarios. The DSO can reject the non-utility electricity generation bids that impose capacity withholding and penalize them. Further, the DSO can reconfigure its system topology and change the status of its normally opened switches. Thus, the DSO control variables for the day-ahead normal operational conditions can be categorized into the following groups:

- The day-ahead commitment of utility-owned, responsive loads, PHEVs, and non-utility-owned distributed energy resources,

- Switching of normally opened switches to change the pattern of power flow and reducing the capacity withholding impacts in the day-ahead horizon. The switching of normally opened switches can be performed for one hours intervals in the first step problem,
- Penalizing of non-utility distributed energy resources that impose market power and withhold their generation capacity,
- Changing the time of use and direct load control fees to encourage consumers to participate in demand response programs.

Based on the above categorization of control variables for the day-ahead normal operational conditions, the objective functions of the first step of the first stage optimization problem can be written as (5):

$$
\begin{aligned}
Min\ \mathrm{F}_1 = & \sum_{Z}\sum_{NOSDA}\sum_{S}\psi\cdot[prob\cdot[W_1\cdot\{\sum_{T}\sum_{I}(c_t^{NUDER}\cdot P_{t,i}^{NUDER} - c_t^{L}\cdot P_{t,i}^{L} + c^{grid}\cdot P_t^{grid} + \\
& c_t^{L}.st_{t,i}\cdot P_i^{PHEV} + c^{ES}\cdot(\left|P_{t,i}^{ES}\right|) + c^{RER}\cdot(P_{t,i}^{PV} + P_{t,i}^{WT}) + (c^{MT} + c^{pul}\cdot\nu_i).P_{t,i}^{MT} \\
& + (c^{up}\cdot\max(0,(\tau_{t,i} - \tau_{t-1,i})) + c^{down}\cdot\max(0,(\tau_{t-1,i} - \tau_{t,i}))) + \\
& \sum_{S}^{NOSRT} prob[\sum_{T}\sum_{I}(c_t^{NUDER}\cdot\Delta P_{t,i}^{NUDER} - c_t^{L}\cdot\Delta P_{s,t,i}^{L} + c^{grid}\cdot\Delta P_{s,t}^{grid} + c^{ES}\cdot\Delta P_{s,t,i}^{ES} + \\
& c^{RER}\cdot(\Delta P_{s,t,i}^{PV} + \Delta P_{s,t,i}^{WT}) + (c^{RD} + c^{pul}\cdot\nu_i)\cdot\Delta P_{s,t,i}^{MT}))\} + W_2\cdot CWI]]
\end{aligned}
\tag{5}
$$

The objective function of the first step problem consists of the following terms: 1) the non-utility DERs energy purchased costs ( $c_t^{NUDER}\cdot P_{t,i}^{NUDER}$ ); 2) the profit of energy sold to consumers( $c_t^{L}\cdot P_{t,i}^{L}$ ); 3) cost/profit of electricity transactions with the upward market ( $c^{grid}\cdot P_t^{grid}$ ); 4) cost/profit of electricity transactions with the PHEVs ( $c_t^{L}.st_{t,i}\cdot P_i^{PHEV}$ ); 5) the energy storage maintenance costs ( $c^{ES}\cdot(\left|P_{t,i}^{ES}\right|)$ ); 6) the intermittent energy generation facilities operational and maintenance costs ( $c^{RER}\cdot(P_{t,i}^{PV} + P_{t,i}^{WT})$ ); 7) the operational and emission costs of microturbines ( $(c^{MT} + c^{pul}\cdot\nu_i).P_{t,i}^{MT}$ ); 8) the start up and start down of microturbine ( $(c^{up}\cdot\max(0,(\tau_{t,i} - \tau_{t-1,i})) + c^{down}\cdot\max(0,(\tau_{t-1,i} - \tau_{t,i}))$ ); 9) the expected cost of energy mismatch purchased from non-utility DERs in real-time horizon ( $c_t^{NUDER}\cdot\Delta P_{t,i}^{NUDER}$ ); 10) the expected profit of energy sold to consumers mismatch in real-time horizon ( $c_t^{L}\cdot\Delta P_{s,t,i}^{L}$ ); 11) the expected mismatch of cost/profit of electricity transactions with the upward market in real-time horizon ( $c^{grid}\cdot\Delta P_{s,t}^{grid}$ ); 12) the expected mismatch of the energy storage maintenance costs in real-time horizon ( $c^{ES}\cdot\Delta P_{s,t,i}^{ES}$ ); 13) the expected mismatch of the intermittent energy generation facilities operational and maintenance costs in real-time horizon ( $c^{RER}\cdot(\Delta P_{s,t,i}^{PV} + \Delta P_{s,t,i}^{WT})$ ); 14) the expected mismatch of operational and emission costs of microturbine in real-time horizon ( $(c^{RD} + c^{pul}\cdot\nu_i)\cdot\Delta P_{s,t,i}^{MT}$ ); and 15) the capacity withholding index ( $CWI$ ).

The constraints of the first step objective functions consist of the following terms.

*A. Electric power balance constraints*

The net injected electricity of each bus consists of the electricity generation minus the electricity consumption of the bus. Thus, the electric power balance constraints of the first step problem can be written as (6):

$$P_{i,t} = P_{i,t}^{NUDER} + P_{i,t}^{MT} + P_{i,t}^{PV} + P_{i,t}^{WT} + P_{i,t}^{ES} + P_{i,t}^{PHEV} - P_{i,t}^{L} \qquad \forall i \in I, \forall t \in T \tag{6}$$

Eq. (6) presents that the net injected active power of the bus equals the sum of the active power of non-utility generation facilities, utility-owned microturbines, photovoltaic arrays, wind turbines, electrical energy storages, plug-in electric vehicles, and loads.

The aggregated electricity generations must be equal to or greater than the electricity consumption. This constraint can be written as (7) for the first step problem:

$$\sum_{j}(P_{i,t}^{NUDER} + P_{i,t}^{MT} + P_{i,t}^{PV} + P_{i,t}^{WT} + P_{i,t}^{ES} + P_{i,t}^{PHEV} - P_{i,t}^{L} - P_{i,j,t}) \geq 0 \qquad \forall i \in I, \forall t \in T \tag{7}$$

The distribution system transacts electricity with the upward market. The transacted electricity with the upward market is the sum of the electricity generations and consumptions in the system that can be presented as (8):

$$P_{t}^{grid} = \sum_{i}(P_{i,t}^{NUDER} + P_{i,t}^{L} - P_{i,t}^{MT} - P_{i,t}^{PV} - P_{i,t}^{WT} - P_{i,t}^{ES} - P_{i,t}^{PHEV}) \qquad \forall t \in T \tag{8}$$

Further, the facilities of the point of common coupling have technical constraints that can be presented as (9):

$$P_{\min}^{grid} \leq P_{t}^{grid} \leq P_{\max}^{grid} \qquad \forall t \in T \tag{9}$$

The load flow constraints and device loading constraints were considered in the optimization process that the detailed formulation of the load flow constraints is available in [23]. The constraints of electricity generation of microturbine are the minimum and maximum limits of electricity generation that can be presented as (10):

$$P_{i}^{MT,min}.\tau_{i,t} \leq P_{i,t}^{MT} \leq P_{i}^{MT,max}.\tau_{i,t} \qquad \forall i \in I, \forall t \in T \tag{10}$$

The $\tau$ variable is the binary decision variable for the commitment of the microturbine.

The ramp rate constraints of electricity generation of microturbine can be presented as (11):

$$\left|(P_{i,t}^{MT} + \Delta P_{i,s,t}^{MT}) - (P_{i,t-1}^{MT} + \Delta P_{i,s,t-1}^{MT})\right| \leq \Delta U_{i}^{MT} \qquad \forall i \in I, \forall s \in S, \forall t \in T \tag{11}$$

The constraints of energy storage facilities can be categorized into the state of charge constraints, the charge and discharge constraints, and the maximum charge limits. Eq. (12) presents the state of charge constraints for the first step problem:

$$0 \le SOC_{i,t} \le SOC_i^{\max} \qquad \forall i \in I, \forall t \in T \tag{12}$$

The state of charge of energy storage in the t[th] simulation step of the first step problem can be written as (13):

$$SOC_{i,t} = SOC_{i,t-1} - \frac{T_p . P_{i,t}^{ES}}{cap_i} . (\lambda_{i,t}^{ch} . \eta_{ch} + \lambda_{i,t}^{dch} . \eta_{dch}^{-1}) \qquad \forall i \in I, \forall t \in T \tag{13}$$

The energy storage maximum discharge and charge constraints can be written as (14):

$$-P_{max,i}^{ES,ch} . \lambda_{i,t}^{ch} \le P_{i,t}^{ES} \le P_{max,i}^{ES,dch} . \lambda_{i,t}^{dch} \qquad \forall i \in I, \forall t \in T \tag{14}$$

$\lambda^{ch}$ and $\lambda^{dch}$ are binary decision variables of charge and discharge of energy storage, respectively [34, 35].

The power generation and consumption of PHEVs are functions of the initial value of stored energy, the navigation distance, and the pattern of usage of PHEVs. Eq. (15) presents the minimum and maximum charge rates of PHEVs. $\gamma^{ch}$ and $\gamma^{dch}$ are binary decision variables of charge and discharge of energy storage, respectively [34, 35]. The ***st*** parameter denotes the status of the connection of PHEV to the network.

$$-P_{max}^{PHEV} . st_{i,t} . \gamma_{i,t}^{ch} \le P_{i,t}^{PHEV} \le P_{max}^{PHEV} . st_{i,t} . \gamma_{i,t}^{dch} \qquad \forall i \in I, \forall t \in T \tag{15}$$

Eq. (16) presents the energy level of PHEVs based on their charge and discharge status.

$$E_{i,t}^{PHEV} = E_{i,t-1}^{PHEV} - T_p . P_{i,t}^{PHEV} . ((\gamma_{i,t}^{dch} / \pi_{dch}^{PHEV}) + \gamma_{i,t}^{ch} . \pi_{ch}^{PHEV}) \qquad \forall i \in I, \forall t \in T \tag{16}$$

The minimum and maximum value of stored energy in PHEV can be presented as (17):

$$E_{min}^{PHEV} \le E_{i,t}^{PHEV} \le E_{max}^{PHEV} \qquad \forall i \in I, \forall t \in T \tag{17}$$

Eq. (18) denotes the desirable energy level of PHEV based on the owner of PHEV departure time:

$$E_{i,t}^{PHEV} = E_{desire}^{PHEV} \qquad \forall i \in I, \forall t = t_{departure} \tag{18}$$

### *2.3.2. Optimal operation in real-time normal conditions*

The DSO updates its database every one minute and optimizes the mismatches of operating points for the next 15 minutes interval. The DSO control variables for the real-time normal operational conditions can be categorized into the following groups:

- Real-time optimal power flow of utility-owned, responsive loads, PHEVs, and non-utility-owned distributed energy resources,
- Penalizing of non-utility distributed energy resources that impose market power and withhold their generation capacity,
- Changing the direct load control fees,
- Switching of normally opened switches to change the pattern of power flow and reducing the capacity withholding impacts in the real-time horizon. It is assumed that the switching of normally opened switches can be performed for 15 minutes intervals in the second step of the first stage problem.

Based on the above categorization of control variables for the real-time normal operational conditions, the objective function of the second step of the first stage optimization problem can be written as (19):

$$Min\ \mathrm{F}_2 = \sum_{Z}\sum_{t}\sum_{i}[W_3 \cdot (c_t^{NUDER}.\Delta P_{t,i}^{NUDER} - c_t^{L}.\Delta P_{t,i}^{L} + c^{grid}.\Delta P_t^{grid} + c^{ES}.\Delta P_{t,i}^{ES} + c^{R}.(\Delta P_{t,i}^{PV} + \Delta P_{t,i}^{WT}) + (c^{RD} + c^{pul}.\nu_i).\Delta P_{t,i}^{MT})) + W_4 \cdot CWI] \quad (19)$$

The objective function of the second step problem consists of the following terms: 1) the expected cost of energy mismatch purchased from non-utility DERs in the real-time horizon ($c_t^{NUDER}.\Delta P_{t,i}^{NUDER}$); 2) the mismatch of profit of energy sold to consumers in the real-time horizon ($c_t^{L}.\Delta P_{t,i}^{L}$); 3) the mismatch of cost/profit of electricity transactions with the upward market in the real-time horizon ($c^{grid}.\Delta P_t^{grid}$); 4) the mismatch of the energy storage maintenance costs in the real-time horizon ($c^{ES}.\Delta P_{t,i}^{ES}$); 5) the mismatch of the intermittent energy generation facilities operations and maintenance costs in the real-time horizon ($c^{R}.(\Delta P_{t,i}^{PV} + \Delta P_{t,i}^{WT})$); 6) the mismatch of the operational and emission costs of microturbine in the real-time horizon ($(c^{RD} + c^{pul}.\nu_i).\Delta P_{t,i}^{MT})$); and 7) the capacity withholding index in real-time operation ($CWI$).

The constraints of the second step objective function consisting of the optimal operation in day-ahead normal conditions constraints that are not presented for the sack of space. Further, the following constraints are considered in the optimal operation in real-time normal conditions.

*A. Electric power balance constraints*

The electric power balance mismatch for the second step problem can be written as (20):

$$\Delta P_{i,s,t} = \Delta P_{i,t}^{NUDER} + \Delta P_{i,s,t}^{MT} + \Delta P_{i,s,t}^{PV} + \Delta P_{i,s,t}^{WT} + \Delta P_{i,s,t}^{ES} - \Delta P_{i,s,t}^{L} \qquad \forall i \in I, \forall s \in S, \forall t \in T \quad (20)$$

Eq. (20) presents that the net mismatch of the injected active power of the bus equals the sum of the mismatches of the active power of non-utility generation facilities, utility-owned microturbines, photovoltaic arrays, wind turbines, electrical energy storages, plug-in electric vehicles, and loads.

The aggregated electricity generation mismatches must be equal to or greater than the electricity consumption mismatches. This constraint can be written as (21) for the second step problem:

$$\sum_{j}(\Delta P_{i,t}^{NUDER}+\Delta P_{i,s,t}^{MT}+\Delta P_{i,s,t}^{PV}+\Delta P_{i,s,t}^{WT}+\Delta P_{i,s,t}^{ES}-\Delta P_{i,s,t}^{L}-\Delta P_{i,j,s,t})\geq 0 \qquad \forall i\in I,\forall s\in S,\forall t\in T \tag{21}$$

The facilities of the point of common coupling have technical constraints that can be presented as (22):

$$P_{\min}^{grid}\leq P_{t}^{grid}+\Delta P_{s,t}^{grid}\leq P_{\max}^{grid} \qquad \forall s\in S,\forall t\in T \tag{22}$$

The constraints of electricity generation mismatches of microturbine can be presented as (23) for the second step problem:

$$P_{i}^{MT,min}.\tau_{i,t}\leq P_{i,t}^{MT}+\Delta P_{i,s,t}^{MT}\leq P_{i}^{MT,max}.\tau_{i,t} \qquad \forall i\in I,\forall s\in S,\forall t\in T \tag{23}$$

The constraints of the energy storage state of charge mismatches can be written as the following constraints:

$$0\leq SOC_{i,t}+\Delta SOC_{i,s,t}\leq SOC_{i}^{\max} \qquad \forall i\in I,\forall s\in S,\forall t\in T \tag{24}$$

$$\Delta SOC_{i,s,t}=\Delta SOC_{i,s,t-1}-\frac{T_p.\Delta P_{i,s,t}^{ES}}{cap_i}.(\lambda_{i,t}^{ch}.\eta_{ch}+\lambda_{i,t}^{dch}.\eta_{dch}^{-1}) \qquad \forall i\in I,\forall s\in S,\forall t\in T \tag{25}$$

The energy storage maximum discharge and charge mismatch constraints can be written as (26):

$$-P_{max,i}^{ES,ch}.\lambda_{i,t}^{ch}\leq P_{i,t}^{ES}+\Delta P_{i,s,t}^{ES}\leq P_{max,i}^{ES,dch}.\lambda_{i,t}^{dch} \qquad \forall i\in I,\forall s\in S,\forall t\in T \tag{26}$$

### *2.4. Simulation of contingent conditions*

The third step of the first stage optimization problem explores the distribution system conditions in the probable external shock conditions. The DSO simultaneously simulates the impacts of external shocks on the system and determines the resiliency and capacity withholding indices for the next 15 minutes.

At the third step of the first stage, the DSO has multiple decision variables to reduce the impacts of external shocks that are presented as:

- Simulation process of the most probable external shock and their impacts on the system,
- Simulation of sectionalizing of distribution system into multi-microgrids in contingent conditions,
- Simulation of real-time optimal power flow of utility-owned, responsive loads, PHEVs, and non-utility-owned distributed energy resources.

In the simulation process, if the sectionalizing of the system process cannot reduce the impacts of external shocks, the switching of normally opened switches are performed and the third step problem sends a request to the first step problem to change the system topology for the remained intervals of day-ahead operational scheduling.

At this step, the simulation of external shocks is carried out to determine the volume of critical loads that are not supplied. If the volume of critical loads that are not supplied is more than a predefined threshold, the first step of the first stage problem is rescheduled. Then, the third step problem is optimized and the conditions of the electricity supply of critical loads are assessed. If the critical loads are not supplied, the process will change the values of time of use and direct load control fees for the next interval of real-time operational scheduling and the simulation of critical conditions are performed.

The objective function of the third step of the first stage system can be proposed as (27):

$$Min\ \mathsf{A}=\sum_{t>t_f}\sum_{k}[W_5\cdot(1-Y_{k,t})+W_6\cdot\sum_{j}X_{k,j})+W_7\cdot CWI] \tag{27}$$

The first term of (27) minimizes the unserved load of the distribution system ($(1-Y_{k,t})$). The second term determines the boundary lines of microgrids and the zero value of $X$ means that the electricity flow in the boundary line equals zero ($\sum_{j}X_{k,j}$). The boundary lines are equipped with normally closed switches that can be opened in contingent conditions to change the topology of the distribution system into multi-microgrids. The third term is the capacity-withholding index that is utilized to minimize the withhold capacity of non-utility facilities in an ex-ante way ($CWI$).

The third step optimization process has a slave problem that optimizes the real-time optimal power flow of utility-owned, responsive loads, PHEVs, and non-utility-owned distributed energy resources distributed energy in multi-microgrids. The objective function of the slave problem is the same as the second step problem and is not presented for the sack of space.

The constraints of the third step of the first stage consist of the following terms.

*A. Electric power balance constraints in contingent conditions*

Eq. (28) presents the electric power balance constraint in the contingent condition that is the net injected electricity of each isolated bus consists of the aggregated electricity injections minus aggregated electricity withdrawals from the bus.

$$\begin{aligned}&P_{k,s,t}^{NUDER}+\Delta P_{k,s,t}^{NUDER}+P_{k,s,t}^{MT}+(P_{k,t}^{PV}+\Delta P_{k,s,t}^{PV})+(P_{k,t}^{WT}+\Delta P_{k,s,t}^{WT})+P_{k,s,t}^{ES}+\\&P_{k,t}^{PHEV}-P_{k,t}^{crit}-Y_{k,t}.(P_{k,s,t}^{ncrit}.D_{k,t})\geq\sum_{j}P_{k,s,t}\\&\forall k\in K,\forall s\in S,\forall t\in T\end{aligned} \tag{28}$$

The aggregated electricity generations must be equal to or greater than the electricity consumptions of the isolated area. This constraint can be written as (29):

$$\begin{aligned}&\sum_{k}P_{k,s,t}^{NUDER}+\Delta P_{k,s,t}^{NUDER}+P_{k,s,t}^{MT}+(P_{k,t}^{PV}+\Delta P_{k,s,t}^{PV})+(P_{k,t}^{WT}+\Delta P_{k,s,t}^{WT})+P_{k,s,t}^{ES}+P_{k,t}^{PHEV}\\&\geq\sum_{k}(P_{k,t}^{crit}+Y_{k,t}.(P_{k,s,t}^{ncrit}.D_{k,t}))\qquad\forall s\in S,\forall t\in T\end{aligned} \tag{29}$$

The $D$ variable presents the duration of deferrable non-critical load commitment that is committed by the optimization process to balance the generation and consumption of electricity in the microgrids. Further, the $Y$ variable denotes that the served non-critical load and the optimization process curtails this load in contingent conditions. The load flow constraints were considered in the optimization process [23].

The constraints of electricity generation of microturbine are the limits of electricity generation and ramp rates that can be presented as (30) and (31), respectively:

$$P_{k,s,t}^{MT,\min} \le P_{k,s,t}^{MT} \le P_{k,s,t}^{MT,\max} \qquad \forall k \in K, \forall s \in S, \forall t \in T \tag{30}$$

$$\left| P_{k,s,t}^{MT} - P_{k,s,t-1}^{MT} \right| \le \Delta U_k^{MT} \qquad \forall k \in K, \forall s \in S, \forall t \in T \tag{31}$$

The constraints of energy storage facilities are categorized into the state of charge constraints, the state of charge of energy storage in the $t^{th}$ simulation step constraints, and the maximum charge limits that are presented by (12), (13), and (14), respectively.

The PHEVs are discharged in contingent conditions to supply the electrical loads. A minimum energy level of PHEV is defined to consider the minimum level of the PHEV owner in contingent conditions based on (32).

$$E_{k,t}^{PHEV} \ge E_{\min}^{PHEV} \qquad \forall k \in K, \forall t \in T \tag{32}$$

Eq. (33) presents the limits of PHEV power.

$$0 \le P_{k,t}^{PHEV} \le P_{min}^{PHEV} \qquad \forall k \in K, \forall t \in T \tag{33}$$

Eq. (34) denotes the change of PHEV energy based on the previous condition of PHEV.

$$E_{k,t}^{PHEV} = E_{k,t-1}^{PHEV} - (T_p . P_{k,t}^{PHEV} . \eta_{dch}^{-1}) \qquad \forall k \in K, \forall t \in T \tag{34}$$

The load control process is performed for the responsive loads that are the non-critical loads. Eq. (35) and Eq. (36) present the percentage of critical and non-critical loads of each bus, respectively.

$$P_{k,s,t}^{crit} = CLPE_{k,t} . (P_{k,t}^{L} + \Delta P_{k,s,t}^{L}) \qquad \forall k \in K, \forall s \in S, \forall t \in T \tag{35}$$

$$P_{k,s,t}^{ncrit} = (1 - CLPE_{k,t}) . (P_{k,t}^{L} + \Delta P_{k,s,t}^{L}) \qquad \forall k \in K, \forall s \in S, \forall t \in T \tag{36}$$

As mentioned earlier, the binary variable $D$ is utilized to commit the non-critical loads. The optimization process determines the optimal scheduling of non-critical loads to minimize the unserved loads. Eq. (37) determines the commitment limits of non-critical loads in non-contingent conditions. Further, Eq. (38) presents the commitment constraints of non-critical loads in scheduling intervals.

$$\sum_{t>t_f} D_{k,t} = 1 \qquad \forall k \in K, \forall t \in T \tag{37}$$

$$\prod_{t>t_f} D_{k,t} = 0 \qquad \forall k \in K, \forall t \in T \tag{38}$$

A resiliency index is defined to evaluate the resiliency level of the system in normal and contingent conditions. The normal and minimum levels of operational conditions are presented by Eq. (39) and Eq. (40), respectively.

$$Q_0^{L,t} = \sum_k \sum_s \sum_t (Pr_s.(P_{k,t}^L + \Delta P_{k,s,t}^L)) \tag{39}$$

$$Q_{min}^{L,t} = \sum_k \sum_s \sum_t (Pr_s.(P_{k,s,t}^{crit} + Y_{k,t}.P_{k,s,t}^{ncrit})) \tag{40}$$

The resiliency index is defined as Eq. (41) that is the inverse deviation of the operational point from its normal conditions.

$$RI = Q_{min}^{L,t} / (Q_0^{L,t} - Q_{min}^{L,t}) \tag{41}$$

### *2.5. Optimal operation in external shock conditions*

The optimal operational scheduling of the system in external shock conditions is the same as the third step of the first stage problem. In the contingent conditions, the distribution system is sectionalized into multi-microgrids based on the fact that the external shocks change the microgrids status into two categories: 1) microgrids that are working in contingent conditions and, 2) microgrids that are working in normal conditions.

The optimization process reads the corresponding values of the optimal scheduling of distributed energy resources, system topology, and the resiliency index of shock state from the third step of the first stage problem database. The demand response program is carried out to control the non-critical loads of microgrids. The commitment of energy storage facilities and PHEVs is performed to balance the generation and consumption of electricity in each microgrid. The objective function in external shock condition can be proposed as (42):

$$Min\ \mathsf{M} = \sum_{t>t_f} \sum_k (W_8.(1 - Y_{k,t}) + W_9.\sum_j X_{k,j}) \tag{42}$$

Same as the third step of the first stage problem, the first term of (42) is the unserved load that is presented by the $Y$ variable ($(1 - Y_{k,t})$). This term minimizes the unserved load of the distribution system. The second term determines the boundary lines of microgrids and the zero value $X$ means the electricity flow in the boundary line equals zero ($\sum_j X_{k,j}$).

The capacity-withholding index is not considered in the second stage optimization objective function based on the fact that the distribution system operator tries to restore its system with all available energy resources.

The constraints of the objective functions consist of Eq. (28)-Eq. (38) and are not presented for the sack of space.

## 3. Optimization algorithm

The optimization problem has the following assumptions and procedures:

- It is assumed that in the contingent conditions, all of the PHEVs are arrived at home parking and are discharged to supply the system loads. The state of charge constraints and the minimum energy level of PHEVs are considered in the optimization process.
- The demand response process utilizes direct load control to determine the status of non-critical load commitment.
- Numerous scenarios for plug-in hybrid electric vehicles, day-ahead electricity prices, real-time electricity price, loads, and intermittent electricity generations are generated [29-31].
- The Monte Carlo stochastic process simulation procedure simulates the location and intensity of the external shocks and demand response program contribution scenarios [36].
- The bidding curves of non-utility generation are generated based on a price-based unit commitment procedure that maximizes the profit of non-utility electricity generation facilities for different day-ahead and real-time horizons. Then, the ARIMA model is utilized to generate different scenarios of the bidding curves. Finally, the scenario reduction process is performed [36].
- The optimization process determines the optimal schedule of the first and second step problems, sectionalizing of the distribution system and, non-critical load, and PHEVs commitment.
- The weighted sum method is utilized to aggregate the proposed objective functions in the context of a multi-objective optimization program. The general form of proposed objective functions can be written as (43) [37]:

$$Min\ f = \sum_{i'=1}^{m'} w_{i'} \cdot f_{i'}(x') \cdot \chi \tag{43}$$

Where, *m'* is the number of objective functions and *f* presents the vector of objective functions of the proposed optimization problem. Further, $\chi$ is the scaling parameter that scales the objective functions based on the fact that the objective functions have different dimensions and cannot be simply added to form a mono-objective function optimization problem [37].

The $\chi$ parameter is defined as (44) [37]:

$$\chi = \frac{1}{f'^{0}_{i'}} \tag{44}$$

Where, the $f_i^{'0}$ is the ideal solution of objective function *i'*. The detailed model of the weighted sum method is available in [37] and are not presented for the sack of space.

The optimization model consists of multiple discrete, continuous, and non-linear state and control variables. The normal operation and contingent conditions optimization procedures are MINLP models. Different MINLP solvers were assessed to solve the proposed optimization problems considering the computational burden, speed and quality of the solutions. Based on the Ref. [15] and [23] solution methods, the DICOPT and SCIP solvers of GAMS are selected for the normal operation and contingent conditions problems, respectively. The DICOPT (DIscrete and Continuous OPTimizer) solver iteratively utilizes the CPLEX and CONOPT3 solvers for Non-Linear Programming (NLP) and Mixed Integer Programming (MIP) solutions, respectively [38]. The SCIP solver is a framework for the fast solution of constraint integer programming [39]. The detailed solution methodology of DICOPT and SCIP solvers are available in [38] and [39], respectively.

Fig. 2 depicts the flowchart of the proposed algorithm. At first, the ARIMA forecasting processes are carried out and the Monte-Carlo simulations are performed. The scenario generation and reduction procedures are performed. Then, the simulations of operational conditions in normal and contingent conditions are performed.

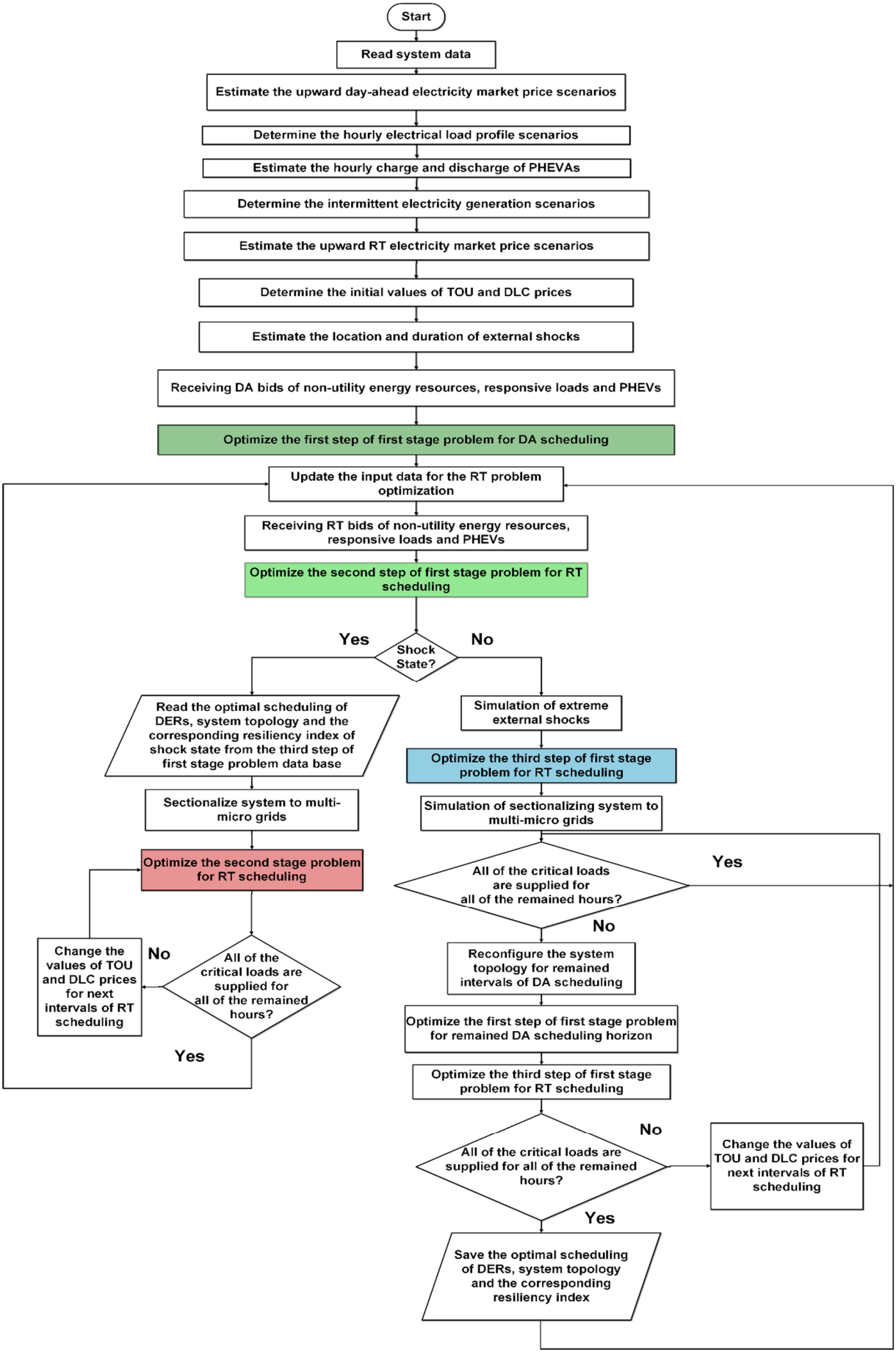


Fig. 2. The overall flowchart of the proposed procedure.

## 4. Simulation Results

### 4.1. Simulation results for 33-bus system

The simulation of the proposed method was carried out for the modified 123-bus and 33-bus test systems.

The outputs of simulations were compared with the results of Ref. [23] for the 33-bus test system to validate the proposed model and algorithm. The data of Ref. [23] was considered for the 33-bus system distributed energy resources. Fig. 3 depicts the 33-bus test system topology.

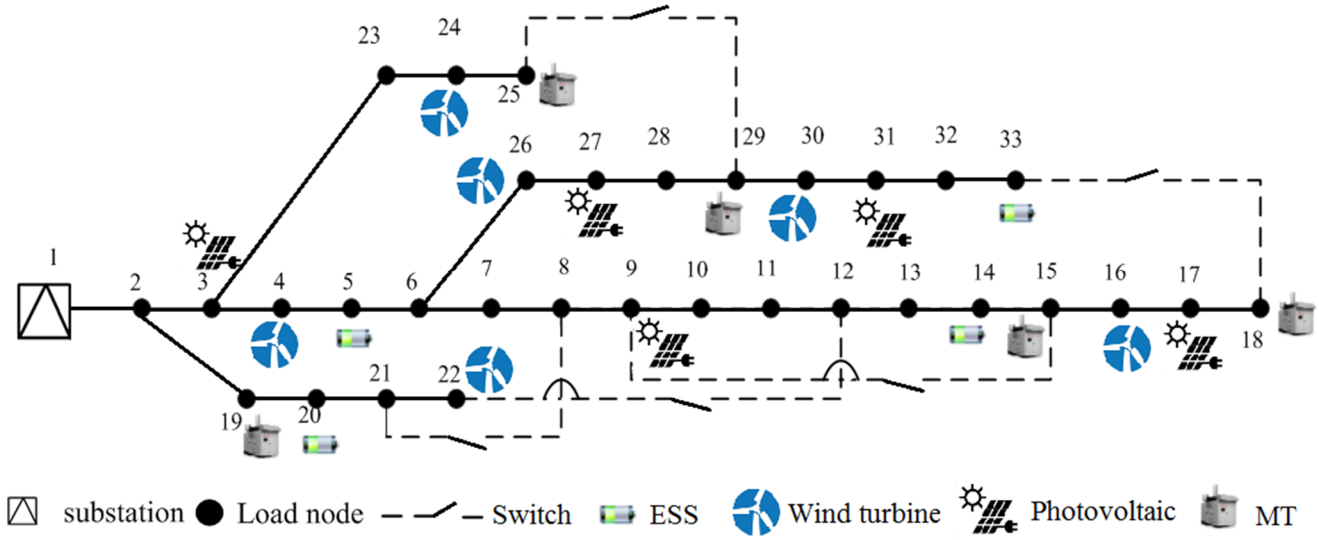


Fig. 3. The modified 33-bus test system.

Table 2 presents the location, capacity, and ownership status of distributed energy resources in Fig. 3.

Table 2. The location, capacity and ownership status of distributed energy resources for the 33-bus test system.

| Type | Bus | Capacity (kW) | Ownership |
|---|---|---|---|
| Microturbine | 15,19 | 500,300 | Utility |
| Electrical energy storage | 5,14,20,33 | 150,150,200,200 | Utility |
| Photovoltaic system | 3,9,17,28 | 60,60,40,50 | Utility |
| Wind turbine | 4,16,22,24,26,30 | 30,85,60,50,50,70 | Utility |
| Microturbine | 18,25,29 | 650,750,750 | Non-utility |

Table 3 presents the parameters of the utility-owned distributed energy resources.

Table 3. The 33-bus system parameters of utility-owned distributed energy resources.

| | | | |
|---|---|---|---|
| $c^{MT}$ | 0.1 $/ kWh | $c^{RD}$ | 0.15 $/ kWh |
| $c^{\Delta MT}$ | 0.15 $/ kWh | $c^{pul}$ | 0.02 $/ kWh |
| $c^{up}$ | 0.2 $/ kWh | $c^{down}$ | 0.2 $/ kWh |
| $c^{grid}$ | 0.15 $/ kWh | $\eta^{ch}$ , $\eta^{dch}$ | 0.95 |
| $c^{ES}$ | 0.4 $/ kWh | | |

The scenario generation and reduction scenarios are presented in Table 4.

Table 4. The scenario generation and reduction scenarios for the 33-bus system.

| System parameter | Value |
|---|---|
| Number of solar irradiation scenarios | 1000 |
| Number of wind turbine power generation scenarios | 1000 |
| Number of demand response contribution scenarios | 1000 |
| Number of day-ahead market load and price scenarios | 1000 |
| Number of real-time market load and price scenarios | 1000 |
| Number of non-utility bidding scenarios | 1000 |
| Number of solar irradiation reduced scenarios | 10 |
| Number of wind turbine power generation reduced scenarios | 10 |
| Number of demand response contribution reduced scenarios | 10 |
| Number of day-ahead market load and price reduced scenarios | 10 |
| Number of real-time market load and price reduced scenarios | 10 |
| Number of non-utility bidding reduced scenarios | 10 |

Figs. 4, 5 present the 33-bus system day-ahead forecasted per-unit electricity generation of photovoltaic arrays and wind turbines for reduced scenarios, respectively.

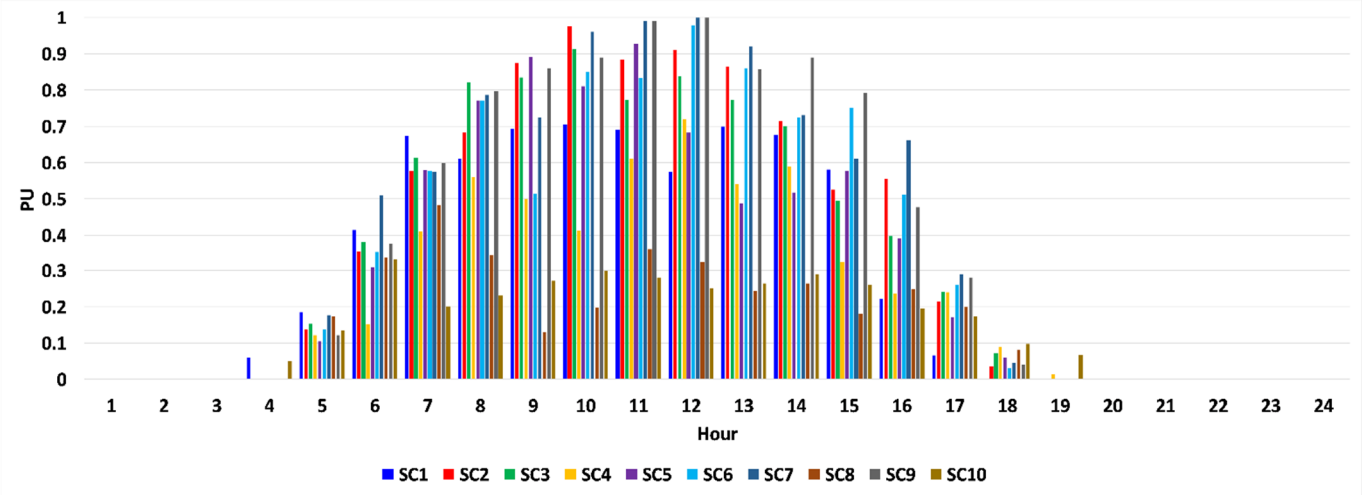


Fig. 4. The 33-bus system day-ahead forecasted per-unit electricity generation of photovoltaic arrays for reduced scenarios.

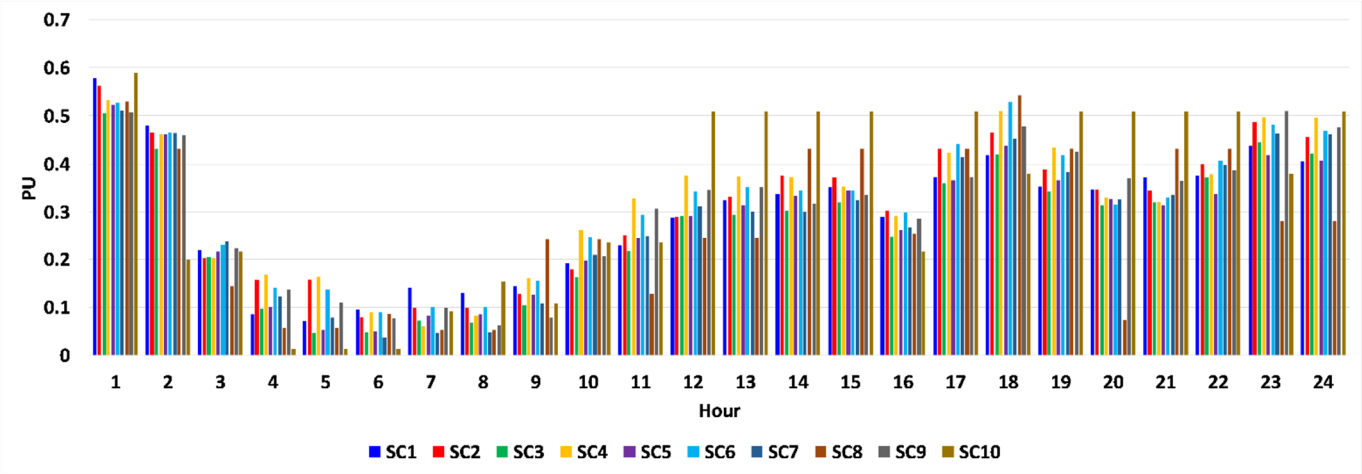


Fig. 5. The 33-bus system day-ahead forecasted per-unit electricity generation of wind turbines for reduced scenarios.

Fig. 6 depicts the 33-bus system forecasted day-ahead electricity price for one of the reduced scenarios.

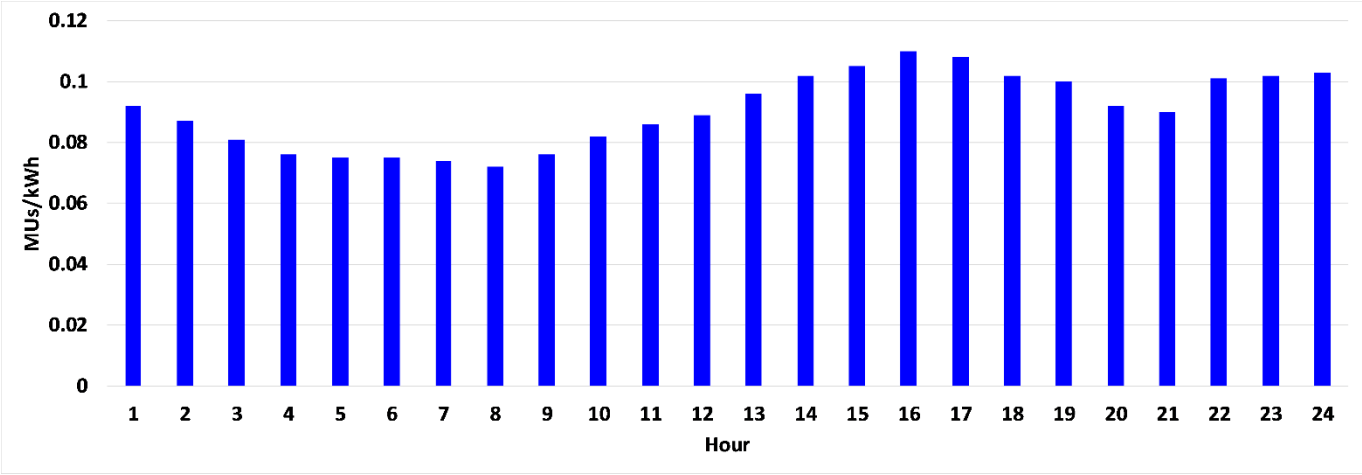


Fig. 6. The 33-bus system forecasted day-ahead electricity price for one of the reduced scenarios.

The first step of the first stage optimization process was carried out for the next 24 hours horizon with one-hour intervals. The simulation process was carried out for the normal operation of the 33-bus system considering the intermittent electricity generation uncertainties. Fig. 7 presents the day-ahead bidding curves of non-utility electricity generation facilities for one of the reduced scenarios.

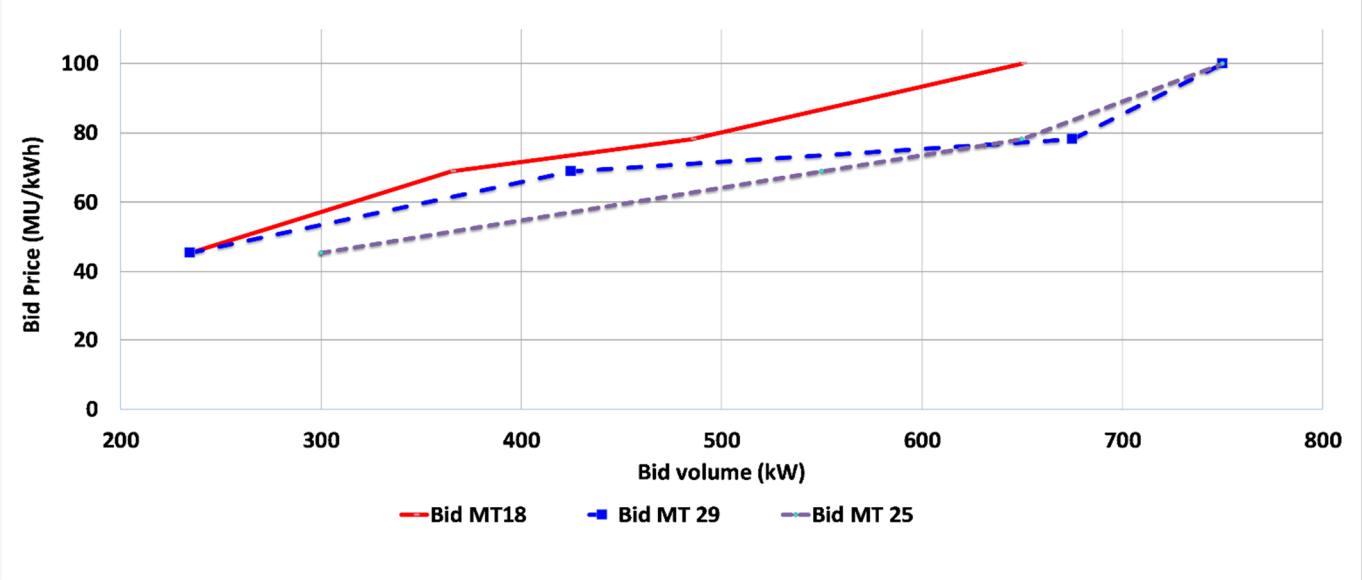


Fig. 7. The day-ahead bidding curves of non-utility electricity generation facilities for one of the reduced scenarios.

Fig. 8 presents the 33-bus system optimal unit commitment of the utility-owned and non-utility owned distributed energy resources.

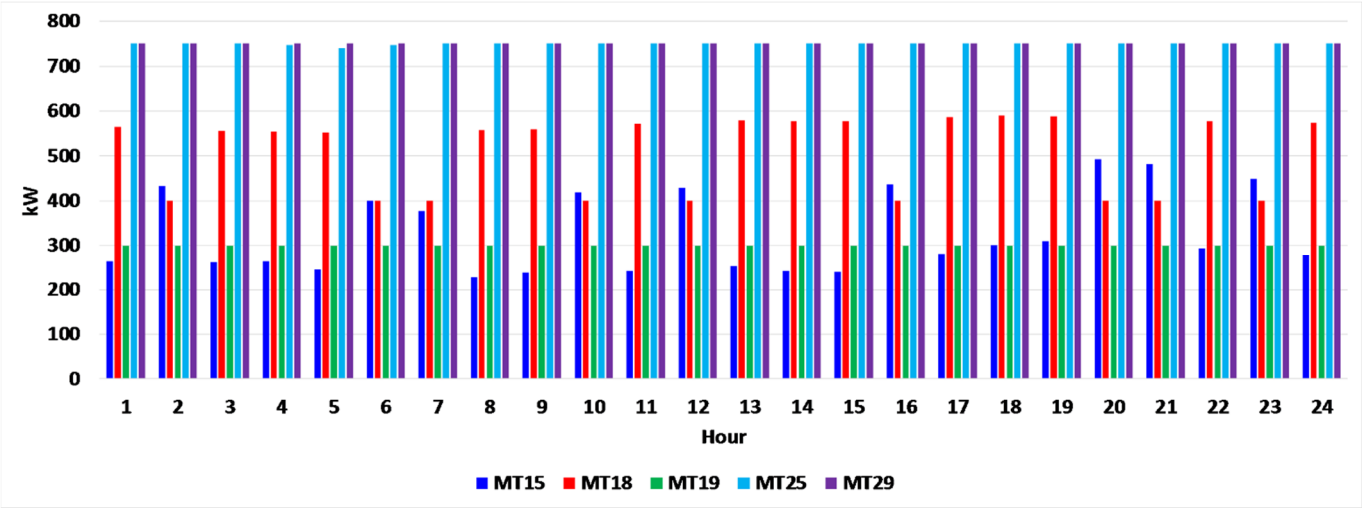


Fig. 8. The 33-bus system optimal unit commitment of the utility-owned and non-utility owned distributed energy resources.

Fig. 9 presents the capacity withholding indices for the first step optimization problem. The average value of the capacity withholding index without the proposed algorithm was about 0.4216. The average value of the capacity-withholding index with the proposed algorithm was about 0.1403, respectively. Further, the maximum value of the capacity-withholding index with the proposed algorithm was about 0.2050. The proposed algorithm reduced the average and maximum values of the capacity-withholding index for day-ahead normal operation conditions by about 66.72% and 72.95%, respectively.

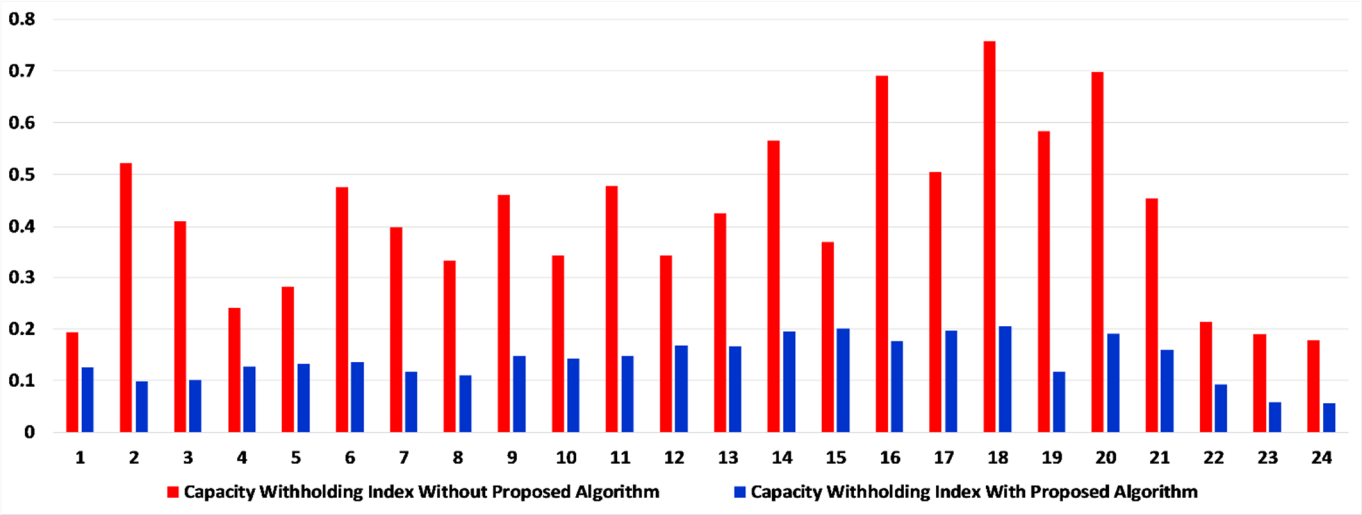


Fig. 9. The 33-bus test system capacity withholding indices for the first step optimization problem.

The second step of the first stage problem updated the forecasting data and the simulation was performed for the next 24 hours with 15 minutes intervals. Fig. 10 depicts the real-time bidding of non-utility facilities.

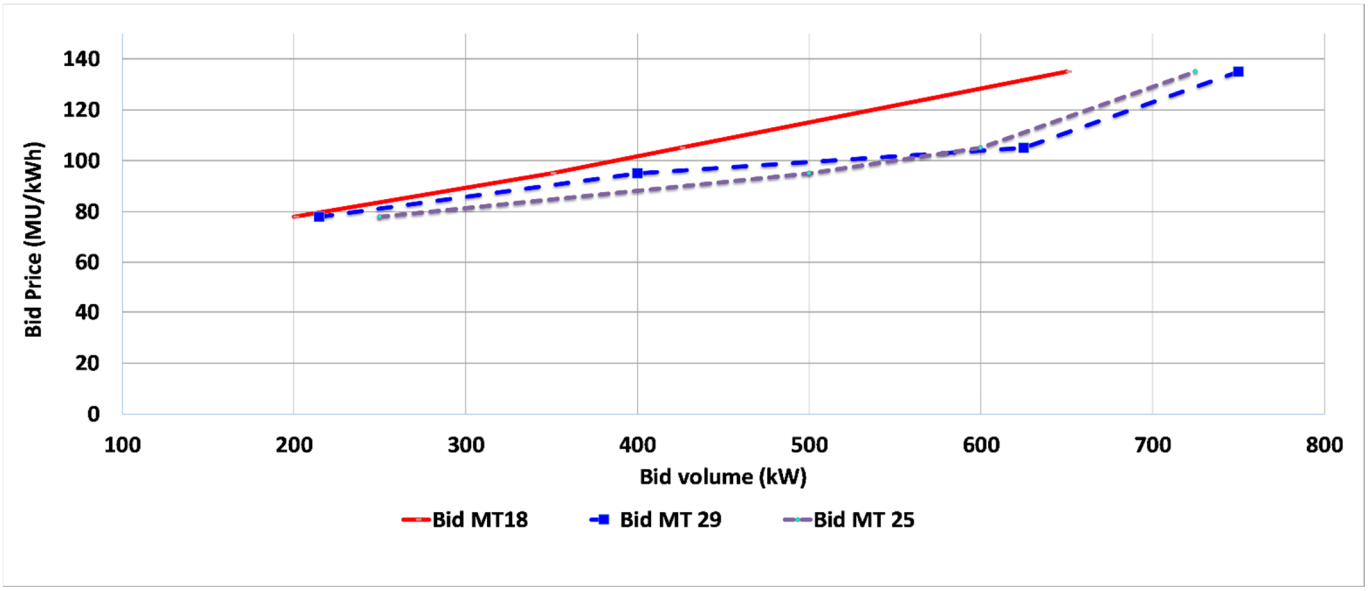


Fig. 10. The real-time bidding of non-utility facilities.

Fig. 11 presents the capacity withholding indices for the second step of the first stage (real-time) optimization problem. The average value of the capacity-withholding index without the proposed algorithm was about 0.4761. The average value of the capacity-withholding index with the proposed algorithm was about 0.1853. The proposed algorithm reduced the average and maximum values of the capacity-withholding index for the day-ahead normal operation conditions by about 59.61% and 61.3%, respectively.

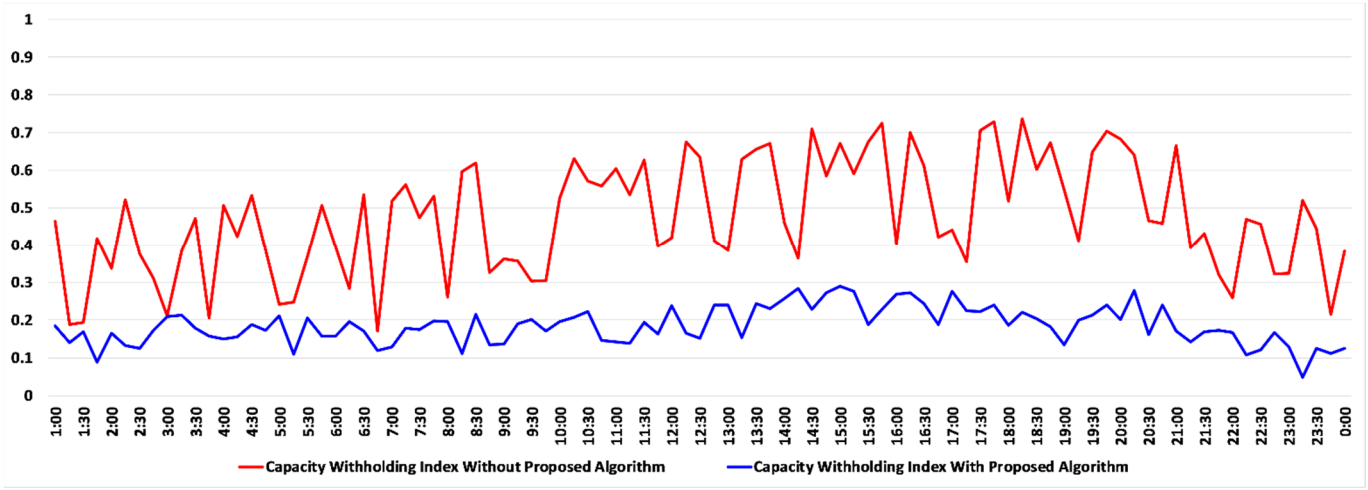


Fig. 11. The 33-bus system capacity withholding indices for the second step of the first stage (real-time) optimization problem.

Fig. 12 (a) and Fig. 12 (b) present the aggregated operational and interruption costs of the 33-bus system without and with the proposed algorithm for the top 48 worst-case external shocks, respectively. As shown in Fig. 12 (a), the worst-case contingency was the 48$^{th}$ contingency that the aggregated operational and interruption costs were about 4239.25 MUs for 19:45-20:00 intervals. The proposed algorithm reduced the corresponding aggregated operational and interruption costs of this contingency to 89.27 MUs. Thus, the proposed algorithm reduced the aggregated operational and interruption costs of the worst-case contingency by about 97.89%. The average values of aggregated operational and interruption costs for the 48 contingencies were about 1983.25 MUs and 167.97 MUs, respectively. Thus, the proposed algorithm reduced the average value of aggregated operational and interruption costs of the worst-case contingencies by about 91.53%.

Fig. 13 presents the capacity withholding indices for the third step of the first stage optimization problem. The average value of the capacity withholding index without the proposed algorithm was about 0.4782. The average value of the capacity-withholding index with the proposed algorithm was about 0.1834. The proposed algorithm reduced the average and maximum values of the capacity-withholding index for the third case by about 61.64% and 64.19%, respectively.

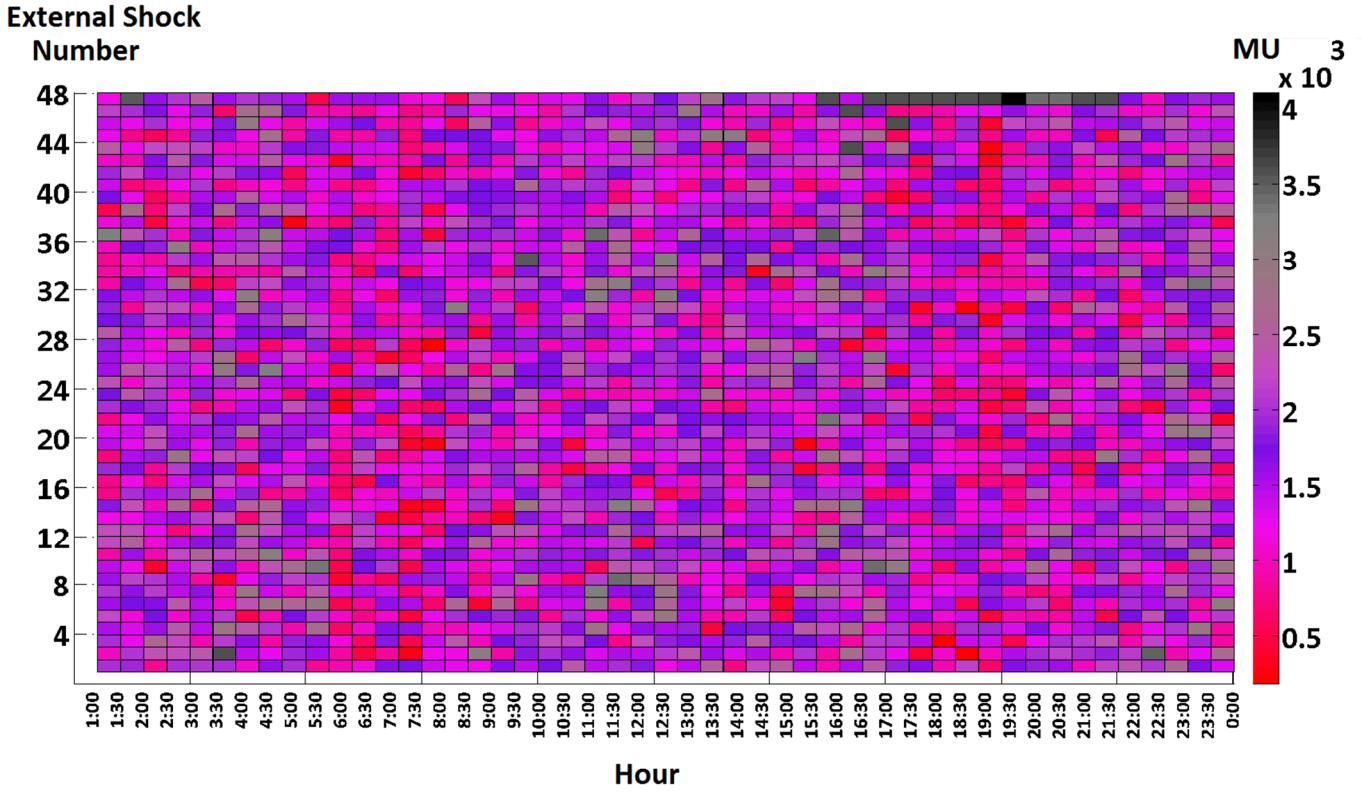


(a)

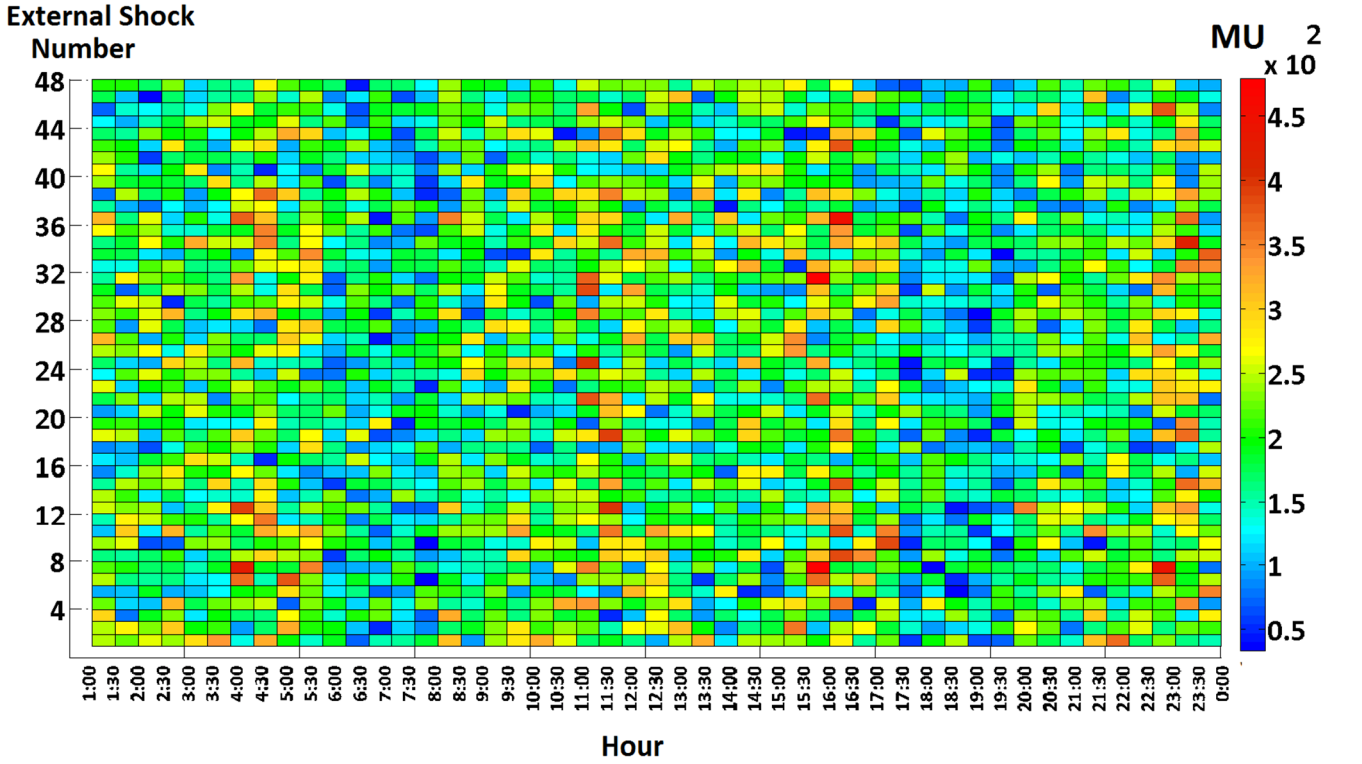


(b)

Fig. 12 (a) The aggregated operational and interruption costs of the 33-bus system for the 48 worst-case external shocks without the proposed algorithm. (b) The aggregated operational and interruption costs of the 33 bus distribution system for the 48 worst-case external shocks with the proposed algorithm.

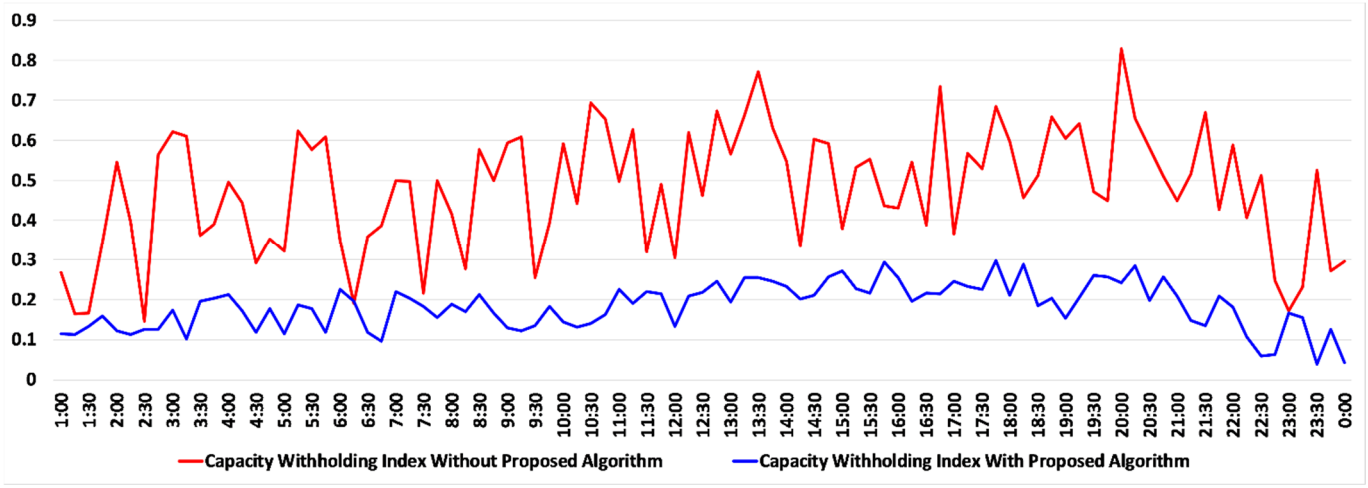


Fig. 13. The 33-bus system capacity withholding indices for different cases of the third step of the first stage (real-time simulation of external shock impacts) optimization problem.

Fig. 14 presents the resiliency index of the 33-bus system for the worst-case external shock conditions without implementing the proposed algorithm for the third step of the first stage optimization problem. The resiliency index of the system with the proposed algorithm tended to infinity. The maximum value of the resiliency index without the proposed algorithm was about 6.5937.

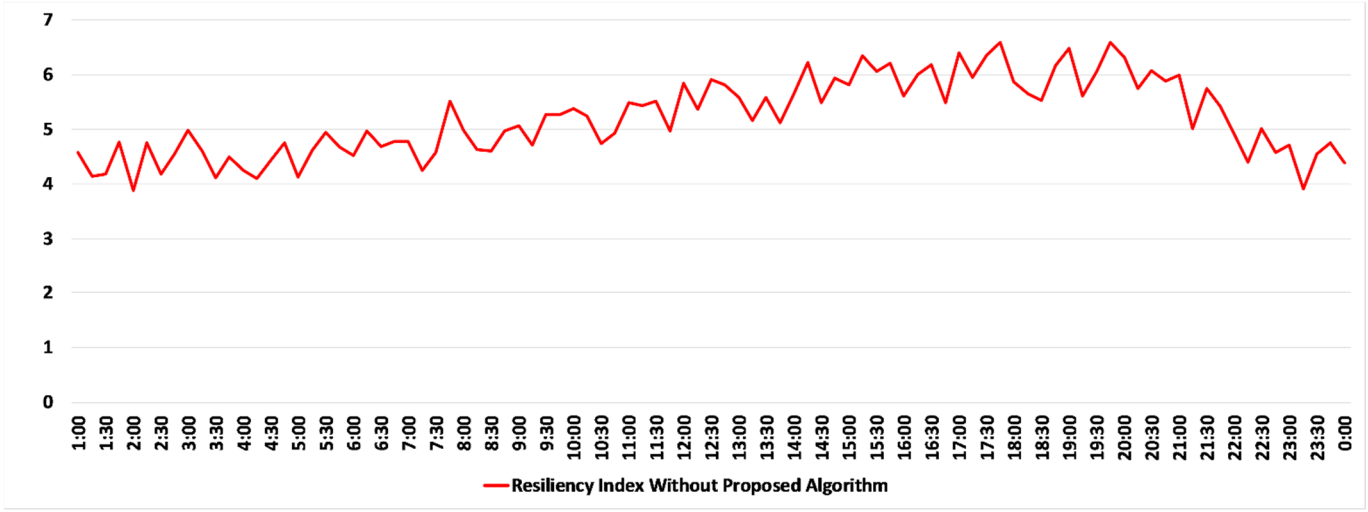


Fig. 14. The resiliency index of the system for the worst-case external shock conditions without implementing the proposed algorithm for the third step of the first stage optimization problem

### 4.2. Simulation results for the 123-bus system

The simulation of the proposed method was carried out for the modified 123-bus test system. A detailed report of 123-bus system simulation outputs is presented. Fig. 15 depicts the topology of the 123-bus test system [36, 40]. Table 5 presents the location, capacity, and ownership status of distributed energy resources of Fig. 15. The simulation of PHEVs was carried out using the model and data of [36].

Table 5. The location, capacity and ownership status of distributed energy resources for the 123-bus test system.

| Type | Bus | Capacity (kW) | Ownership |
|---|---|---|---|
| Microturbine | 13,73,76,78,101,108 | 80,140,140,150,160 | Utility |
| Electrical energy storage | 20,42,90,97 | 150,200,60,150 | Utility |
| Photovoltaic system | 14,15,29,39,57,69,82,95,106 | 60,60,60,80,40,80,60,40,60 | Utility |
| Wind turbine | 5,9,18,31,41,46,51,62,86,103,112 | 80,60,100,80,30,80,95,60,100,85,60 | Utility |
| Microturbine | 21,35,44,48,49,67,81,87,93 | 180,120,140,100,160,110,80,140,100 | Non-utility |

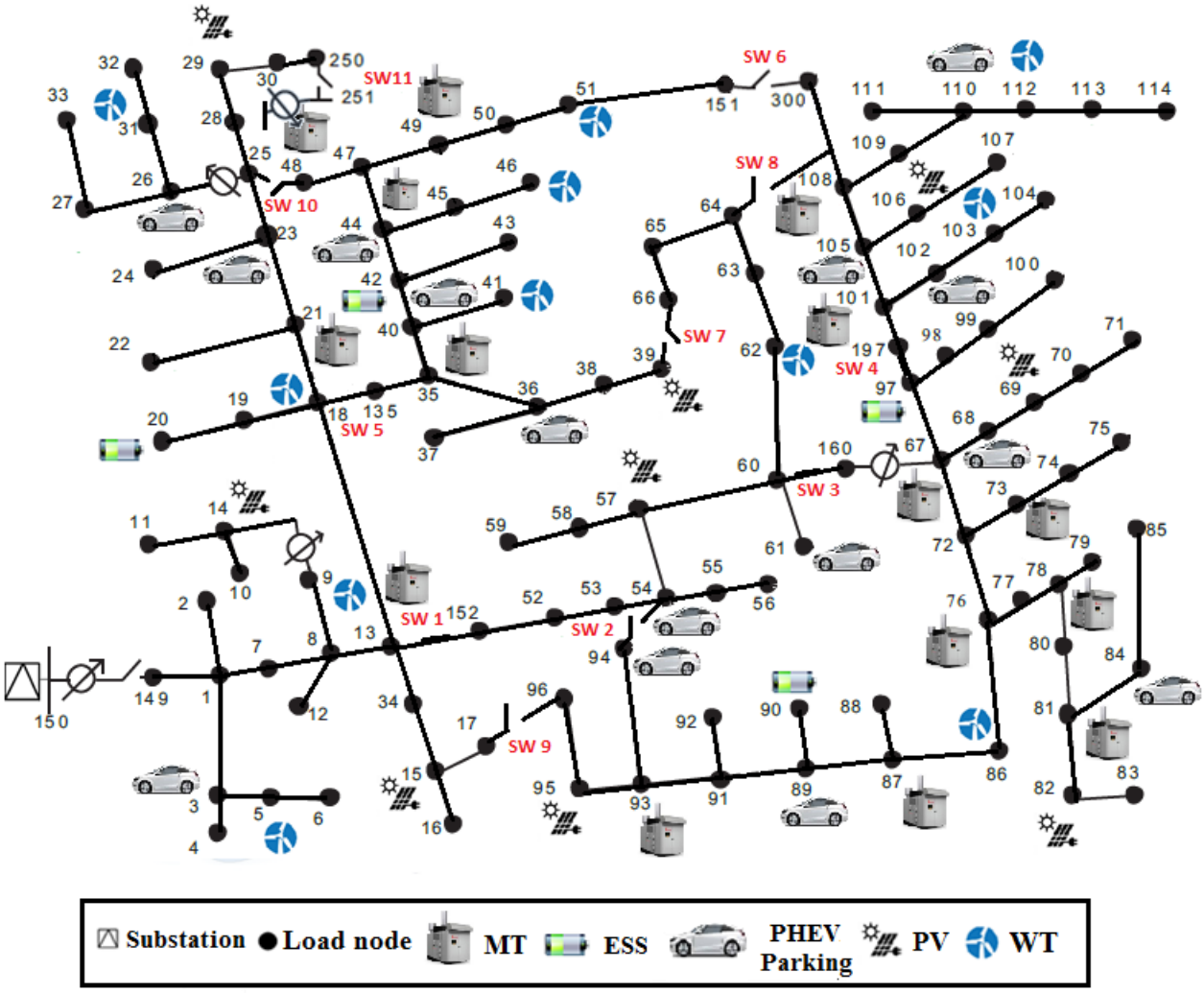


Fig. 15. The modified 123-bus test system.

Table 6 presents the parameters of the utility-owned distributed energy resources.

Table 6. The 123-bus system parameters of utility-owned distributed energy resources.

| | | | |
|---|---|---|---|
| $c^{MT}$ | 0.1 $/ kWh | $c^{RD}$ | 0.15 $/ kWh |
| $c^{\Delta MT}$ | 0.15 $/ kWh | $c^{pul}$ | 0.02 $/ kWh |
| $c^{up}$ | 0.2 $/ kWh | $c^{down}$ | 0.2 $/ kWh |
| $c^{grid}$ | 0.15 $/ kWh | $\eta^{ch}$ , $\eta^{dch}$ | 0.95 |
| $c^{ES}$ | 0.4 $/ kWh | | |

The scenario generation and reduction scenarios are presented in Table 7.

Table 7. The scenario generation and reduction scenarios.

| System parameter | Value |
|---|---|
| Number of solar irradiation scenarios | 1000 |
| Number of wind turbine power generation scenarios | 1000 |
| Number of PHEVs contribution scenarios | 1000 |
| Number of demand response contribution scenarios | 1000 |
| Number of day-ahead market load and price scenarios | 1000 |
| Number of real-time market load and price scenarios | 1000 |
| Number of non-utility bidding scenarios | 2000 |
| Number of solar irradiation reduced scenarios | 10 |
| Number of wind turbine power generation reduced scenarios | 10 |
| Number of PHEVs contribution reduced scenarios | 10 |
| Number of demand response contribution reduced scenarios | 10 |
| Number of day-ahead market load and price reduced scenarios | 10 |
| Number of real-time market load and price reduced scenarios | 10 |
| Number of non-utility bidding reduced scenarios | 20 |

Figs. 16, 17, and 18 present the 123-bus system day-ahead forecasted load, electricity generation of photovoltaic arrays, and wind turbines for one of the reduced scenarios, respectively. Fig. 19 presents the 123-bus system forecasted day-ahead electricity price for one of the reduced scenarios.

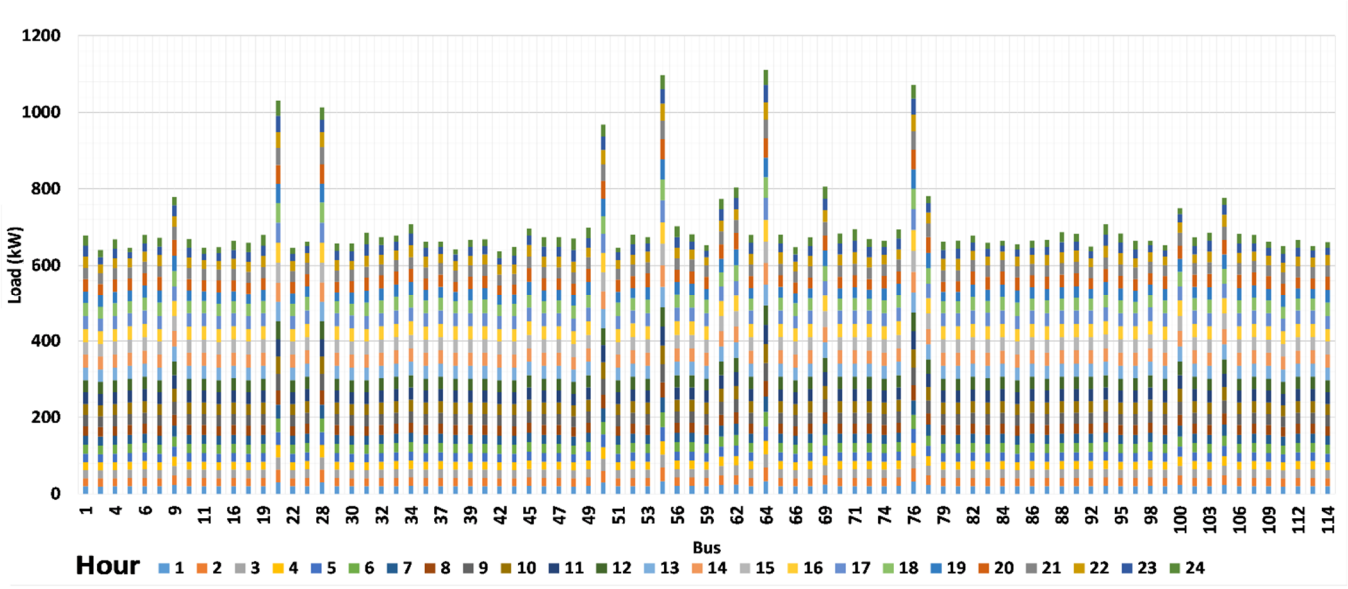


Fig. 16. The 123-bus system day-ahead forecasted electrical load for one of the reduced scenarios.

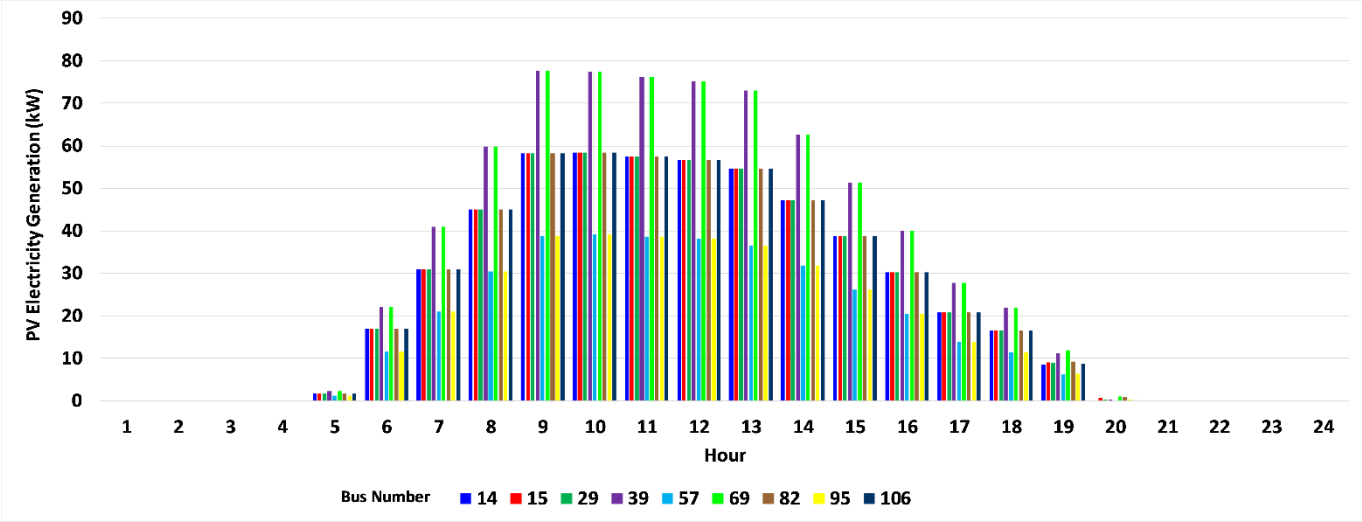


Fig. 17. The 123-bus system forecasted photovoltaic electricity generation for one of the reduced scenarios.

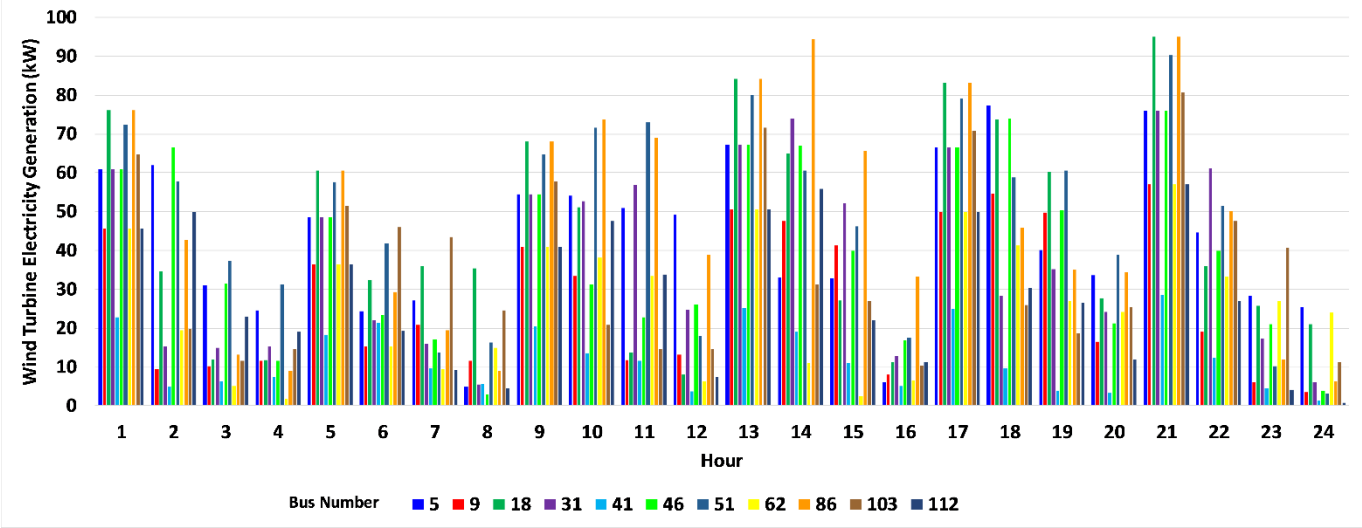


Fig. 18. The 123-bus system forecasted wind turbine electricity generation for one of the reduced scenarios.

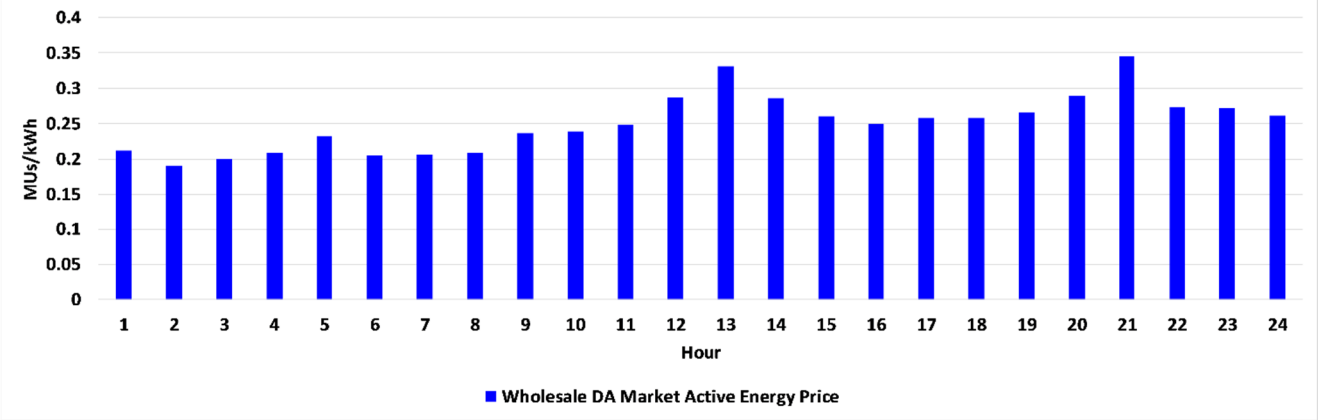


Fig. 19. The 123-bus system forecasted day-ahead electricity price for one of the reduced scenarios.

Table 8 presents different states of the 123-bus system topology based on the status of normally opened switches.

Table 8. Different states of the 123-bus system topology based on the status of normally opened switches.

| | Normally opened switches status | | | | | | | | | | |
|---|---|---|---|---|---|---|---|---|---|---|---|
| Topology Number | SW1 | SW2 | SW3 | SW4 | SW5 | SW6 | SW7 | SW8 | SW9 | SW10 | SW11 |
| 1 | 1 | 0 | 1 | 1 | 1 | 0 | 0 | 0 | 0 | 0 | 0 |
| 2 | 1 | 0 | 1 | 1 | 1 | 0 | 1 | 1 | 0 | 0 | 0 |
| 3 | 1 | 0 | 1 | 1 | 1 | 0 | 0 | 0 | 0 | 1 | 0 |
| 4 | 1 | 0 | 1 | 1 | 0 | 0 | 0 | 0 | 0 | 0 | 1 |
| 5 | 1 | 0 | 1 | 1 | 0 | 0 | 1 | 0 | 0 | 0 | 0 |
| 6 | 1 | 1 | 1 | 1 | 1 | 0 | 0 | 0 | 1 | 0 | 0 |
| 7 | 1 | 0 | 1 | 1 | 1 | 0 | 0 | 0 | 1 | 1 | 0 |
| 8 | 1 | 0 | 1 | 1 | 1 | 0 | 0 | 0 | 0 | 1 | 1 |
| 9 | 1 | 0 | 1 | 1 | 1 | 0 | 0 | 0 | 0 | 0 | 1 |
| 10 | 0 | 0 | 1 | 1 | 1 | 1 | 0 | 1 | 1 | 0 | 0 |
| 11 | 1 | 0 | 1 | 1 | 0 | 0 | 0 | 0 | 0 | 0 | 0 |
| 12 | 1 | 0 | 1 | 1 | 1 | 1 | 0 | 0 | 0 | 0 | 0 |
| 13 | 1 | 0 | 1 | 1 | 1 | 1 | 0 | 0 | 0 | 1 | 0 |
| 14 | 1 | 0 | 1 | 1 | 1 | 0 | 1 | 0 | 0 | 0 | 0 |
| 15 | 1 | 1 | 1 | 1 | 1 | 0 | 0 | 0 | 0 | 0 | 0 |
| 16 | 1 | 1 | 1 | 1 | 1 | 0 | 0 | 0 | 1 | 0 | 0 |
| 17 | 1 | 0 | 1 | 1 | 1 | 0 | 0 | 1 | 0 | 0 | 0 |
| 18 | 0 | 1 | 1 | 1 | 1 | 0 | 0 | 0 | 0 | 0 | 0 |
| 19 | 1 | 0 | 1 | 1 | 1 | 1 | 0 | 0 | 1 | 0 | 0 |

### 4.2.1. Simulation results of the first step of the first stage problem

The first step of the first stage optimization process was carried out for the next 24 hours horizon with one-hour intervals. Three cases were considered for the normal operation of the 123-bus system. The first case only considered the intermittent electricity generation uncertainties. In the second case, the energy storage facilities were considered in the optimization process. In the third case, the PHEVs were considered in the problem. Finally, the results of the three cases were compared. Fig. 20 presents the day-ahead bidding curves of non-utility electricity generation facilities for one of the reduced scenarios. The outputs of the first case simulations were compared with the results of Ref. [15] for the 123-bus test system to validate the proposed model and algorithm.

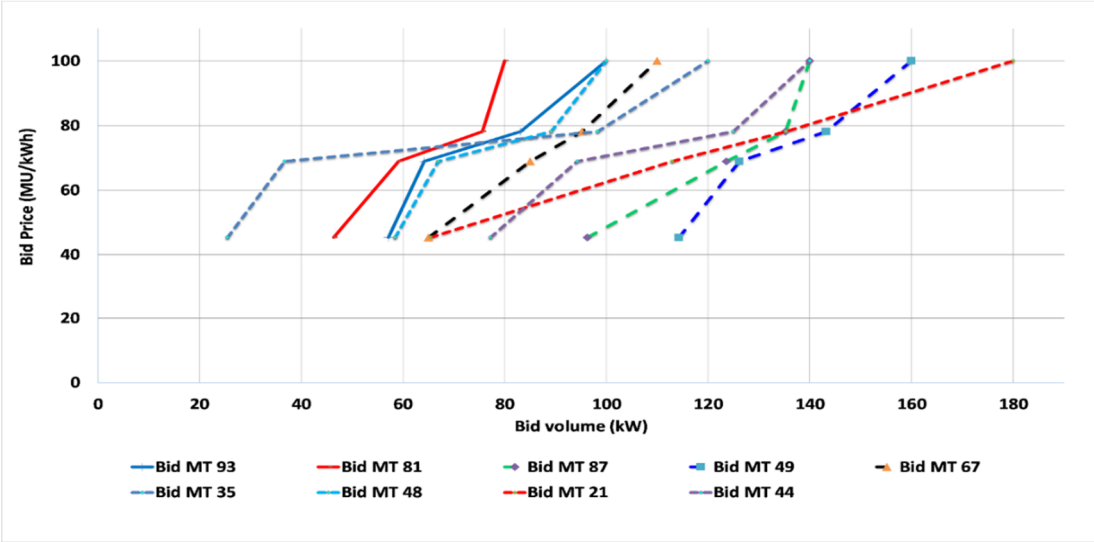


Fig. 20. The day-ahead bidding curves of non-utility electricity generation facilities for one of the reduced scenarios.

Further, for the third case, three scenarios of time of use fees, direct load control fees, and prices of electricity were considered. Fig. 21 The electricity purchased and sold price and direct load control fees for the third case.

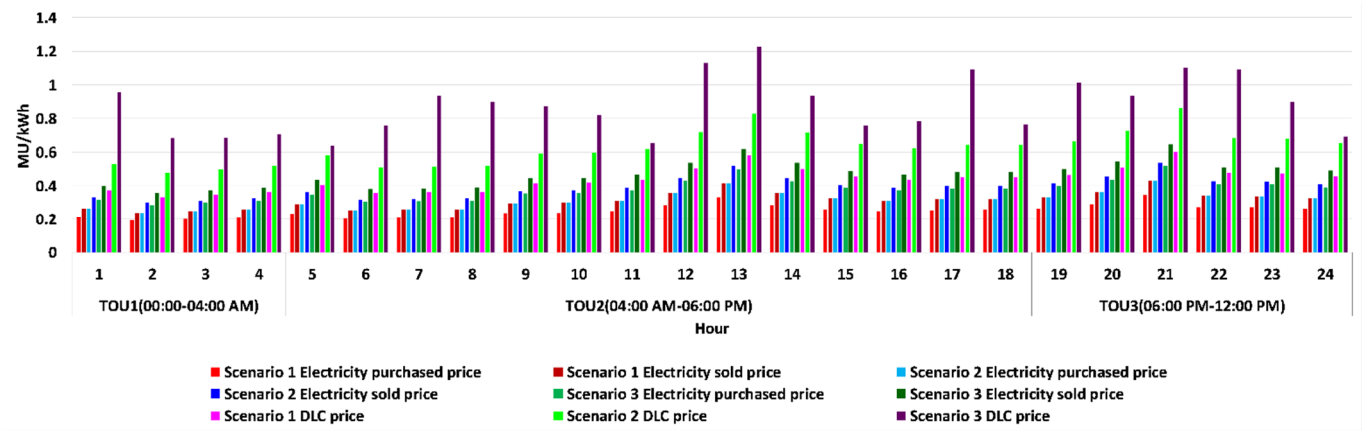


Fig. 21. The electricity purchased and sold price and direct load control fees for the third case.

Table 9 shows the values of the objective function of the first step for three cases and three scenarios of the purchased and sold price and direct load control fees. The minus values presented the profit of the system that compromised profits of energy sold to consumers, PHEVs, and upward network. By comparing the values of Table 9, it could be concluded that the energy storages commitment increased the profit of the system by about 16.306$ concerning the first case. In this case, the energy storage facilities were charged in the intervals that the price of electricity was low and they were discharged for the intervals that the price of electricity was high. The PHEV commitment increased the profit of the system by about 121.551$ concerning the second case based on the fact that the PHEVs behaved like moving energy storage facilities. Thus, the third scenario of the third case was the optimal day-ahead scheduling and it corresponded to the third scenario of demand response and electricity prices. Hence, all of the third case study values were calculated based on the third scenario of time of use fees, direct load control fees, and electricity prices.

Table 9. The values of the objective function of the first step for three cases and three scenarios of purchased and sold price and direct load control fees for the 123-bus system.

| Case | Scenario of time of use fees, direct load control fees, electricity sold and purchase prices | Objective function of first step problem |
|---|---|---|
| 1 | -- | -2774.513 |
| 2 | -- | -2790.819 |
| 3 | 1 | -2835.912 |
| 3 | 2 | -2876.326 |
| 3 | 3 | -2912.370 |

Figs. 22, 23, 24 present the optimally allocated apparent power of non-utility owned distributed energy resources for the three cases based on the bidding values of non-utility distributed energy resources.

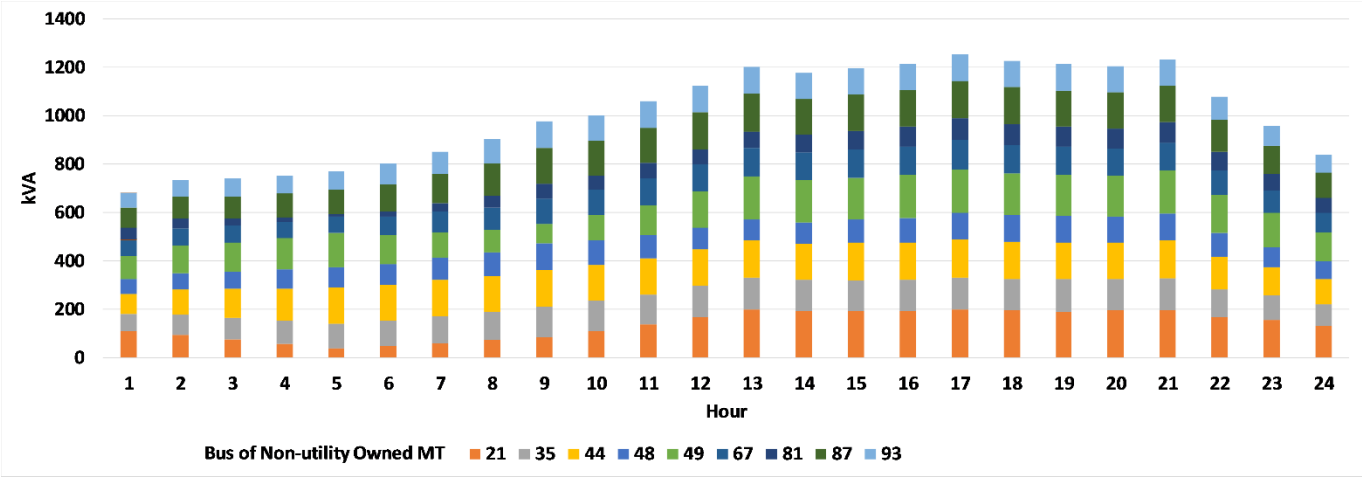


Fig. 22. The optimally allocated apparent power of non-utility owned distributed energy resources for the first case.

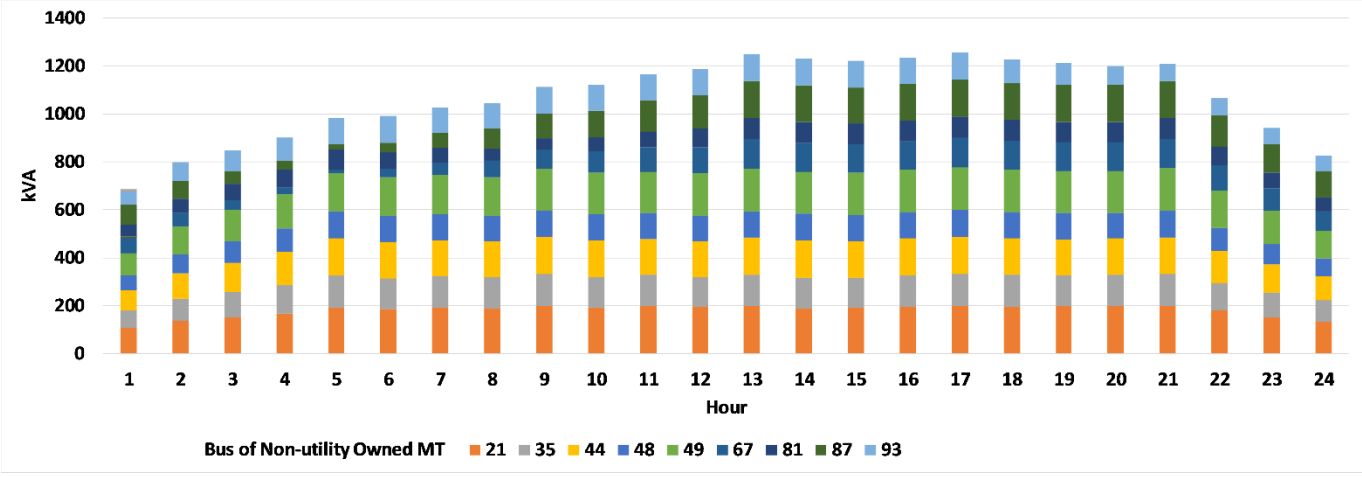


Fig. 23. The optimally allocated apparent power of non-utility owned distributed energy resources for the second case.

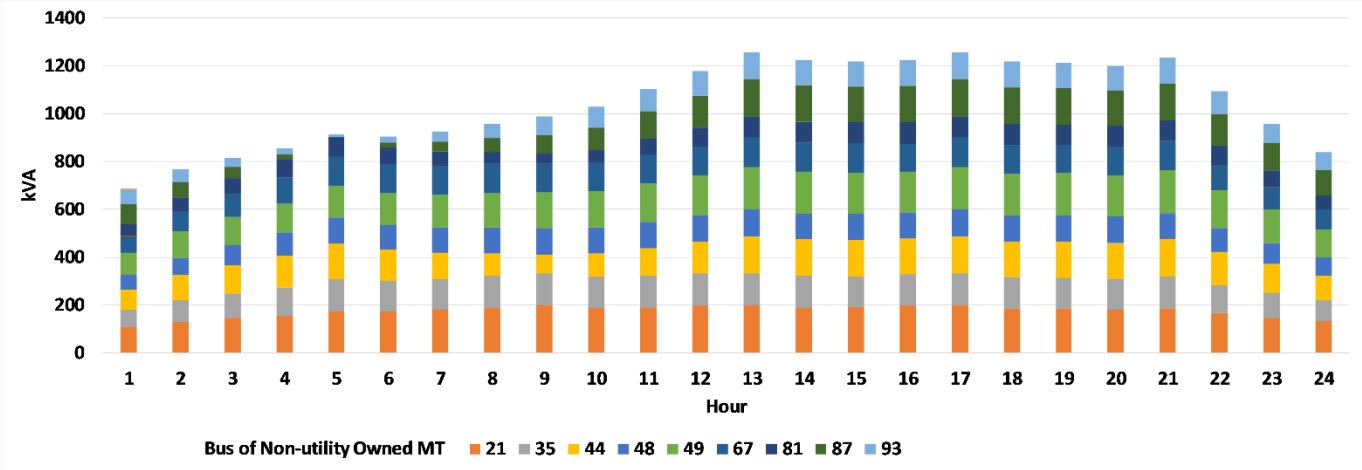


Fig. 24. The optimally allocated apparent power of non-utility owned distributed energy resources for the third case.

Figs. 25, 26, 27 present the 123-bus system optimal unit commitment of the utility-owned and non-utility owned distributed energy resources for the first, second, and third cases, respectively. The energy generation facilities tracked the electrical loads and the ramp rates of microturbines highly limited the deviations of electricity generation of these devices. By comparing the results, it could be concluded that the average electricity generation of the microturbines in the second case and third case were increased by about 3.44% and 3.29%, respectively. The commitment of energy storage facilities and their constraints led to an increase in electricity generation in the second case. Further, the energy consumption of PHEVs led to an increase in electricity generation in the third case.

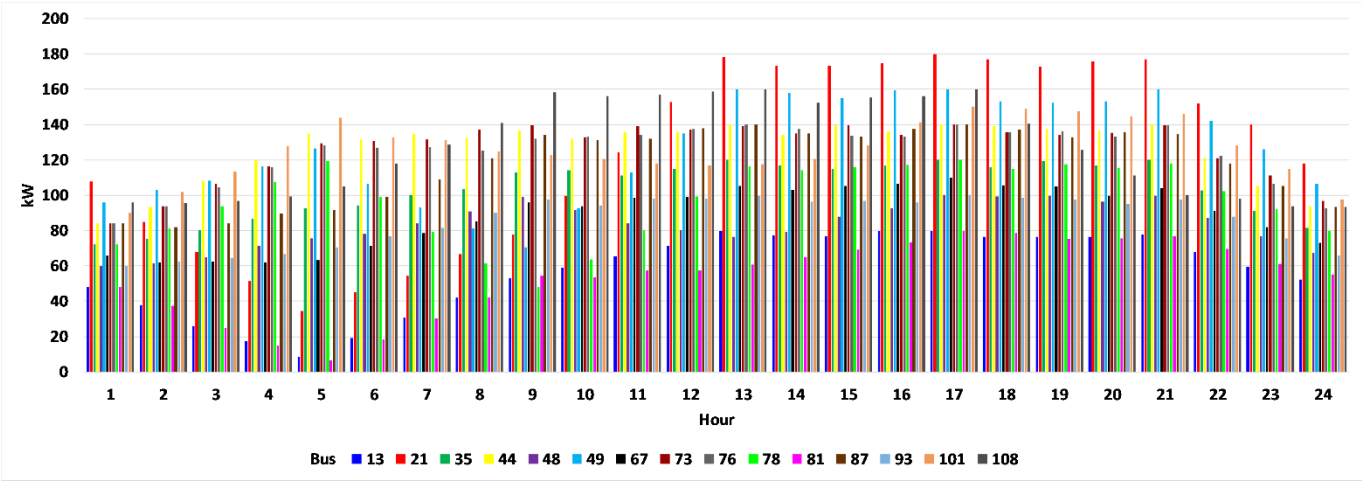


Fig. 25. The optimal unit commitment of utility-owned and non-utility owned distributed energy resources for the first case.

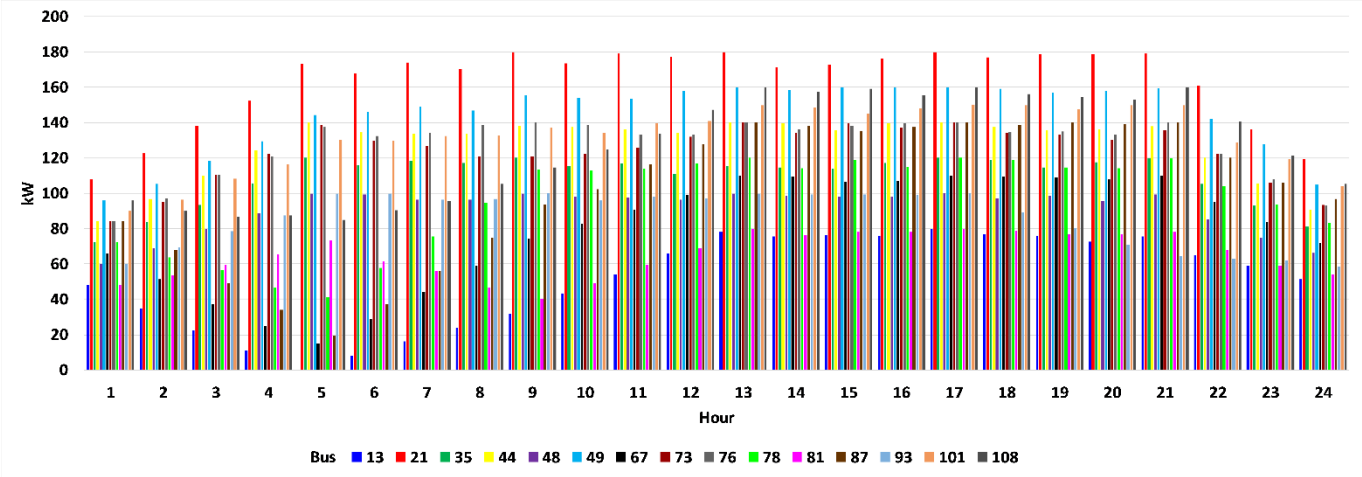


Fig. 26. The optimal unit commitment of utility-owned and non-utility owned distributed energy resources for the second case.

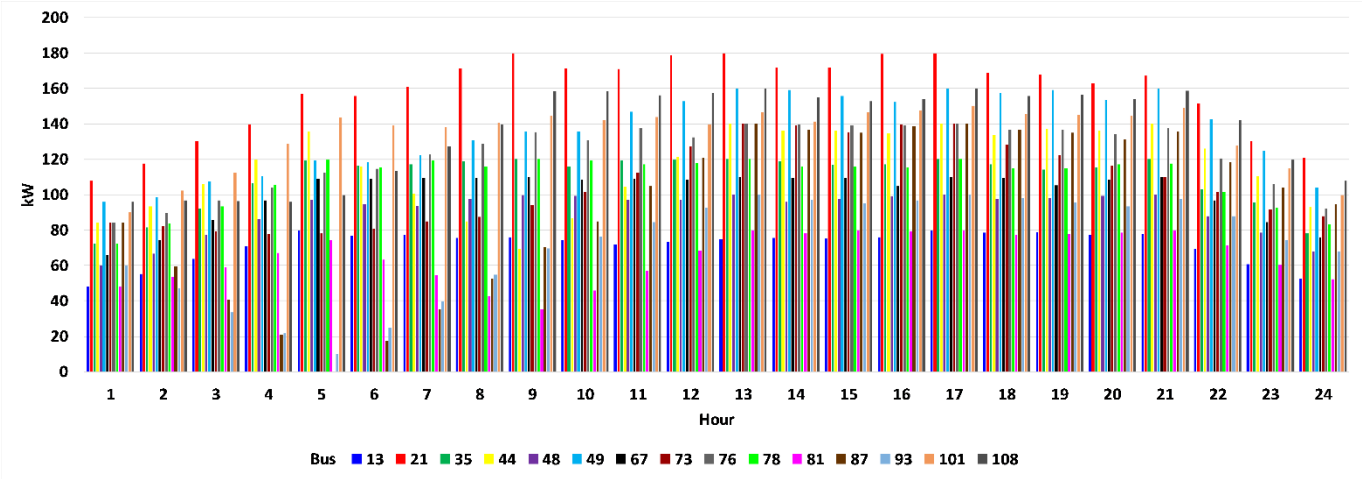


Fig. 27. The optimal unit commitment of utility-owned and non-utility owned distributed energy resources for the third case.

Fig. 28 presents the transacted energy with the upward market for three cases. The negative value of Fig. 28 presented the values of the electricity sold to the upward network. By comparing the results of Fig. 28 for three cases, it could be concluded that the proposed method increased the energy generation of system facilities. Further, the system decreased the energy import from the upward market and exported more electricity to the market to increase its profit. The energy storage commitment for the second case highly increased the electricity transaction capability of the system. However, the PHEVs commitment and their energy consumption were reduced the system's electricity transaction capability. Thus, the electricity transactions with the upward market were reduced in the third case concerning the second case.

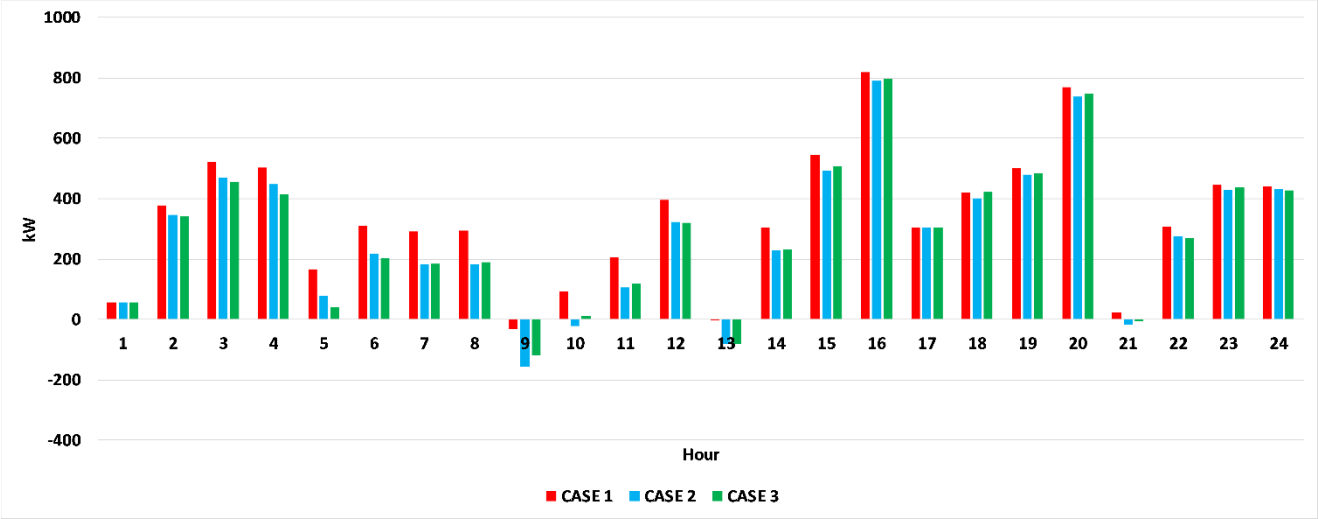


Fig. 28. The optimal transacted electricity with the upward electricity market for different cases.

Fig. 29 presents the optimal values of the electrical power of energy storage facilities for the third case. The optimization process charged the energy storage devices in the low load and low electricity price conditions to supply the electric load of the system in the peak load intervals based on the fact that the wind turbine electricity generation of bus 41 reached its minimum value and the microturbine of 35 and 44 buses reached to their maximum limits.

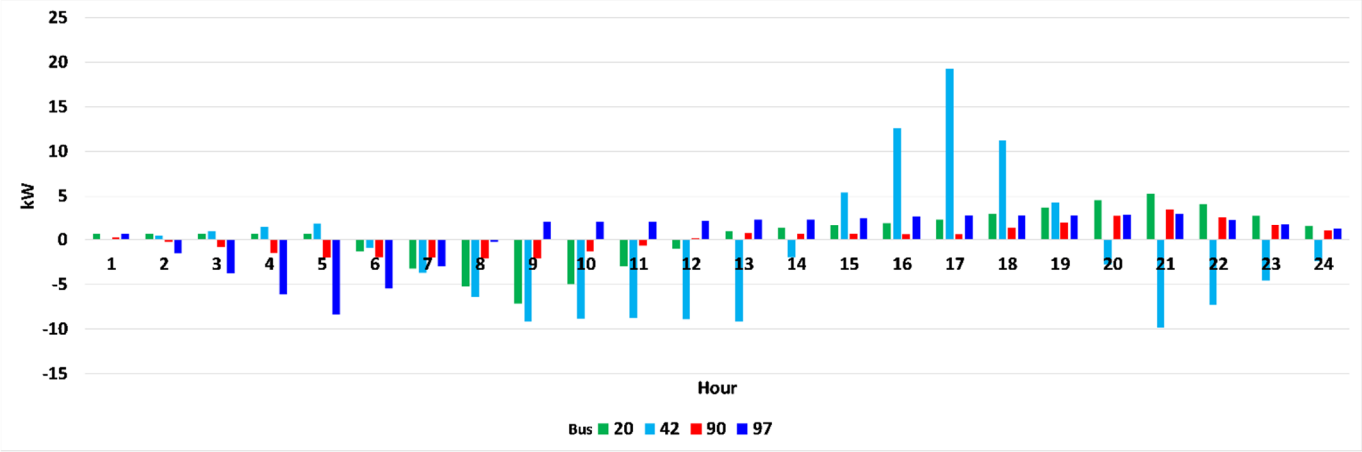


Fig. 29. The optimal values of electrical power of energy storage facilities for the third case.

Fig. 30 presents the electrical power of PHEVs for the third case study. The optimization process determined the energy level of each PHEV based on its departure time, which are depicted by the minus values. The PHEVs charging processes were accomplished for the low load conditions that corresponded to the off-peak intervals. Further, the optimization process discharged the energy of PHEVs to supply the peak load interval. Finally, for the 21:00-24:00 interval, the PHEVs of 3, 23, 236, 40, 84, 105, and 110 buses were charged. The optimization process charged the PHEVs of 54, 61, 89, 94, and 102 buses for the next interval of the day-ahead horizon.

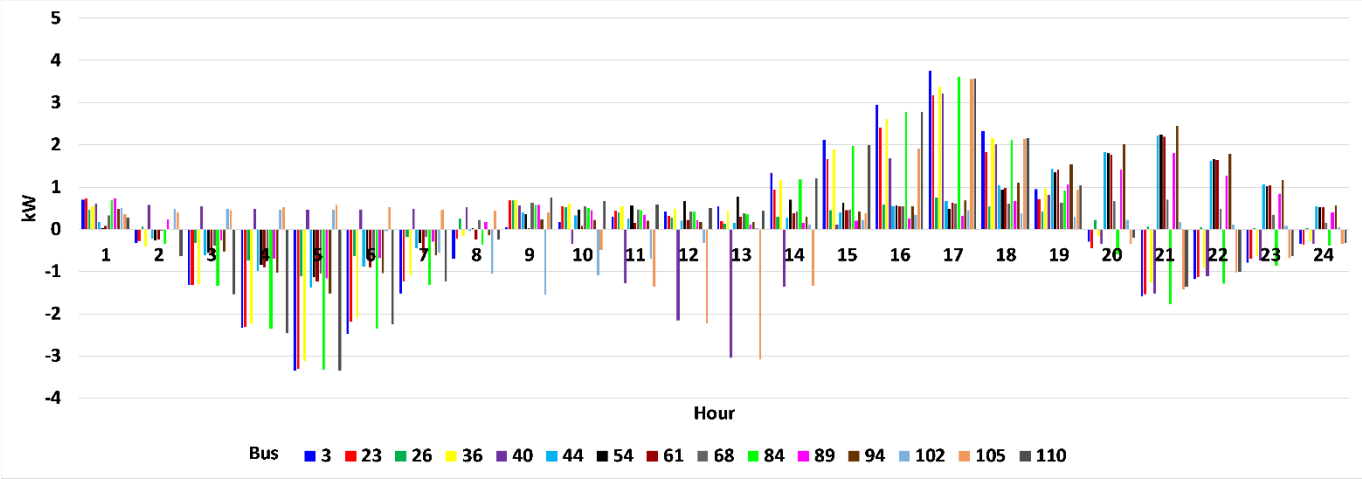


Fig. 30. The electrical power of PHEVs for the third case.

For assessing the proposed algorithm, the capacity withholding indices for different cases were calculated. Fig. 31 presents the capacity withholding indices for different cases of the first step optimization problem. The average values of the capacity withholding index without the proposed algorithm for the first, second, and third cases were about 0.2953, 0.2492, and 0.2237, respectively. The average values of the capacity-withholding index with the proposed algorithm for the first, second, and third cases were about 0.124, 0.1174, and 0.1121, respectively. Further, the maximum values of the capacity withholding index with the proposed algorithm for the first, second, and third cases were about 0.1889, 0.1813, and 0.1730, respectively. It could be concluded that the proposed algorithm successfully reduced the average and maximum values of the capacity-withholding index for the third case of day-ahead normal operation conditions by about 49.88% and 55.38%, respectively.

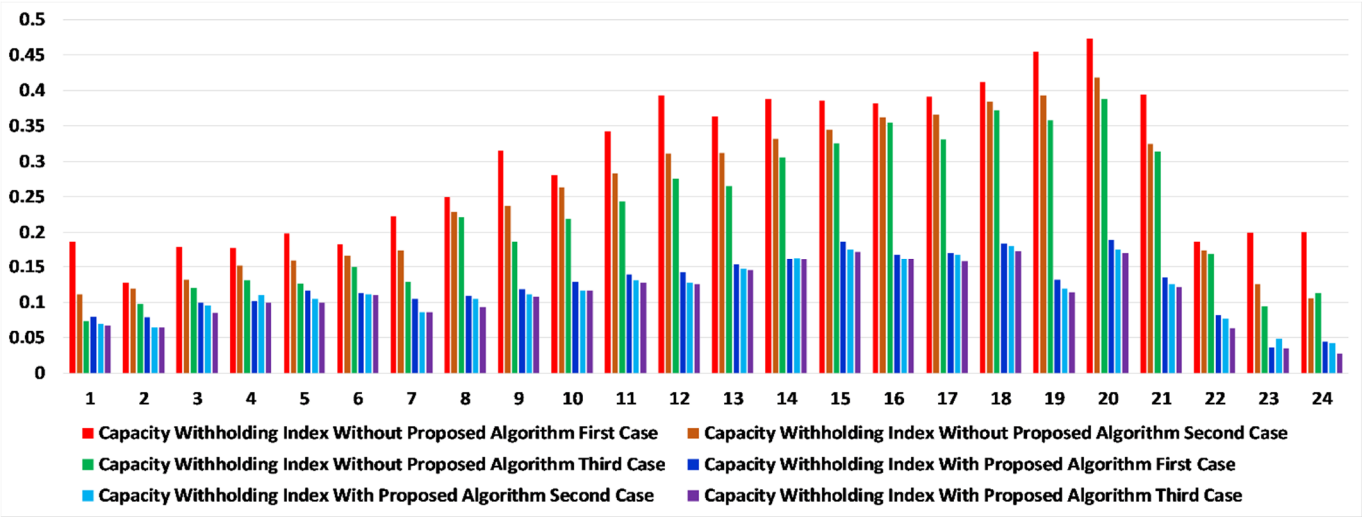


Fig. 31. The capacity withholding indices for different cases of the first step optimization problem.

### 4.2.2. Simulation results of the second step of the first stage problem

The second step of the first stage problem updated the forecasting data and the simulation was performed for the next 24 hours with 15 minutes intervals. The load forecasting process was performed for the next 15 minutes. Fig. 32 presents the real-time electrical load forecasting for different forecasting intervals. Fig. 33 depicts the real-time bidding of non-utility facilities. Fig. 34 depicts the aggregated mismatches of utility and non-utility distributed generation electrical power generations for different values of the real-time electrical load of the system.

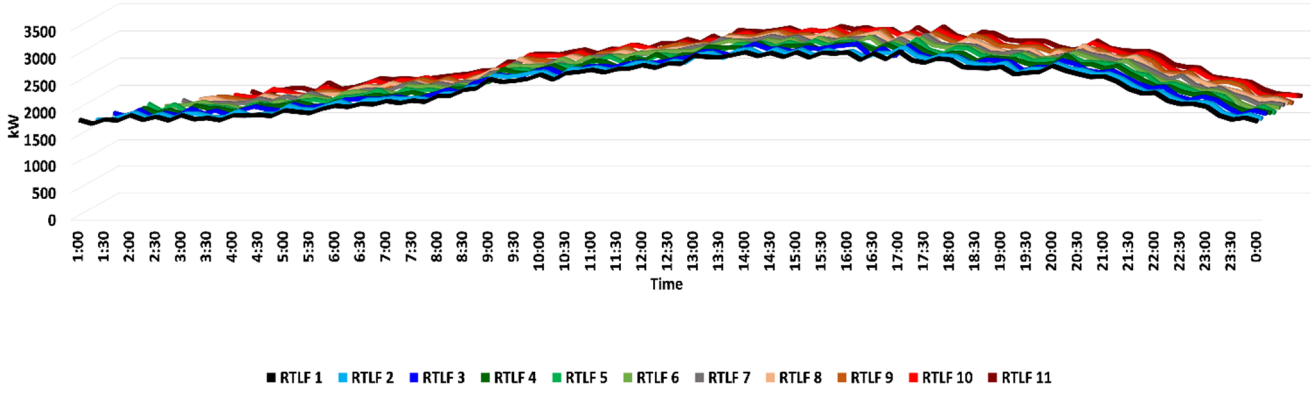


Fig. 32. The 123-bus system forecasted real-time electrical load.

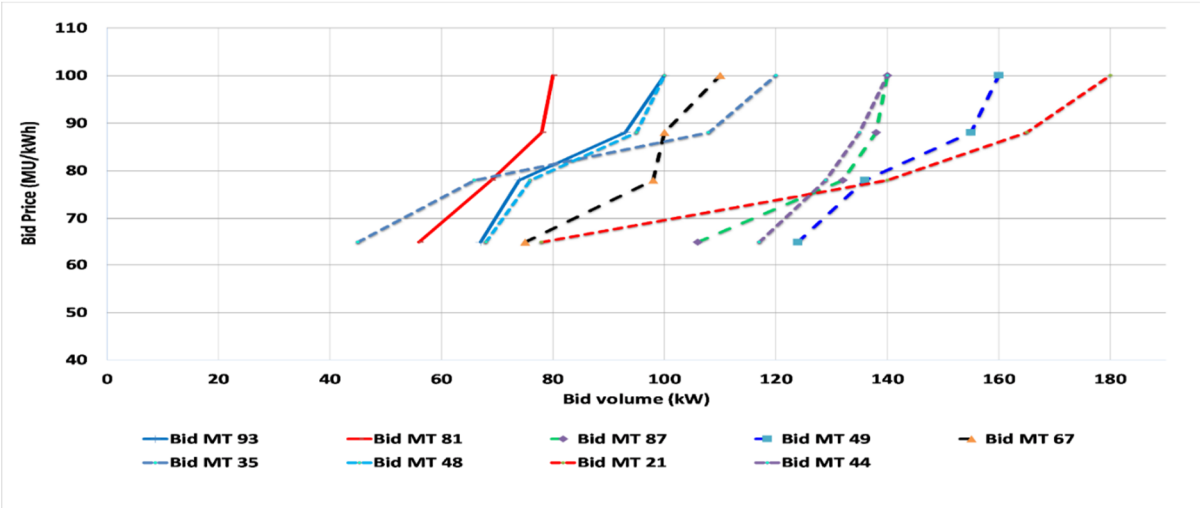


Fig 33. The real-time bidding of electricity generation of non-utility facilities.

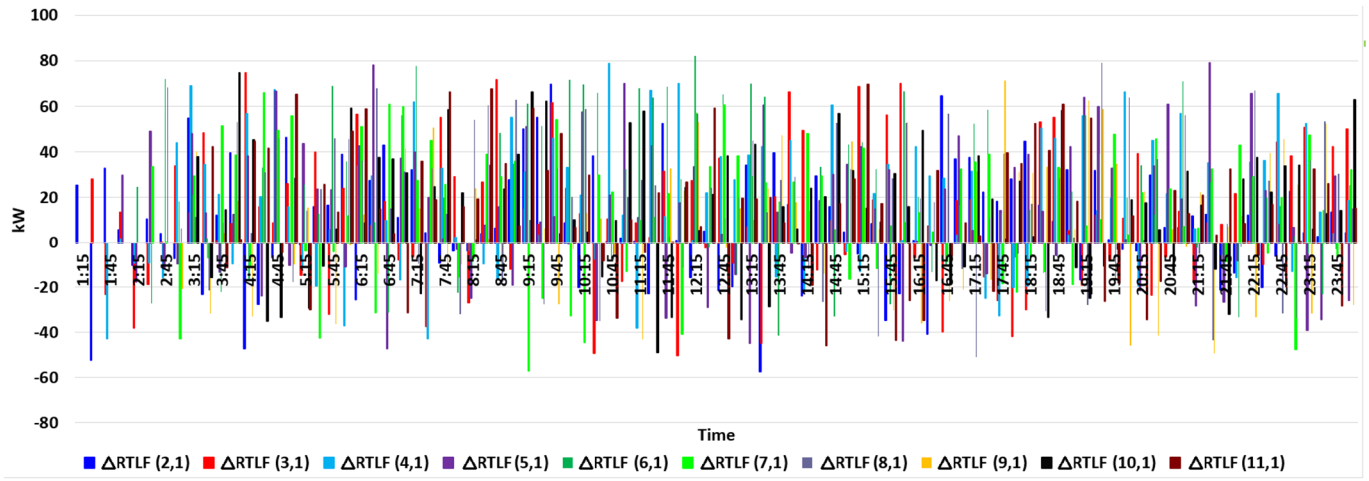


Fig. 34. The aggregated mismatches of utility and non-utility distributed generation electrical power generations for different values of the real-time electrical load.

The capacity withholding indices for different real-time load forecasting cases were determined. Fig. 35 presents the capacity withholding indices for different cases of the second step of the first stage (real-time) optimization problem. The average values of the capacity-withholding index without the proposed algorithm for the first, second, and third cases were about 0.3224, 0.2753, and 0.2477, respectively. The average values of the capacity-withholding index with the proposed algorithm for the first, second, and third cases were about 0.1483, 0.1420, and 0.1364, respectively. The proposed algorithm reduced the average and maximum values of the capacity-withholding index for the third case of day-ahead normal operation conditions by about 44.93% and 47.61%, respectively.

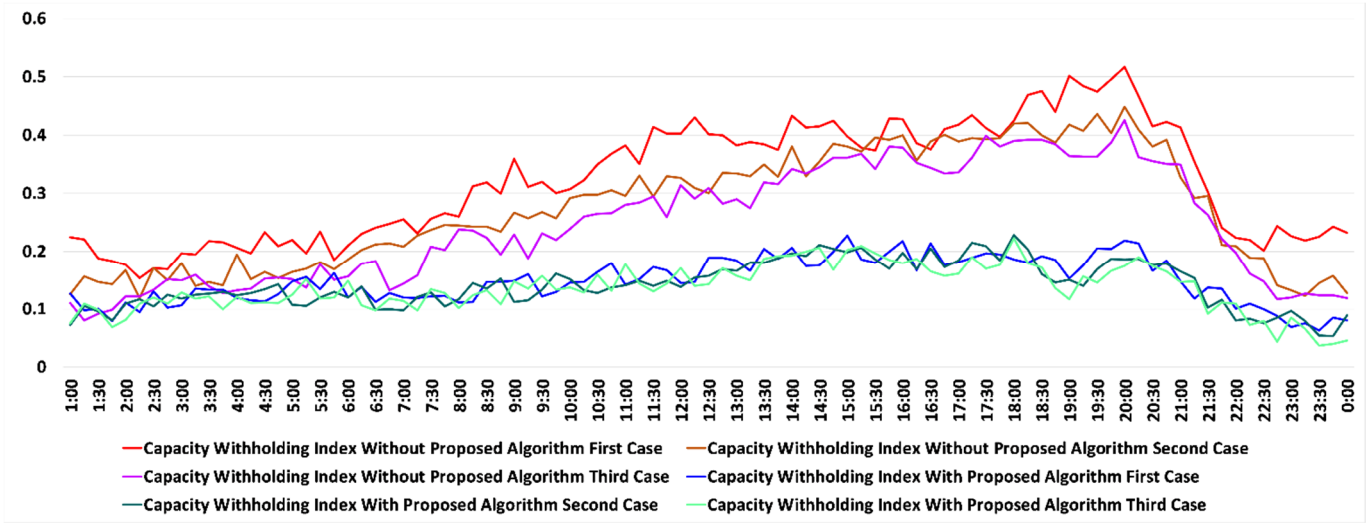


Fig. 35. The capacity withholding indices for different cases of the second step of the first stage (real-time) optimization problem.

### 4.2.3. Simulation results of the third step of the first stage problem

The third step of the first stage problem simulation was performed for multiple external shocks and the next 24 hours with 15 minutes intervals. The third step problem explored the system conditions for the worst-case of external shocks.

It was assumed that all of the 123-bus system lines were equipped with normally closed sectionalizers that could be opened in the contingent condition to form a multi-microgrids system. The total number of simulated external shocks was 512 that consisted of multiple contingencies. Figs. 36 (a), (b) present the aggregated operational and interruption costs of the distribution system without and with the proposed algorithm for the top 96 worst-case external shocks for the third case, respectively. As shown in Fig. 36 (a), the worst-case contingency was the 96 contingency that the aggregated operational and interruption costs were about 14852 MUs for 20:30-20:45 interval. The proposed algorithm reduced the corresponding aggregated operational and interruption costs of this contingency to 1765 MUs. Thus, the proposed algorithm reduced the aggregated operational and interruption costs of the worst-case contingency by about 88.11%. The average values of aggregated operational and interruption costs for the 96 contingencies were about 8096 MUs and 2039 MUs, respectively. Further, the proposed algorithm reduced the average value of aggregated operational and interruption costs of the worst-case contingencies by about 74.81%.

Figs. 37 (a) and (b) present the number of optimal microgrid formations for the top 96 worst-case external shocks. As shown in Figs. 37 (a) and (b), the third step of the first stage optimization process determined the optimal topology of the distribution system by sectionalizing the system into multi-microgrids.

Figs. 38 (a) and (b) present the optimal topology and demand response programs in the day-ahead and real-time optimization intervals. As shown in Fig. 38, the optimal day-ahead scheduling determined the optimal topology of the system based on the real-time normal operation and the simulation of external shocks. The switching of normally opened switches was performed in the day-ahead and real-time horizons to change the pattern of load flow, reduce the impacts of external shocks, and reduce the capacity withholding of non-utility electricity generation facilities. The third scenario of the demand response program was selected as the optimal demand response alternative for the day-ahead and real-time optimization horizons.

The capacity withholding and resiliency indices were determined for different real-time external shock cases. Fig. 39 presents the capacity withholding indices for the third step of the first stage optimization problem. The average values of the capacity withholding index without the proposed algorithm for the first, second, and third cases were about 0.5173, 0.5055, and 0.4740, respectively. The average values of the capacity-withholding index with the proposed algorithm for the first, second, and third cases were about 0.1639, 0.1574, and 0.1545, respectively. The proposed algorithm reduced the average and maximum values of the capacity-withholding index for the third case by about 67.40% and 71.05%, respectively.

Fig. 40 presents the resiliency index of the system for the worst-case external shock conditions without implementing the proposed algorithm for the third step of the first stage optimization problem. The resiliency index of the system with the proposed algorithm tended to infinity based on the fact that the optimization process maximized the resiliency index. The maximum values of the resiliency index for the first, second, and third cases without the proposed algorithm were about 2.5211, 4.3937, and 7.8081, respectively.

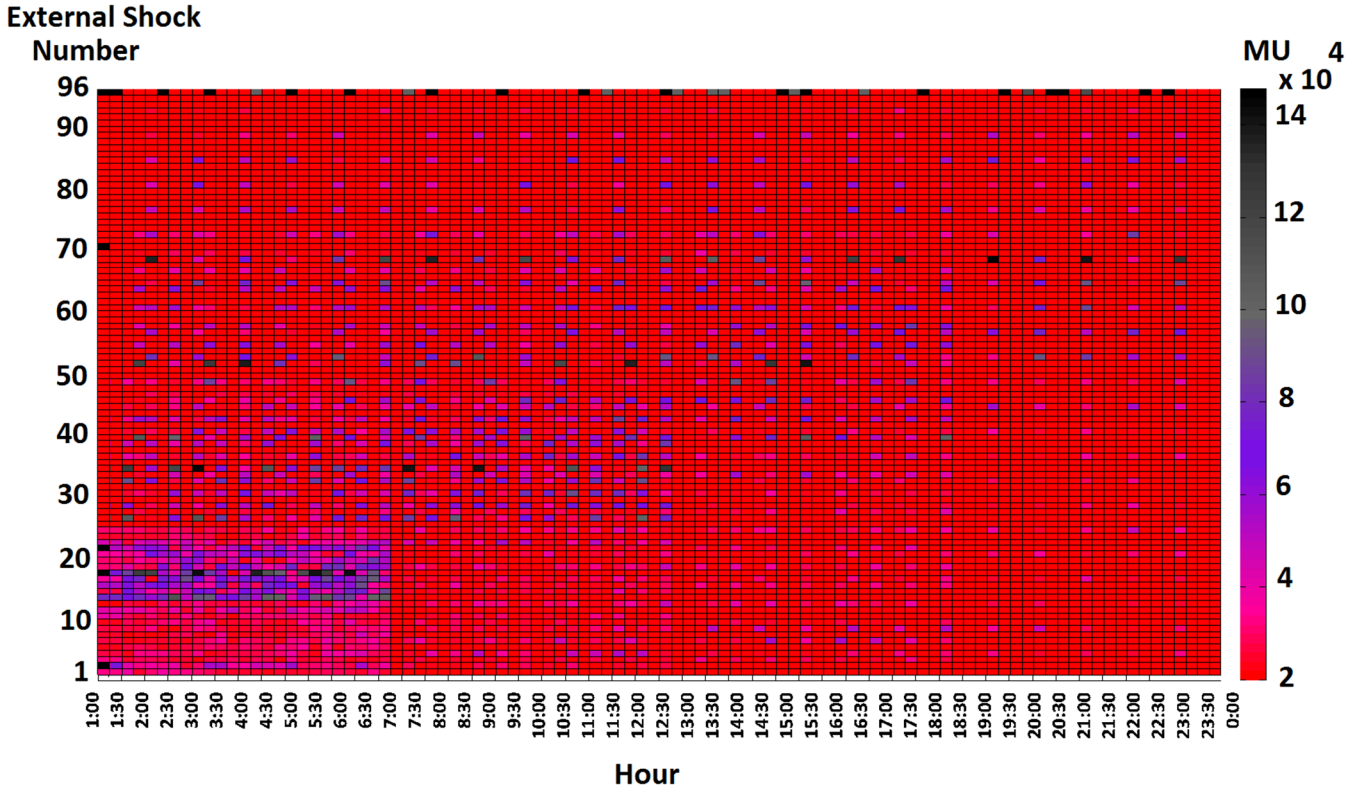


(a)

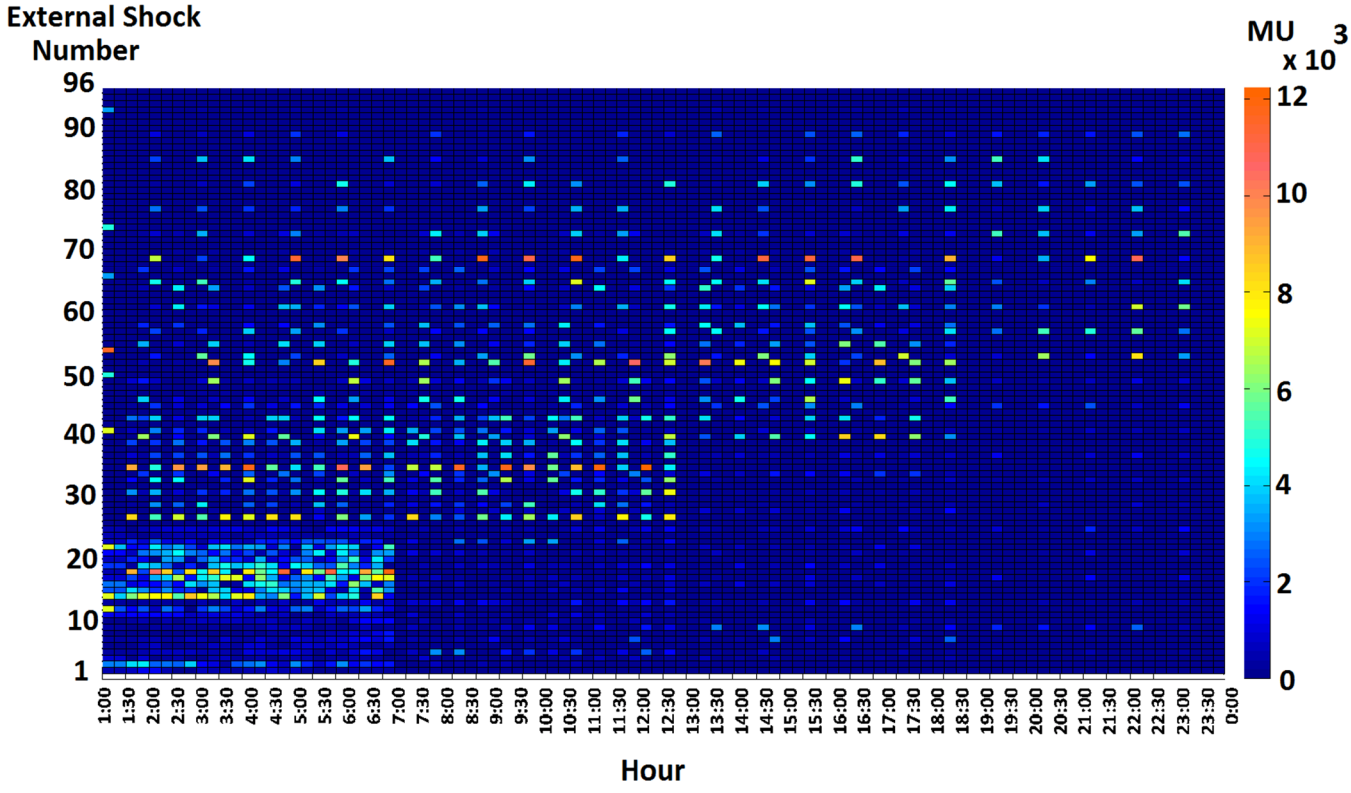


(b)

Fig. 36 (a) The aggregated operational and interruption costs of the distribution system for the 96 worst-case external shocks without the proposed algorithm for the third case. (b) The aggregated operational and interruption costs of the distribution system for the 96 worst-case external shocks with the proposed algorithm for the third case.

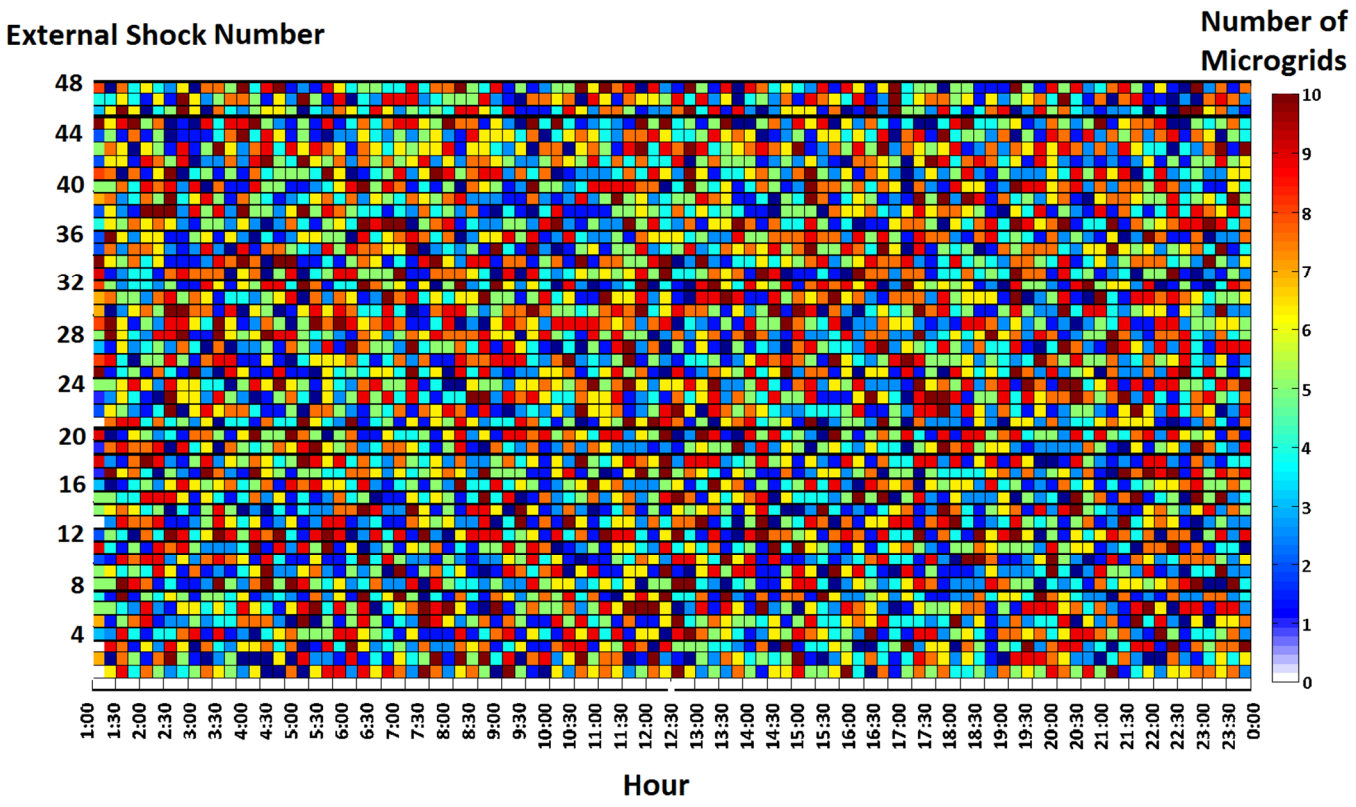


(a)

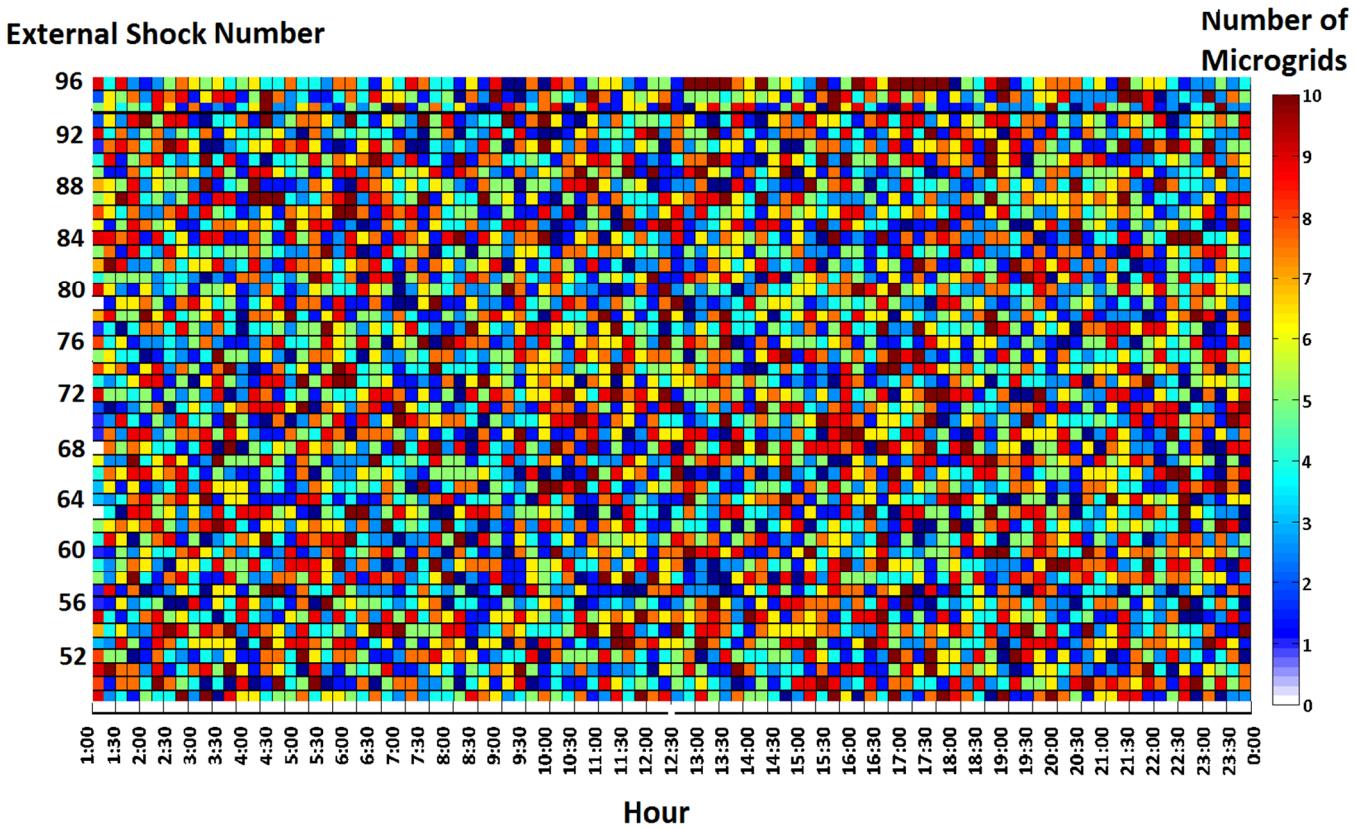


(b)

Fig. 37. (a) The number of optimal microgrid formations for the top 1-48 worst-case external shocks. (b) The number of optimal microgrid formations for the top 49-96 worst-case external shocks.

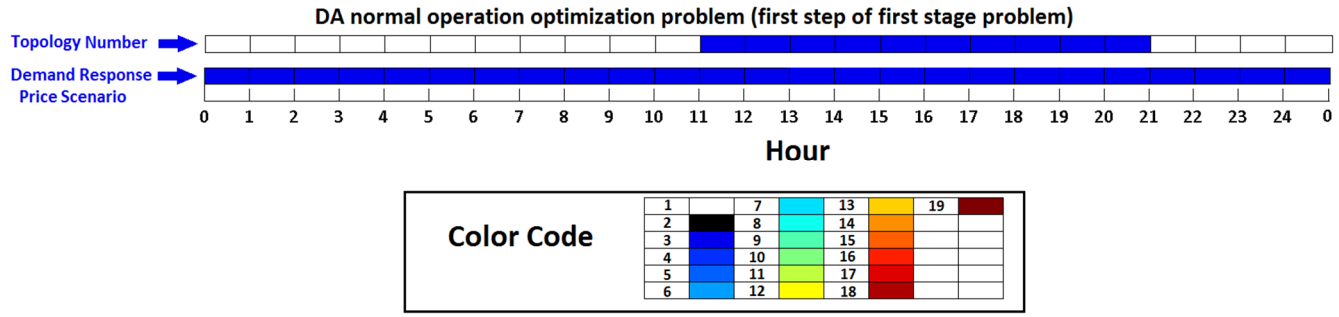


(a)

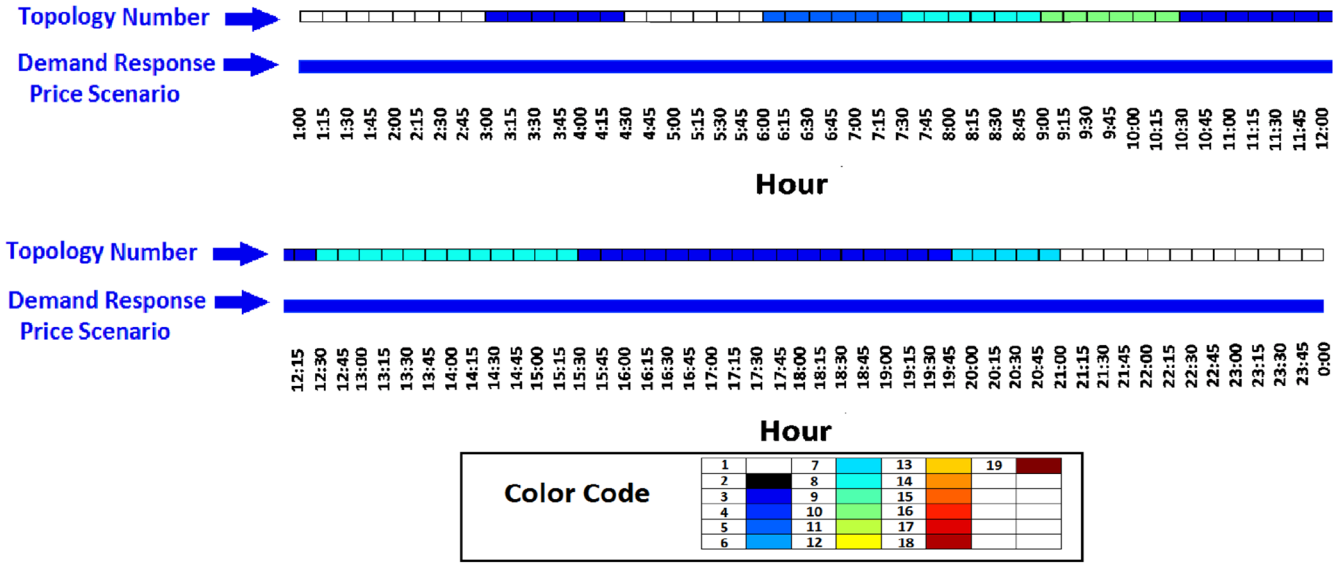


(b)

Fig. 38. (a) The optimal topology state of system and demand response programs in day-ahead optimization intervals. (b) The optimal topology state of system and demand response programs in real-time optimization intervals.

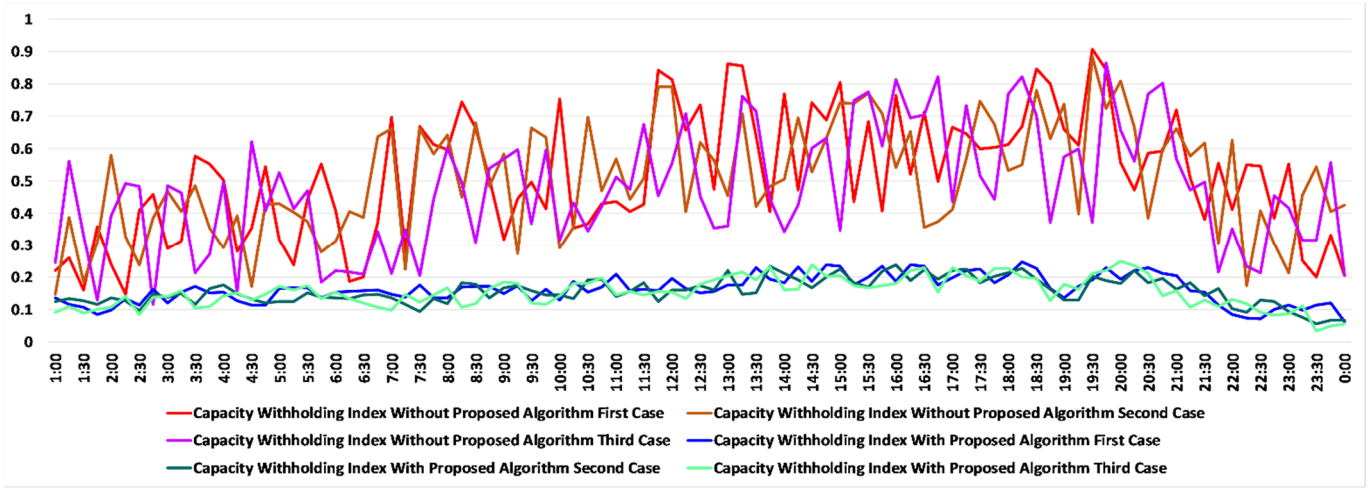


Fig. 39. The capacity withholding indices for different cases of the third step of the first stage (real-time simulation of external shock impacts) optimization problem.

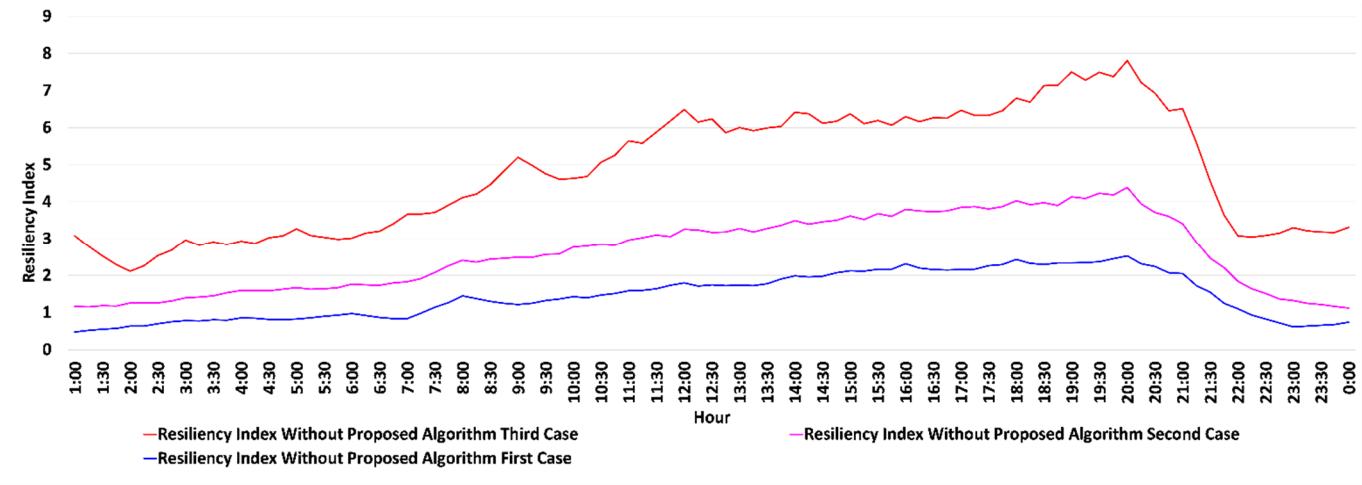


Fig. 40. The resiliency index of the system for the worst-case external shock conditions without implementing the proposed algorithm for the third step of the first stage optimization problem.

### 4.2.4. Simulation results of the second stage problem

The proposed method was assessed for the external shock conditions that were 512 contingencies and the results of the most credible contingency are presented. The status of system topology for the most credible external shock is shown in Fig. 41. The first contingency occurred in lines 67-60 (zone 1) that isolated the 67-114 buses from the system for 13:00. Then, a contingency occurred in lines 18-35 (zone 2) that isolated the 35-51 buses from the system for 17:00.

It was assumed that the system restoration process in the faulted areas was carried out in the last second of the corresponding interval of simulation. Further, the third demand response program scenario was selected for real-time operational scheduling from the day-ahead optimization process results. Same as the day-ahead optimization process, three cases of simulations for the most credible contingency were carried out. The first case determined the optimal energy dispatch of DERs to minimize the shed load. The second case considered the optimal demand response program for the first case. The third case assessed the impacts of PHEVs commitment for the second case. The optimization results are presented for 13:00, 17:00, and 21:00 to explore the detailed outputs of the algorithm and the effectiveness of the optimization process.

The objective functions of the optimization procedure in contingent conditions maximized the served loads and the resiliency index of the system. As shown in Fig. 37 and Fig. 41, the distribution system was optimally sectionalized into ten microgrids. The optimization process sectionalized the system into (1-8) and (9-10) microgrids for the first and second contingencies, respectively. It was assumed that the microgrids (1-8) and (9-10) formed Zone 1 and Zone 2, respectively.

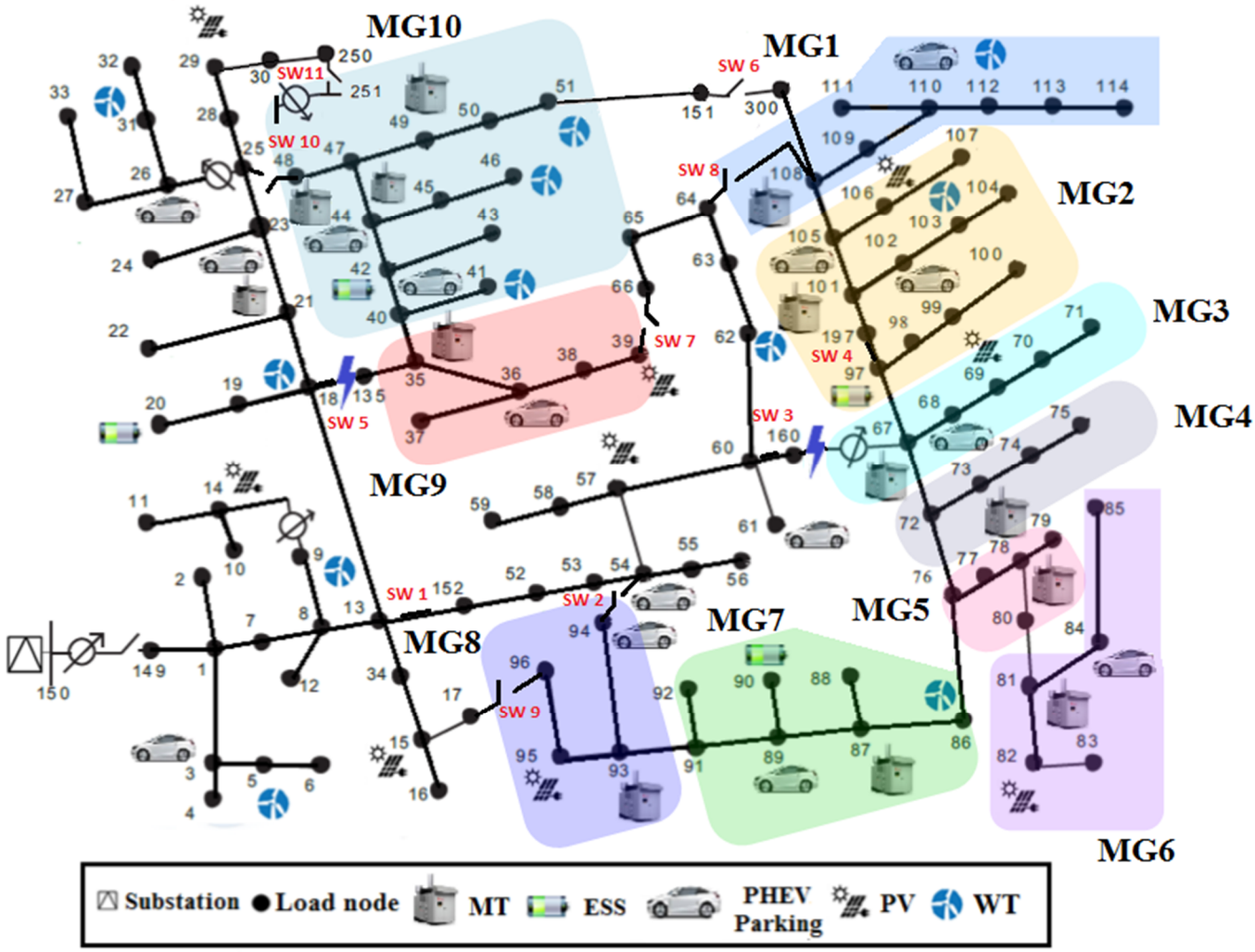


Fig. 41. The sectionalizing process of the distribution system for the worst-case external shocks.

Table 10 presents the served non-critical load index and resiliency index for the described contingencies. The proposed method served all of the critical loads. The served non-critical load index was the summation of the *Y* variable. As shown in Table 10, the served non-critical load index for the second case was increased by about 23.247% concerning the first case. The served non-critical loads in the second case and the third case was increased to 99.95% and 100% of the non-critical load values, respectively. The PHEVs were highly committed by the DSO to supply the non-critical loads. Further, the resiliency index took the values 7.049 and 2334.346 for the first and second cases, respectively. However, the resiliency index for the third case tended to infinity based on the fact that the demand response and PHEVs contributions highly increased the values of the served non-critical loads in the contingent conditions.

Table 10. The served non-critical load index and resiliency index for the worst-case contingencies.

| | **Served non-critical load index** | | **Resiliency index** | |
|---|---|---|---|---|
| | **Contingency** | | **Contingency** | |
| **Case** | **1** | **2** | **1** | **2** |
| **1** | 84.704 | 24.650 | 7.049 | 3.552 |
| **2** | 107.951 | 28.00 | 2334.346 | ∝ |
| **3** | 108 | 28.00 | ∝ | ∝ |

Table 11 presents the values of responsive load commitment variables for the third case that the "1/0" values of variables present the "OFF/ON" status of the responsive load control process. The system utilized the responsive load commitment process to balance the generation and consumption values and it shifted the non-critical energy consumption from peak periods to non-peak periods. The values of unserved non-critical loads were about 52%, 30%, and 18% for 21:00, 17:00, and 13:00 hours, respectively. The proposed procedure flatted the load profile and clipped the peak load of 13:00 and 17:00 hours. The optimization process fully supplied the critical loads and shifted the non-critical loads to other intervals to balance the values of energy generation and consumptions and minimize the non-served loads.

Table 11. The status of commitment of responsive loads.

| | | | | | | | | | | | | | | | | | | | | | |
|---|---|---|---|---|---|---|---|---|---|---|---|---|---|---|---|---|---|---|---|---|---|
| **Contingency** | **#1** | **Bus** | | **68** | **69** | **70** | **71** | **73** | **74** | **75** | **76** | **77** | **79** | **80** | **82** | **83** | **84** | **85** | **86** | **87** | **88** |
| | | **Hour** | **13** | 0 | 0 | 1 | 0 | 0 | 0 | 0 | 0 | 1 | 0 | 0 | 1 | 1 | 0 | 0 | 0 | 0 | 0 |
| | | | **17** | 0 | 0 | 0 | 0 | 1 | 0 | 0 | 1 | 0 | 0 | 0 | 0 | 0 | 1 | 0 | 0 | 0 | 0 |
| | | | **21** | 1 | 1 | 0 | 1 | 0 | 1 | 1 | 0 | 0 | 1 | 1 | 0 | 0 | 0 | 1 | 1 | 1 | 1 |
| | | **Bus** | | **90** | **92** | **94** | **95** | **96** | **98** | **99** | **100** | **102** | **103** | **104** | **106** | **107** | **109** | **111** | **112** | **113** | **114** |
| | | **Hour** | **13** | 0 | 0 | 1 | 1 | 0 | 0 | 0 | 0 | 0 | 0 | 0 | 1 | 1 | 0 | 1 | 0 | 0 | 0 |
| | | | **17** | 0 | 1 | 0 | 0 | 0 | 0 | 1 | 0 | 1 | 1 | 1 | 0 | 0 | 0 | 0 | 1 | 1 | 1 |
| | | | **21** | 1 | 0 | 0 | 0 | 1 | 1 | 0 | 1 | 0 | 0 | 0 | 0 | 0 | 1 | 0 | 0 | 0 | 0 |
| | **#2** | **Bus** | | **35** | **37** | **38** | **39** | **41** | **42** | **43** | **45** | **46** | **47** | **48** | **49** | **50** | **51** | | | | |
| | | **Hour** | **17** | 0 | 1 | 0 | 0 | 0 | 0 | 0 | 0 | 1 | 0 | 0 | 1 | 1 | 0 | | | | |
| | | | **21** | 1 | 0 | 1 | 1 | 1 | 1 | 1 | 1 | 0 | 1 | 1 | 0 | 0 | 1 | | | | |

Figs. 42, 43, and 44 depict the optimal microturbine electricity generations of the multi-microgrids system for the first, second and third cases, respectively. As discussed in Table 11 results, the electricity generations of microturbines of 48, 49, 73, 78, and 101 buses were shifted from 17:00 to 19:00 and 17:00 to 13:00 for the second and third cases, respectively. The PHEV commitment in the optimization process changed the commitment schedule of microturbines of 44, 84, 94, and 102 buses for the third case concerning the second case. This process reduced the electricity generation of these facilities based on the fact that the PHEVs electricity injection into the system led to gain more profit for the system.

By comparing the second case and third case results, the average electricity generations of microturbines were decreased by about 31.59% and 31.44%, respectively. The non-critical responsive loads were shifted to other intervals. As shown in Table 11, the not-served non-critical loads were supplied by the PHEVs and microturbines.

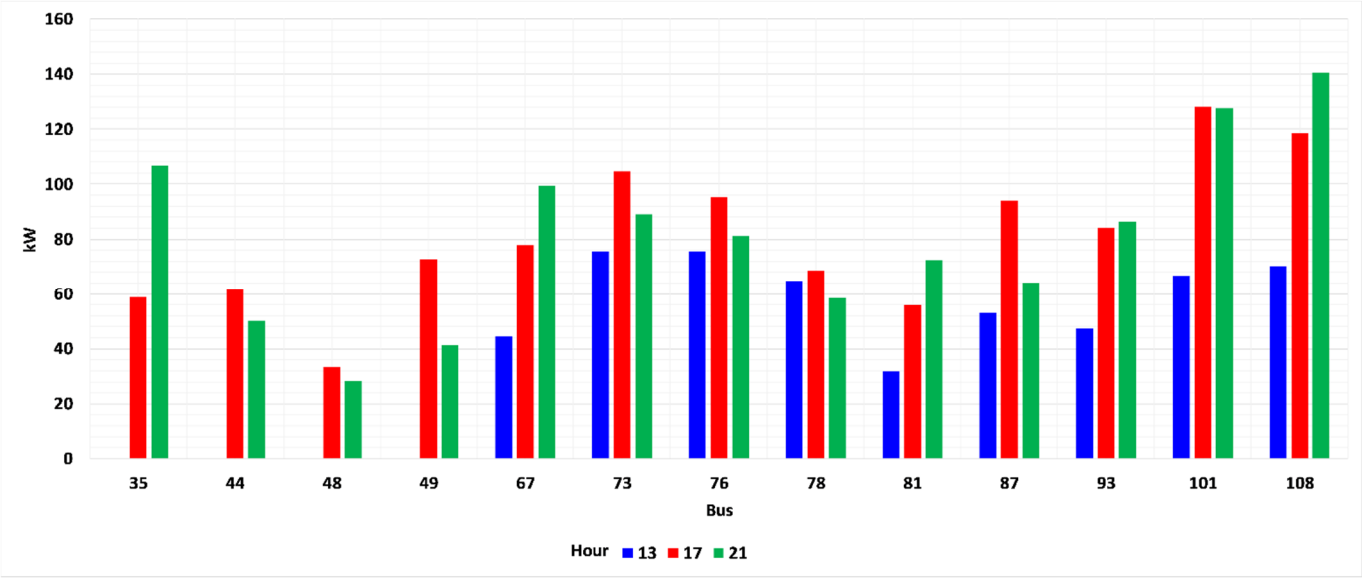


Fig. 42. The optimal microturbine electricity generations for the multi-microgrids system for the first case of external shock conditions.

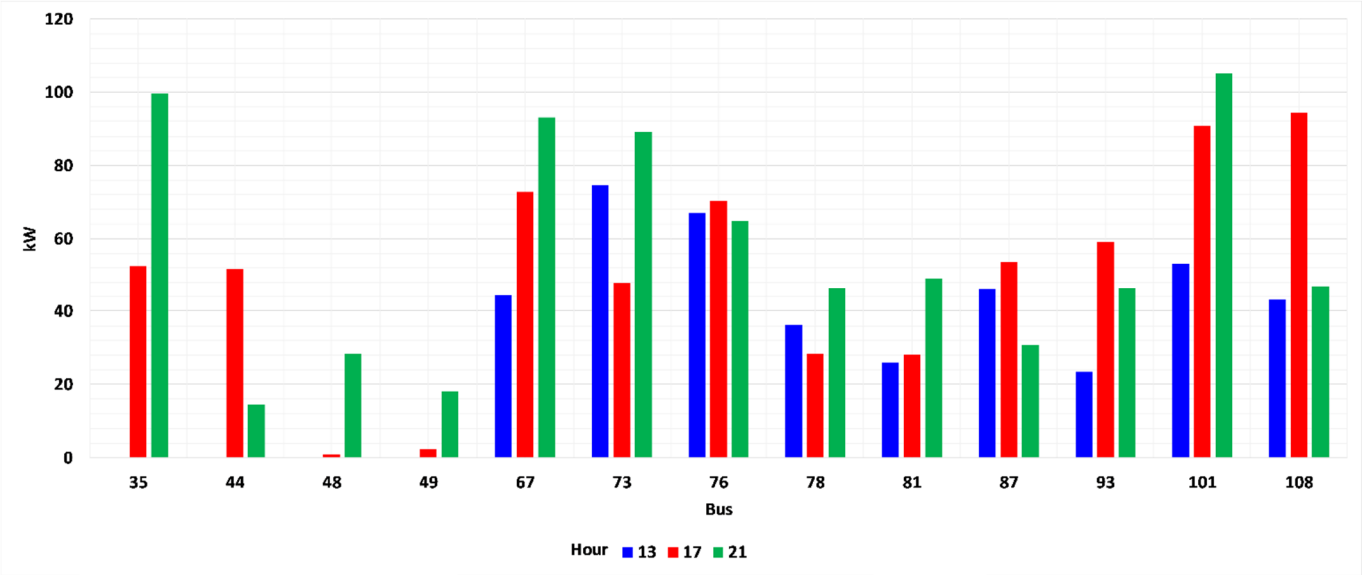


Fig. 43. The optimal microturbine electricity generations for the multi-microgrids system for the second case of external shock conditions.

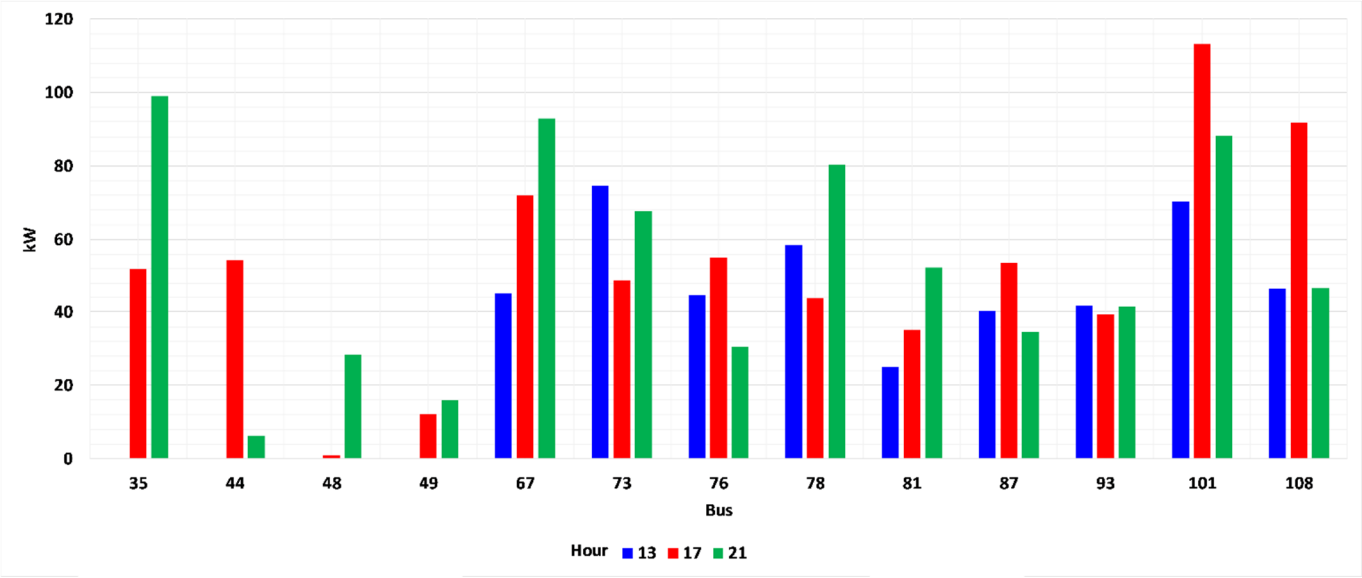


Fig. 44. The optimal microturbine electricity generations for the multi-microgrids system for the third case of external shock conditions.

Fig. 45 and Fig. 46 present the electrical power and energy of PHEVs for the third case of contingency conditions, respectively. The PHEVs were discharged in contingent conditions to balance the energy generations and consumptions. As shown in Fig. 46, the PHEVs of 68, 84, 102, 105, and 110 buses were heavily discharged for 21:00. The PHEVs supplied the unserved non-critical loads for the third case.

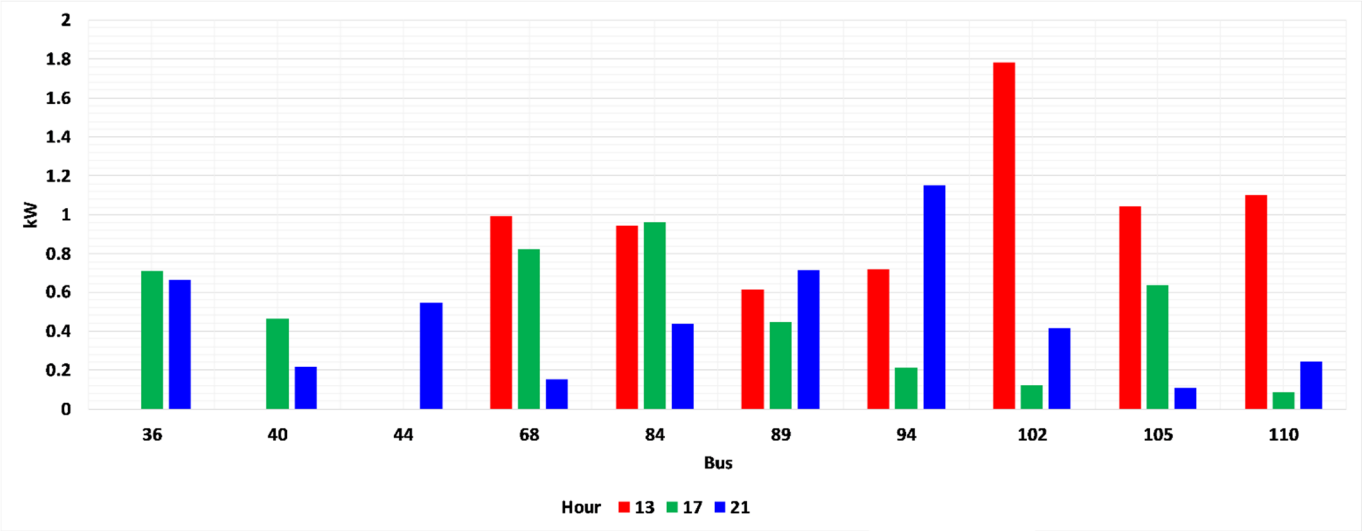


Fig. 45. The electrical power of PHEVs for the third case study in contingent conditions.

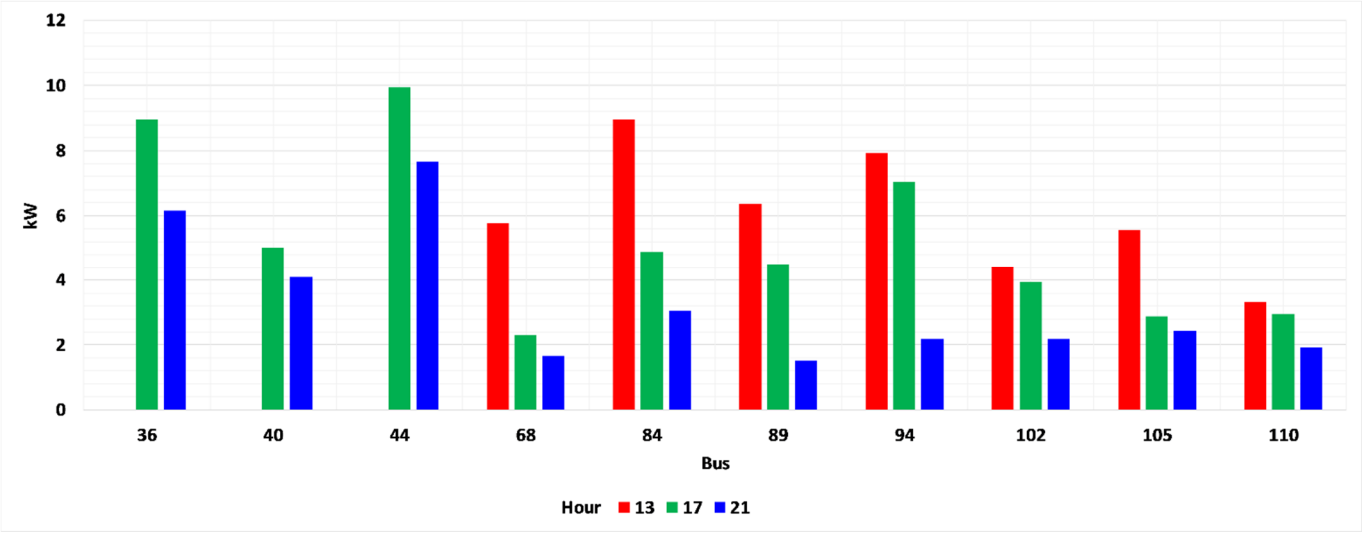


Fig. 46. The energy of PHEVs for the third case study in contingent conditions.

The simulation was carried out on a PC (AMD A10-5750M processor, 4×2.5 GHz, 8 GB RAM). The maximum simulation time for the normal operational condition was about 6217 seconds. Further, the maximum simulation time for the worst-case contingent condition was about 225.7 seconds. Table 12 presents the simulation times, continuous variables, discrete variables, and total equations of the optimization model for different cases.

Table 12. The simulation times, continuous variables, discrete variables, and total equations of the optimization model for different cases.

| Operation Mode | Case | | CPU time (sec) | Continuous variables | Discrete variables | Total equations |
|---|---|---|---|---|---|---|
| Normal | 1 | | 2145 | 1512637 | 720 | 1592632 |
| | 2 | | 3765 | 1535677 | 768 | 1637680 |
| | 3 | | 6217 | 1536487 | 948 | 1638040 |
| Worst-case contingent condition | 1 | Zone 1 | 23.9 | 18425 | 293 | 20403 |
| | | Zone 2 | 76.9 | 267553 | 2928 | 276712 |
| | 2 | Zone 1 | 26.4 | 18425 | 321 | 20459 |
| | | Zone 2 | 115.4 | 267553 | 3036 | 276928 |
| | 3 | Zone 1 | 29 | 19445 | 321 | 20969 |
| | | Zone 2 | 196.7 | 272413 | 3036 | 279358 |

In conclusion, the proposed optimization framework was successfully scheduled the utility-owned and non-utility owned distributed generation resources in day-ahead and real-time horizons for normal and contingent conditions. Further, the proposed algorithm explored the real-time operational conditions for different external shock impacts and changed the scheduling of system resources and performed the distribution system reconfiguration. Finally, the process determined the optimal sectionalizing of the distribution system into multi-microgrids to minimize the impacts of external shocks and scheduled the multi-microgrid system energy resources.

## 5. Conclusion

This paper addressed a multi-stage day-ahead and real-time operational scheduling of utility-owned and non-utility owned distributed energy resources considering the capacity-withholding opportunities of non-utility facilities. The proposed method determined the capacity withholding and resiliency indices and optimally switched the normally opened switches in day-ahead and real-time scheduling horizons to minimize the system's costs. Further, the process explored the adequacy of system resources in real-time normal operational conditions considering external shock impacts and sectionalized the system into multi-microgrids to mitigate the impacts of the external shocks. The proposed algorithm was assessed for the 33-bus and 123- bus test systems. The process successfully reduced the average value of aggregated operational and interruption costs of the 33-bus and 123-bus test systems by about 91.53% and 74.81%, respectively. Further, the proposed framework reduced the average and maximum values of the 33-bus system capacity-withholding index for real-time external shock conditions by about 61.64% and 64.19%, respectively. The authors are working on different capacity withholding indices to consider in the proposed algorithm. Further, the authors are working on the coordinated bidding of non-utility modelling and simulations.

## Acknowledgment

J.P.S. Catalão acknowledges the support by FEDER funds through COMPETE 2020 and by Portuguese funds through FCT, under POCI-01-0145-FEDER-029803 (02/SAICT/2017).

## References

1- Z. Li, M. Shahidehpour, F. Aminifar, A. Alabdulwahab, Y. Al-Turki," Networked microgrids for enhancing the power system resilience", *Proceedings of the IEEE*, 2017, **105**, pp. 1289-1310.

2- D.T. Ton, W.P. Wang, "A more resilient grid: The US department of energy joins with stakeholders in an R&D plan", *IEEE Power and Energy Magazine,* 2015, **13**, pp. 26-34.

3- Z. Li, Y. Xu, "Temporally-coordinated optimal operation of a multi-energy microgrid under diverse uncertainties", *Applied Energy,* 2019, **240**, pp. 719-729.

4- E. Grover-Silva, M. Heleno, S. Mashayekh, G. Cardoso, R. Girard, G. Kariniotakis,"A stochastic optimal power flow for scheduling flexible resources in microgrids operation", *Applied Energy,* 2018, , **229**, pp. 201-208.

5- N. Nikmehr, S. Najafi-Ravadanegh,"Optimal operation of distributed generations in micro-grids under uncertainties in load and renewable power generation using heuristic algorithm", *IET Renewable Power Generation*, 2015, **9**, pp. 982-990.

6- A. Rabiee, M. Sadeghi, J. Aghaei, A. Heidari, "Optimal operation of microgrids through simultaneous scheduling of electrical vehicles and responsive loads considering wind and PV units uncertainties", *Renewable and Sustainable Energy Reviews,* 2016, **57**, pp. 721-739.

7- H. Chamandoust , G. Derakhshan, S.M Hakimi , S. Bahramara, "Tri-objective optimal scheduling of smart energy hub system with schedulable loads", *J. Clean. Prod.* , 2019, **236**, 117584.

8- H. Chamandoust , G. Derakhshan, S. Bahramara, “Multi-objective performance of smart hybrid energy system with Multi-optimal participation of customers in day-ahead energy market”, *Energy Build.*, 2020, 216, 109964.
9- H. Chamandoust , G. Derakhshan, S.M Hakimi , S. Bahramara, “Tri-objective scheduling of residential smart electrical distribution grids with optimal joint of responsive loads with renewable energy sources, *J. Energy Storage*, 2020, **27**, 101112.
10- H. Chamandoust , G. Derakhshan, S. Bahramara, “Day-ahead scheduling problem of smart micro-grid with high penetration of wind energy and demand side management strategies”, *Sustainable Energy Technologies and Assessments*, 2020, **40,**100747.
11- H. Chamandoust , A. Hashemi, S. Bahramara, “Energy management of a smart autonomous electrical grid with a hydrogen storage system”, *Int. J. Hydrogen Energy,* 2021, **46**, 17608-17626.
12- F. Sheidaei, A. Ahmarinejad, “Multi-stage stochastic framework for energy management of virtual power plants considering electric vehicles and demand response programs”, *Int. J. Electr. Power Energy Syst*., 2020, **120**, 106047.
13- A. Rezaee Jordehia, Mohammad Sadegh Javadi, João P. S. Catalão, “Optimal placement of battery swap stations in microgrids with micro pumped hydro storage systems, photovoltaic, wind and geothermal distributed generators”, *Int. J. Electr. Power Energy Syst*., 2021, **125**, 106483.
14- F. Sheidaei, A. Ahmarinejad, M. Tabrizian, M. Babaei, “A stochastic multi-objective optimization framework for distribution feeder reconfiguration in the presence of renewable energy sources and energy storages”, *J Energy Storage,* 2021, **40**, 102775.
15- Z. Wang, J. Wang, “Self-healing resilient distribution systems based on sectionalization into microgrids”, *IEEE Trans. on Power Sys.,* 2015, **30**, pp. 3139-3149.
16- A. Hussain, V.H. Bui, H.M. Kim, ”Resilience-oriented optimal operation of networked hybrid microgrids”, *IEEE Transactions on Smart Grid,* 2017, **10**, pp. 204-215.
17- S. Chanda, A.K. Srivastava,”Defining and enabling resiliency of electric distribution systems with multiple microgrids”, *IEEE Trans. on Smart Grid,* 2016, **7**, pp. 2859-2868.
18- S.A. Arefifar, Y.A. Mohamed, T.H. El-Fouly,”Comprehensive operational planning framework for self-healing control actions in smart distribution grids”, *IEEE Transactions on Power Systems*, 2013, **28**, pp. 4192-4200.
19- A. Hussain, V.H. Bui, H.M. Kim,” A resilient and privacy-preserving energy management strategy for networked microgrids”, *IEEE Transactions on Smart Grid,* 2016, 9, pp.2127-2139.
20- J. Zhu, Y. Yuan, W. Wang,” An exact microgrid formation model for load restoration in resilient distribution system”, *Int. J. Electr. Power Energy Syst*., 2020, **116**, 105568.
21- M. Figueroa-Candia, F.A. Felder, D.W. Coit, “Resiliency-based optimization of restoration policies for electric power distribution systems”, *Electr. Power Syst. Res.*, 2018, **161**, pp. 188-198.
22- H. Farzin, M. Fotuhi-Firuzabad, M. Moeini-Aghtaie, “Enhancing power system resilience through hierarchical outage management in multi-microgrids”, *IEEE Transactions on Smart Grid,* 2016, **7**, pp. 2869-2879.
23- M. Zadsar, M.R. Haghifam, S.M.M. Larimi, ”Approach for self-healing resilient operation of active distribution network with microgrid”, *IET Gener. Transm. Distrib*., 2017, **11**, pp. 4633-4643.
24- S. Mousavizadeh, T.G. Bolandi, M.R. Haghifam, M. Moghimi, J. Lu, ”Resiliency analysis of electric distribution networks: A new approach based on modularity concept”, *Int. J. Electr. Power Energy Syst*., 2020, **117**, 105669.

25- A. Hussain, V.H. Bui, H.M. Kim, "Microgrids as a resilience resource and strategies used by microgrids for enhancing resilience", *Applied Energy,* 2019, **240,** pp. 56-72.

26- B. Balasubramaniam, P. Saraf, R. Hadidi, E.B. Makram," Energy management system for enhanced resiliency of microgrids during islanded operation", *Electr. Power Syst. Res.*, 2016, **137**, pp. 133-141.

27- T. Khalili, M. Tarafdar Hagh, S. Gassem Zadeh, S. Maleki,"Optimal reliable and resilient construction of dynamic self-adequate multi-microgrids under large-scale events", *IET Gener. Transm. Distrib*., 2019, **10**, pp. 1750 - 1760.

28- A. Khodaei, "Resiliency oriented microgrid optimal scheduling", *IEEE Trans. on Smart Grid,* 2014, **5**, pp. 1584-1591.

29- A. Eichhorn, H. Heitsch, W. Römisch,"Stochastic optimization of electricity portfolios: Scenario tree modeling and risk management", *Handbook of power systems* II, 2010, Springer, Berlin, Heidelberg.

30- H. Heitsch, W. Römisch,"Scenario reduction algorithms in stochastic programming", *Computational optimization and applications*, 2003, **24,** pp.187-206.

31- S. Salarkheili, M. Setayesh Nazar, "New indices of capacity withholding in power markets", *Int. Trans. on Elec. Energy Syst.*, 2015, **25**, pp. 180-196.

32- S. Salarkheili, M. Setayesh Nazar," Capacity withholding analysis in transmission constrained electricity markets", *IET Gener. Transm. Distrib*., 2016, **10**, pp. 487-495.

33- S. Salarkheili, M. Setayesh Nazar, " Capacity withholding assessment in the presence of integrated generation and transmission maintenance scheduling", *IET Gener. Transm. Distrib*., 2017, **11**, pp. 3903-3911.

34- M.S. Javadi, K. Firuzi, M. Rezanejad, M. Lotfi, M. Gough, J.P.S. Catalão, "Optimal Sizing and Siting of Electrical Energy Storage Devices for Smart Grids Considering Time-of-Use Programs", *IECON 2019, 45th Annual Conference of the IEEE Industrial Electronics Society*, 2019, https://doi.org/10.1109/IECON.2019.8927263.

35- M.S. Javadi, K. Firuzi, M. Rezanejad, M. Lotfi, M. Gough, A. Esmaeel Nezhad, J.P.S. Catalão, "Optimal Spinning Reserve Allocation in Presence of Electrical Storage and Renewable Energy Sources", *2019 IEEE International Conference on Environment and Electrical Engineering and 2019 IEEE Industrial and Commercial Power Systems Europe (EEEIC / I&CPS Europe)*, 2019, https://doi.org/10.1109/EEEIC.2019.8783696.

36- A. Bostan, M. Setayesh Nazar, M. Shafie-khah, J.P.S. Catalão, "An integrated optimization framework for combined heat and power units, distributed generation and plug-in electric vehicles", *Energy*, 2020, vol. 202, 117789.

37- F.S. Lobato, V. Steffen Jr., "Multi-objective optimization problems concepts and self-adaptive parameters with mathematical and engineering applications", 2017, *Springer Press*.

38- https://www.gams.com/latest/docs/S_DICOPT.html (last checked 07/18/2021)

39- https://www.gams.com/latest/docs/S_SCIP.html (last checked 07/18/2021)

40- M.E. Baran, M.E., F.F. Wu, 'Network reconfiguration in distribution systems for loss reduction and load balancing', *IEEE Trans. Power. Del.,* 1989, **4**, pp. 1401-1407.